DISSOLVED GASES IN HYDROTHERMAL PLUMES FROM ARTIC VENT FIELDS

Anne Stensland

Master of Science Thesis

Department of Earth Science

University of Bergen

October 2013

Abstract

Recent discoveries of active vent fields on slow and ultraslow spreading ridges have revealed that hydrothermal activity is more common than previously assumed. In the Norwegian-Greenland Sea, two such vent fields are found; the Jan Mayen vent fields (71°N and 6°E) and Loki`s Castle (73°30′N and 8°E). Both these systems are located on the ultraslow spreading Mohns Ridge, but they differ profoundly in the geochemical fluid and gas composition. This study presents dissolved hydrogen (H_2), methane (CH_4) and helium isotope (^3He) concentrations in the hydrothermal plume above the two vent fields. The results are based on samples collected during research cruises to the Norwegian Greenland Sea in the period 2007-2012.

The plume at the Loki's Castle rises 400 m from 2400 to 2000 m, and is characterized by considerable amounts of CH_4 and H_2. The rise-height is thus 50-200 m higher than observed in most hydrothermal fields in the Atlantic and Pacific Oceans. Dilution factors for the buoyant and the non-buoyant plume was calculated to be 1700 and 8900, respectively. The thermal output from Loki's Castle (1300 MW) was estimated to be comparable to that of the Rainbow field due to similar ^3He input. Loki's Castle is situated between different ocean current systems, causing extensive mixing and transportation of the plume. Elevated ^3He concentrations close to the seafloor indicate either deep water transport from the north or hydrothermal input from the ridge below. Comparison to the deep seawater at the East Pacific Rise, where the spreading rate is 7.5 times faster and the ^3He input 6 times larger than at the AMOR, indicating a correlation between spreading rates and the magnitude of hydrothermal activity. Because of background concentrations up to 5 and 7 nM for H_2 and CH_4, respectively, reliable evidence for hydrothermal input requires values higher than these. Methane anomaly at a depth 2319 m indicate a possible new vent field southwest of Loki's Castle.

The non-buoyant plume at the Jan Mayen vent fields (JMVF) was characterized by moderate CH_4 and low H_2 concentration, and rose 150 m above the Troll Wall and 200 m above the Soria Moria vent field. The dilution factor for the non-buoyant plume was estimated to be 9500 at the Troll Wall vent field. Diffuse venting occurring at the Troll Wall was characterized by the moderate CH_4 and very low H_2. The CH_4 produced here may be of biogenic origin, produced by methanogenesis at or below the seafloor. The H_2 content in the water column in 2011 was about 26 times higher than observed in any other year. This excess H_2 probably originated from an eruptive event at the seafloor in the JMVF area.

The results demonstrate that determination of the dissolved gas composition provides vital information on processes occurring in the surface and subsurface at Artic vent fields.

Acknowledgments

Without the eminent help and guidance from my supervisors this thesis would never come together. For this I owe a great thanks to Rolf Birger Pedersen, Ingunn H. Thorseth and Tamara Baumberger. I would also like to give thanks to all the scientists whom have taken part of the cruises I have participated in. A special thanks to the great Marvin D. Lilley and Eric Olsen for allowing me to analyze data they obtained over the years.

I also want to acknowledge Alden Denny for being the ArcGis wizard that he is. And a great thank you to Elinor Bartle for helping to be a better writer.

Thanks to my great friends Marie Songve, Jørn Ådneram, Joar Svindland, Daniel Aasheim and Vegard Hausken for making these past 5 years the best in my life. Morten Grefstad, thank you for all the laughs and all your patience.

Contents

1. Introduction

1.1 Objective

In the spring of 1977 on the Galapagos Rift, the first hydrothermal deep-sea vent field was discovered (Corliss et al., 1979). Since the discovery, it has been established that circulation of seawater through the oceanic crust and sediments is crucial for the transportations of volatiles and heat to the ocean water. Stein and Stein [1994] estimated that of the total global ocean heat flux of $32*10^{12}$ W, 34 ±12 % originates from hydrothermal flow. Estimating fluxes and sizes of hydrothermal fields at mid-ocean spreading ridges is essential for understanding the effect of hydrothermal circulation on ocean chemistry, on its geology and the mineralization of the oceanic crust. The latter may also have important economical concequences in the future.

Ultraslow spreading ridges are defined as ridges with spreading rates <20mm/y. (e.g Dick et al., 2003; German et al., 2010). Ultraslow spreading ridges are typically found on two parts of the global ridge system; the Artic Mid-Ocean Ridge (AMOR) and the Southwest Indian Ridge (SWIR) (Dick et al., 2003). Hydrothermal venting was previously believed to be rare or absent at these ridges because ultraslow spreading can result in extremely thin crust and abundant exposure of mantle material (Dick et al., 2003; Michael et al., 2003; Pedersen et al., 2010). It was not until 1997 that hydrothermal activity was discovered on ultraslow spreading ridges (SWIR) (German et al., 1998; Pedersen et al., 2005; Connelly et al., 2007). Over the last decade approximately twenty active and extinct vent sites have been located on the AMOR, mostly by water column anomalies or dredging (Olafsson et al., 1990; Hannington et al., 2001; Snow et al., 2001; Edmonds et al., 2003; Nygaard et al., 2003; Pedersen et al., 2005 Connelly et al., 2007; Pedersen et al., 2010a). Bordered by the Iceland hot spot in the south, the AMOR gradually evolves from being a magmatically robust system to a magmatically starved system in the north. The reason for this evolution is the decreasing spreading rates and therefore a decreasing volcanic influence in the south-north direction (Pedersen et al., 2010a). This contrast enables a large variability in the geology and geochemistry of vent fields potentially present.

Introduction

The high temperature volatiles which are emitted from hydrothermal vents, will rise up in the water column where they progressively mix with the surrounding water. The heated, chemical rich water will rise until neutral buoyancy is established underneath a density layer (e.g Lupton 1985). The hydrothermal plume then disperse under this layer. The composition of the hydrothermal plume can in many ways give us an understanding of how the hydrothermal circulation affects the ocean chemistry. Through concentrations of dissolved species one may estimate how much hydrothermal activity there is in the area. Comparing the hydrothermal plumes in the Norwegian-Greenland Sea to plumes found in other parts of the world can indicate differences and similarities between oceans. Another aspect of plume investigations concerns how the dissolved gases are consumed/oxidized over time and by what processes.

In this study I investigate the methane, hydrogen and helium content of the hydrothermal plumes of the two deep-sea vent fields first discovered at the AMOR. These fields, the Jan Mayen vent fields and the Loki`s Castle vent field, are located at the northern and southern end of the Mohns Ridge in the Norwegian-Greenland Sea, respectively.

Specific objectives for the study are:

- Deduce a general pattern of the non-buoyant plume at both vent fields and investigate possible deviations from the general pattern.
- Compare these vent fields with other vent fields
- Investigate the mixing and consumption in the hydrothermal fluids.
- Estimate the dilution of the hydrothermal plumes.
- Address the possibilities of additional vent fields being present in the regions.

The water column samples on which the thesis is built, were collected during 5 different cruises with the R/V G.O.Sars to this area between 2007 and 2012. Measurements of hydrogen and methane concentrations were done shipboard by Marvin D. Lilley, Eric Olsen and Tamara Baumberger from 2007-2011. In 2012 the measurements of these parameters were performed by Tamara Baumberger and Anne Stensland (the author). In addition to hydrogen and methane, samples for ^{3}He isotope and concentration analysis were also collected.

1.2 The path through the hydrothermal system

Seawater may be able to circulate within the crust if certain requirements are met. One needs the presence of a heat source, either magma or newly solidified rock. Because of this, circulation of fluids usually occurs at or in association with mid-ocean spreading ridges. A second requirement is a permeable medium, usually faulted or fissured igneous rock (e.g. Tivey, 2007). During the journey from the seafloor to depths of 1-4 km the seawater will undergo extreme changes in temperature, volatile concentrations and composition as it approaches the magma chamber (e.g. Kelley et al., 2002). The first reaction phase (low temperature alteration) starts in the so-called "recharge" zone with relative low temperatures (40°C-60°C) (Alt, 1995). In this zone, primary solid phases (e.g. basaltic glass, olivine and plagioclase) are altered into secondary minerals, such as ferric mica, smectite and Fe-oxyhydroxides (e.g. Tivey, 2007). The second step, deeper in the crust, is precipitation of smectite and chlorite, which will cause a decrease of Mg and an increase of Ca^{2+}, H^{+} and Na^{+} in the penetrating fluid (e.g Alt, 1995). This reaction phase takes place at elevated temperatures. If the temperature exceeds 150°C, anhydrite will precipitate and cause a depletion of Ca^{2+} and SO_4^{2-} in the fluid (e.g. Bischoff and Seyfried, 1978; Alt, 1995; Tivey, 2007). As the fluid penetrates deeper, another alteration process occurs, where anorthite is altered into albite (albitization). In this process Na^{+} and Si are added to the crust in substitution for Ca^{2+}, which is released into the fluid. The seawater is at this point slightly acidic, anoxic, Mg poor and alkali rich compared to initial seawater (e.g. Tivey, 2007). The last alteration stage takes place at the "reaction zone", which defines the deepest part of the circulation system (Alt, 1995). It is believed that this zone occurs near the sheeted dyke-gabbro interface or within the gabbroic layer of the crust (e.g. Kelley and Delaney, 1987; Alt, 1995; Kelley et al., 2002). In this zone the fluid leaches metals and sulfur from the rocks. Volatiles from magma, such as He, CO_2, H_2 and CH_4, may also be added to the fluid (e.g Alt, 1995; Tivey, 2007). As igneous rock obtains its volatile content from the mantle, the initial mantle composition reflects the volatiles available (Kelley et al., 2002). From this point the modified seawater rises as a heated buoyant fluid through the up-flow zone. The chemistry of the hydrothermal fluid is determined by three factors: (1) temperature of the surrounding rock, (2) how much water has made the same journey and reacted with the available rock (water/rock ratio) and (3) the composition of the host rock (Kelley et al., 2002). The hydrothermal fluid will now have a temperature of 350-400°C and a pH between 2 and 6 (e.g

Bischoff and Seyfried, 1978; Alt, 1995). Relative to seawater, the hydrothermal fluid will be enriched in Li, K, Rb, Cs, SiO_2, Fe, H_2S, CO_2, He, H_2 and CH_4 (e.g Kelley et al. 2002). As the fluid emits from the seafloor it meets cold, oxygen-rich seawater. The dramatic change in temperature causes precipitation of anhydrite, barite, silica, sphalerite and chalcopyrite (Kelley et al., 2002). When hydrothermal fluids are emitted from high temperature vents, the fluids are less dense than the surrounding water. The fluids therefore form buoyant plumes that rise rapidly through the water column (e.g. Lupton and Craig, 1981; Lupton et al., 1985; de Angelis et al., 1993). Density layers in the water column are products of temperature and salinity. When the warm, less dense vent fluids come in equilibrium with a density layer, neutral buoyancy is established, generally several hundred meters above the venting site (e.g. Lupton and Craig, 1981; Lupton et al., 1985; de Angelis et al., 1993). When neutral buoyancy is established, the plume starts spreading out along the density layer (e.g. Lupton et al., 1981; 1985). When spread out, the plume is called a non-buoyant plume. This non-buoyant plume will have slightly higher temperature and an enrichment of chemical compounds compared to the surrounding seawater. The non-buoyant may therefore also be referred to as a chemical plume.

1.3 Previous studies on hydrothermal plumes

Previous work done on hydrothermal plumes had many different objectives. Temperature, salinity, redox potential and particle anomalies in the water column are often used to identify and quantify the hydrothermal plume (e.g. Rudnicki et al 1994; James et al., 1995; German et al., 1996). Another method used for quantifying plumes is to consider the hydrography. Speer and Rona [1989] established a mathematical model that estimates the thermal flux at a level of neutral buoyancy. Such a model has been utilized at both the Rainbow and TAG vent fields at the MAR (Rudnicki et al. 1994; German et al. 1996). Measurements of dissolved chemical species in the water column are one of the most commonly used techniques for identifying a hydrothermal plume. However, the compounds which are measured vary. Methane (CH_4), hydrogen (H_2) , Fe, Mn, and ^{3}He are some of the most abundantly measured species but also other plume characteristics such as pH and Eh are commonly analyzed (e.g. Kelley et al., 1998; Connolly et al., 2007; German et al., 2010). The hydrothermal systems presented in this thesis are situated on an ultraslow spreading ridge. Connolly et al. [2007] published an article

on hydrothermal plumes on the Knipovich Ridge. The Knipovich Ridge is an ultraslow spreading ridge of the AMOR system and thus the most closely related to the two vent systems presented here. The methods used for plume detection by Connolly et al. (2007) include optical backscatter anomalies, CH_4, total dissolvable Mn (TdMn) and adenosine triphosphate (ATP). Optical backscatter anomalies were detected using a deep-tow side scan/ sensor string and (TdMn) and ATP were analyzed shipboard in water column samples.

In this thesis the focus is on three dissolved chemical species: CH_4, H_2 and ^3He.

1.4 Sources for H_2, CH_4 and ^3He

Although the chemical species emit from the same vent, the sources of the volatiles differ profoundly. In this section the sources for each of the dissolved gas species that is focused on in this thesis are presented.

1.4.1 CH_4 Source

According to Welhan (1988), methane venting from hydrothermal vent systems has four primary sources:

1. Biogenic production of methane, which mainly occurs at low temperatures.
2. Thermal decomposition of biological material, which occurs at high to moderate temperatures (>100°C). This is normally referred to as thermogenic production of methane.
3. Degassing of juvenile carbon species (CO_2) and subsequent reduction to CH_4.
4. Abiotic synthesis. This process occurs preferentially at high temperatures (>300-400).

The first two sources are influenced by biological matter, while 3 and 4 are abiotic processes. Biogenic methane is produced from the metabolic and biosynthetic activities of organisms and is common in diffuse venting hydrothermal systems. Thermogenic methane is produced from thermal decomposition of organic material that has undergone diagenic processes (McCollom and Seewald. 2007). Thermogenic production of methane is low at hydrothermal systems without a sedimentary influence. However, at sediment influenced vent fields the thermogenic input of methane makes up a relative large percentage of the total methane input to the hydrothermal circulation (Welhan 1988).

Abiotic production of methane is a purely chemical process with no participation of organic material (Welhan 1988). Abiotic production is due to either direct loss of volatiles at the magmatic stage, or to rock leaching during hydrothermal fluid penetration (Welhan, 1988). Another type of such abiotic reactions is Fischer-Tropsch-type (FTT) reactions (e.g. Horita and Berndt, 1999; Bradley and Summons, 2010*)*. FTT reactions use surface catalyzed reduction of oxidized carbon to methane and other light hydrocarbons under excess H_2 conditions (e.g. Bradley and Summons, 2010). This reaction type has been suggested to explain the elevated hydrocarbon concentrations in hydrothermal fluids from ultramafic hosted systems (e.g. Proskurowski et al. 2008). Although FTT reactions may occur in hydrothermal systems, it appears as if FTT are not the predominant producers of methane in these environments (McCollom 2008). Methane may also be produced abiotically by Sabatier reactions, which is the reduction of CO_2 to methane without the release of other alkanes as occurs in FTT reactions (Horita and Berndt, 1999; Seewald et al. 2006; Fiebig et al., 2007; McCollom and Seewald, 2007; Bradley and Summons, 2010). Methane is unstable and oxidizes in hydrothermal plumes due to the high energy yield of methane. CH_4 oxidation rates are therefore significantly enhanced in plumes compared to background seawater. The methane oxidation rates have been measured by de Angelis et al. (1993) at the Endeavour segment of the Juan de Fuca Ridge. The oxidation rates in this area were measured to be up to 0.15 day^{-1}, corresponding to turnover in approximately a week (de Angelis et al., 1993).

1.4.2 H_2 source

Hydrogen gas in hydrothermal fluids may have a variety of origins. Serpentization of mantle rocks is a known source of H_2 (and CH_4) at slow and ultraslow spreading ridges where ultra-mafic rocks are exposed. The production of H_2 is induced by the oxidation of Fe^{2+} in primary mantle minerals such as olivine and pyroxene to Fe^{3+}, and the formation of secondary minerals such as magnetite and serpentine (Marcaillou et al., 2011). The following three reactions show how H_2 is produced during the transformation of primary to secondary minerals (Marcaillou et al. 2011).

$$(2Fe_{0,5}Mg_{1,5}SiO_4) + 7/3H_2O \rightarrow (Mg_3Si_2O_5(OH)_4) + (1/3Fe_3O_4) + (1/6H_2) \quad (1)$$

olivine — serpentine — magnetite

$$(2Fe_{0,5}Mg_{1,5}Si_2O_6) + 7/3H_2O \rightarrow (Mg_3Si_2O_5(OH)_4) + (1/3Fe_3O_4) + (1/6H_2) + 2SiO_2aq \quad (2)$$

Opx — serpentine — magnetite

$$Fe^{2+}+H_2O \rightarrow Fe^{3+}+H_2 \quad (3)$$

Equation (1) and (2) both display serpentinization reactions. These reactions occur in ultra-mafic hosted systems, in less mafic hosted systems, however, the reactions will not be the same. Equation (3) is a general reaction that occurs when hot mafic lava comes in contact with seawater, such as during eruptions at submarine volcanoes. Hydrothermal alteration of basalt produces secondary minerals that contain Fe^{2+} in the structures. A result of this is that hydrothermal alteration of basalt produces less H_2 than at ultra-mafic systems (e.g. McCollom and Seewald, 2007). However, there are other options for H_2 production in hydrothermal systems. As seawater approaches the recharge limb of the hydrothermal circulation zones, the reaction rates increase. This temperature-induced increased reactivity may produce additional H_2 in basaltic hosted systems (e.g. McCollom and Seewald. 2007).

Hydrogen in the non-buoyant plume is suggested to be oxidized within a couple of hours after venting, because hydrogen is a favorable electron donor, and gives a high energy yield during its oxidation. The energy yield from this process is much higher than from methane oxidation (Petersen et al., 2011). For example, Petersen et al., (2011) reported that the aerobic hydrogen oxidation at the Logatchev vent could provide up to 7 times more energy per kg compared to the methane oxidation there. This difference in energy yield is the reason why methane remains longer in the water column than hydrogen.

1.4.3 ^{3}He source

^{3}He is believed to be of primordial origin, which means that the presence of ^{3}He in the ocean reflects input from the mantle. Such inputs usually originate from submarine hydrothermal vents and volcanoes (e.g. Resing et al., 2004). This helium isotope is not produced or consumed by any reaction at the surface, which makes ^{3}He a very effective tracer for hydrothermal activity (e.g. Kelley et al., 2002). Together with heat it is the most effective tracer used in tracing hydrothermal vent fields. It has also been suggested that the ^{3}He concentration is proportional to the spreading rate (e.g Lupton, 1995).

As both H_2 and CH_4 show varying residence time in the hydrothermal plume, comparing them to ^3He makes it possible to assess the original source fluids as well as the chemical evolution of the plume by aging (Lilley et al., 1995; Lupton, 1995; Massoth et al.,1998; McLaughlin, 1998; Kelley et al., 2002;).

2 Geological Setting

The AMOR has been defined as the spreading ridge north of 66°, and can be divided into six segments: (1) The Kolbeinsey Ridge, (2) The Mohns Ridge, (3) the Knipovich Ridge, (4) the Molley Ridge, (5) the Lena trough and (6) the Gakkel Ridge (Pedersen et al., 2010a). The Jan Mayen vent fields and the Loki`s Castle vent field are located at the two opposite ends of the Mohns Ridge in the Norwegian Greenland Sea (Fig. 1). The two vent fields show a great variation in geology and geochemistry that will be explained further in the following pages.

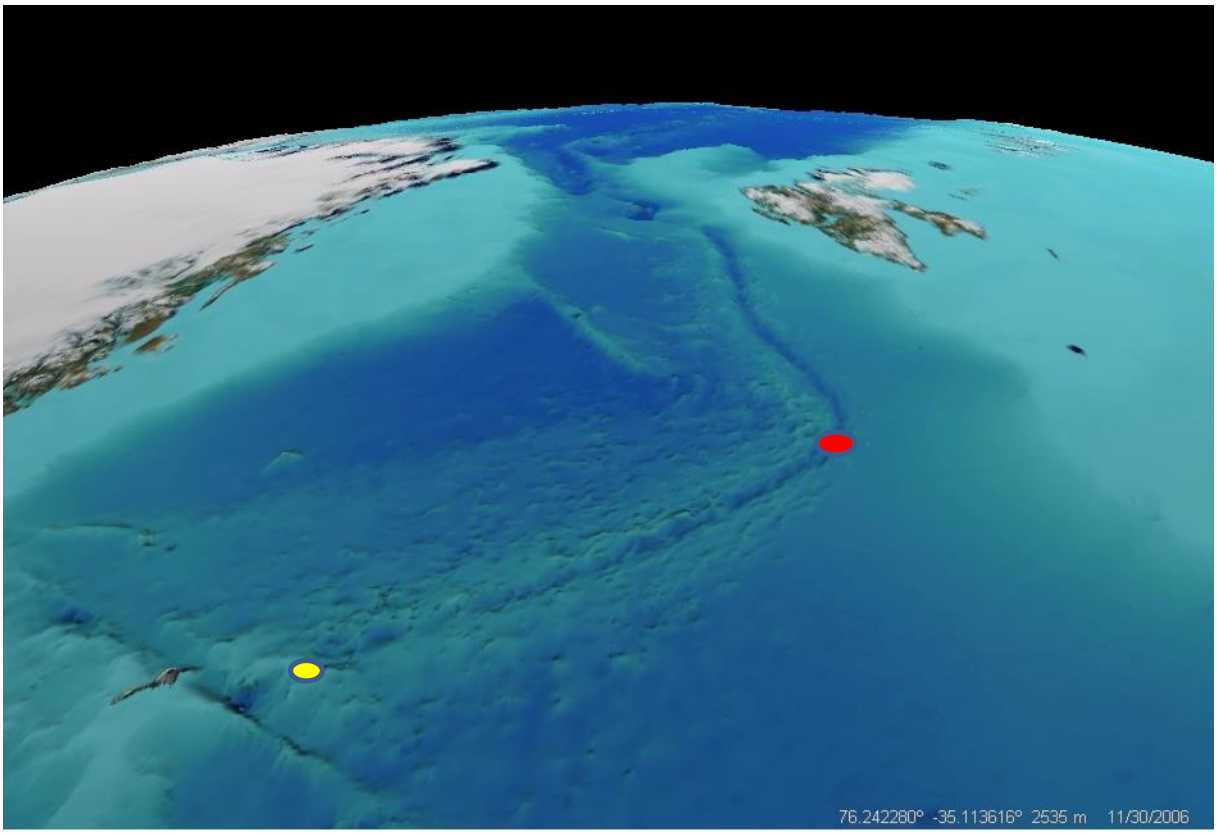

Figure 1: Location of the Jan Mayen vent fields (yellow circle) and the Loki's Castle vent field (red circle) on the opposite end of the Mohns Ridge.

2.1 The Jan Mayen vent fields

The Jan Mayen vent fields consist of two separate vent fields; the Troll Wall and the Soria Moria vent fields. The fields, which were discovered in 2005, are located near the southern termination of the Mohns Ridge at 71°N and 6°E and are separated by approximately 5 km (Pedersen et al., 2010a). The end-member fluid composition of the Troll Wall vent field and the Soria Moria vent field is 0.01–0.9 mM for methane and 0.01–0.1 mM for hydrogen (Pedersen et al., 2010a).

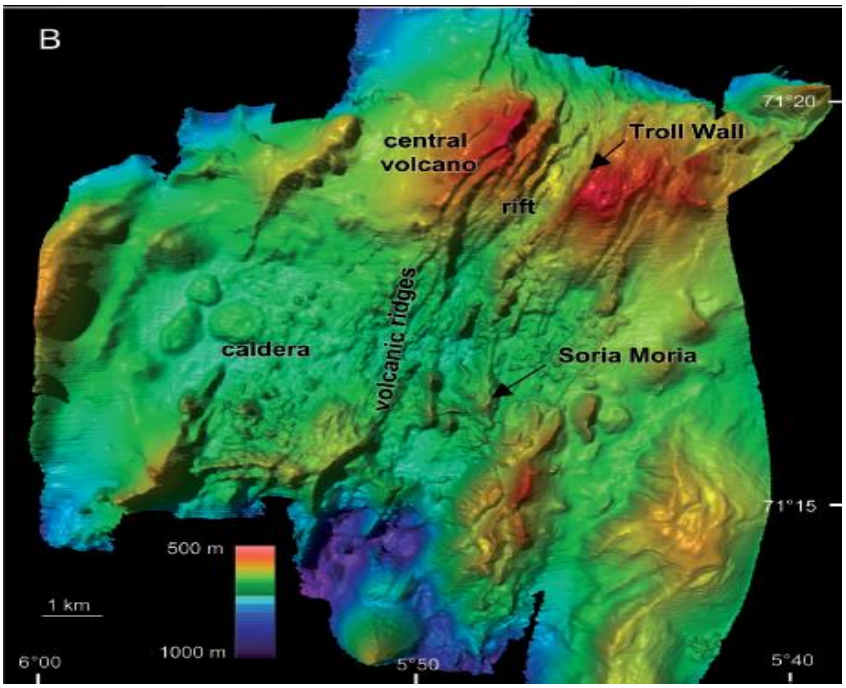

Figure 2. Bathymetric map showing the southernmost part of the Mohns ridge and the location of the Troll Wall and Soria Moria vent fields (from Pedersen et al., 2010a).

2.1.1 Troll Wall vent field

The Troll Wall vent field is a high temperature venting site at about 550 m water depth with vent fluid temperatures reaching 270 °C. (Pedersen et al., 2010a) There are at least 10 major vent sites in the area with multiple chimneys found at each site (Fig. 2). Chimneys reach a height of 10 m and are located on hydrothermal mounds, which sit on top of talus deposits. The chimneys are mainly composed of anhydrite, barite, sphalerite and pyrite. Hydrothermal fluids diffuse through the seafloor surrounding the chimneys. These areas are also covered with extensive white bacterial mats. The temperature gradient through these bacterial mats is

steep with a seawater temperature close to zero and a temperature 15 cm below the seabed of 80 °C (Pedersen et al., 2010a).

2.1.2 Soria Moria vent field

The Soria Moria vent field is another high temperature field located 5 km south of the Troll Wall vent field. In contrast to the Troll Wall, Soria Moria is located on a volcanic ridge that covers an area of 7 km^2 (Pedersen et al., 2010a). Hydrothermal fluids are discharged at about 700 m water depth at two different settings. Here white smoker, turbulent fluids are emitted from 8-9 m tall sulfide chimneys and clear, lower temperature fluids erupt from barite and silica structures (Fig. 3) (Pedersen et al., 2010a). The vent fluid temperature at Soria Moria reaches generally the same level as that of the Troll Wall vent field, about 270 °C.

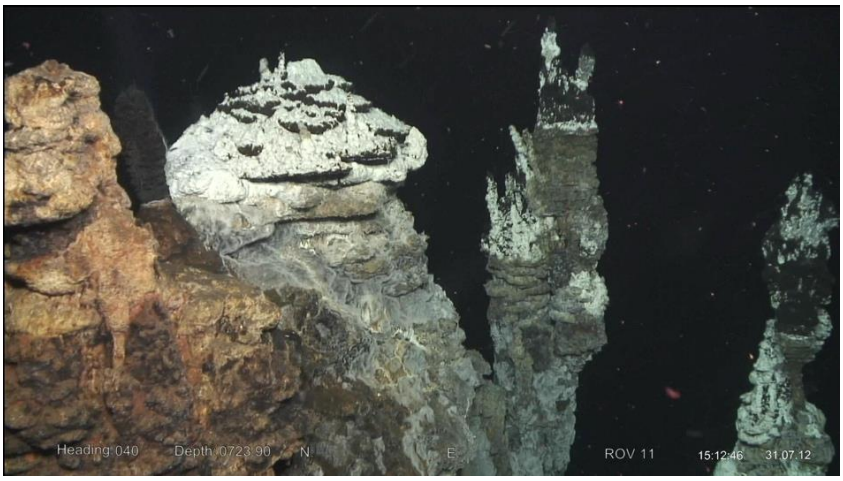

Figure 3. The vent «Kremtoppen», located at the Soria Moria vent field.

2.2 The Loki's Castle vent field

The Loki's Castle vent field was discovered in 2008 (Pedersen et al., 2010a; 2010b). The high temperature venting site is located at about 2400 m water depth on the crest of a volcanic ridge, where the Mohns Ridge transitions into the Knipovich Ridge. The field is situated near the northwestern margin of the rift valley, where sedimentary deposits tower 100 m above the rift-valley floor. The chimneys at this hydrothermal field are located on two sulfide mounds that are separated by 150 m, and are estimated to be 20-30 m high. There are four major active, black smoker chimneys up to 13 m tall, which release volatiles and fluids at temperatures of 310-320 °C (Fig. 4). The end-member concentrations of methane and

hydrogen at the Loki's Castle vent field are 15 and 5 mM, respectively (Pedersen et al., 2010a). The end-member concentrations were measured on 3 cruises over 3 years, and the CH_4/H_2 ratio in the vents remained the same in each year (Pedersen et al., 2010b).

Figure 4. Sampling of high-temperature vent fluids from one of the four chimneys at Loki`s Castle.

2.3 Hydrography in the Norwegian-Greenland Sea

Hydrothermal plumes are strongly influenced by the local hydrography. A basic understanding of the hydrography in this arctic region is therefore necessary.

The circulation in the Norwegian-Greenland Sea has been found to be consistent with a cyclonic gyre (Fig 5) (Johannesen, 1986; Blindheim and Rey, 2004). The coldest surface temperature in the Nordic Seas is found within the central gyre in the Greenland Sea (Fig 5) (Swift, 1986). The East Greenland current flows along the eastern coast of Greenland. The current has two major branches, the Jan Mayen current and the East Icelandic Current, respectively (Blindheim and Rey, 2004). The Jan Mayen current is the southern current of the central Greenland Sea gyre. In the northern part of the gyre the West Spitsbergen Current re-circulates into the East Greenland Current (Blindheim and Rey, 2004). In this merger, the West Spitsbergen Current meets waters from the Atlantic returning from the Artic (Blindheim and Rey, 2004). This mixing results in the Re-circulating Atlantic Water that exists as an intermediate water mass in the Norwegian-Greenland Sea (Blindheim and Rey, 2004). Below the intermediate water layer, deeper layers fill the basins with water originating from the

Arctic Ocean (Malmberg, 1983; Meincke and Rudels, 1995; Malmberg and Jönsson, 1997; Blindheim and Rey, 2004). This artic deep water can be identified by either its distinct temperature or salinity, and is found at a depth between 1100 and 2400 m (e.g Blindheim and Østerhus, 2005; Jütterström and Jeansson, 2008).

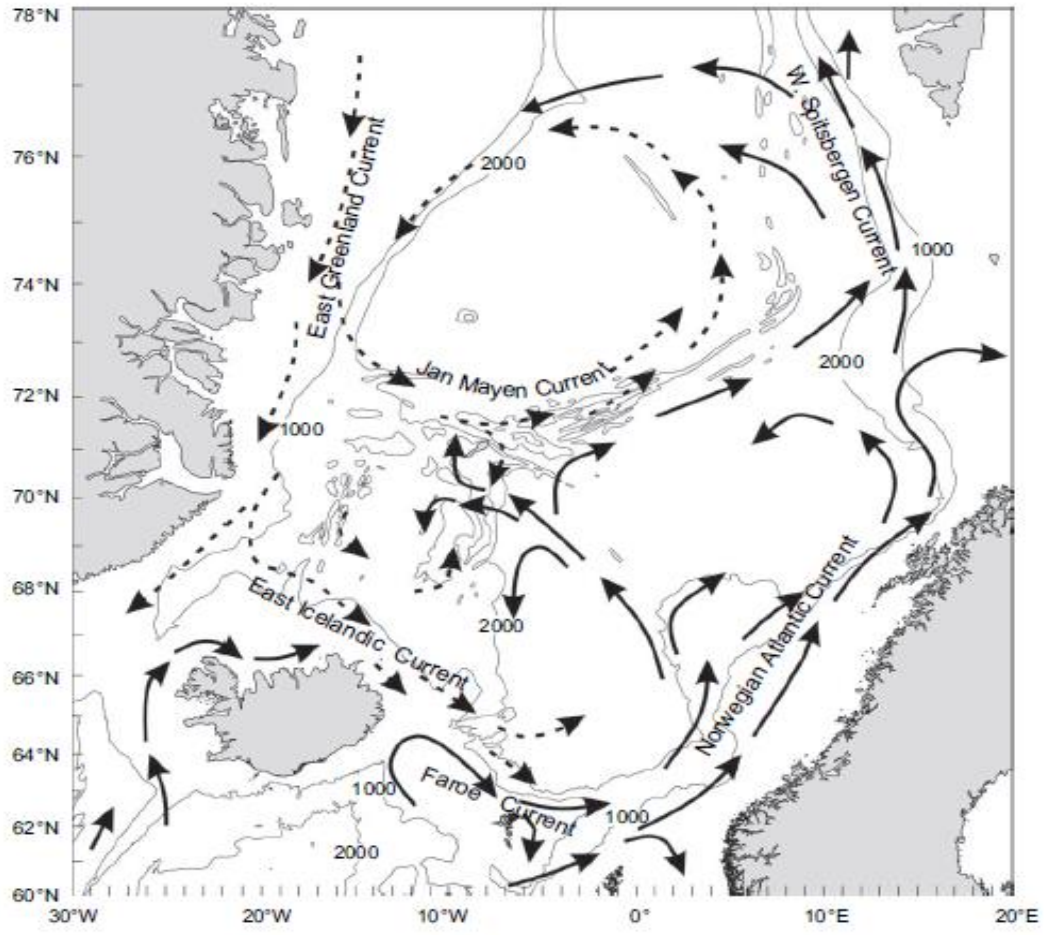

Figure 5. Ocean current systems in the Norwegian-Greenland Sea. The stapled lines indicate cold, deeper water masses than the solid lines (From Blindheim and Rey, 2004).

3 Materials and Methods

This thesis is based on water column samples and data collected during CGB cruises to the Norwegian Greenland Sea with the R/V G.O. Sars in the period 2007-2012. The water column samples were collected using a CTD (conductivity, temperature, density) probe with a Neskin water bottle rosette (911plus Seabird).

Methane and hydrogen analysis were done in the shipboard laboratories shortly after sampling from the CTD bottle rosette. 100 ml of bubble free water was injected into 140 ml syringes. After sampling, a 40 ml head space of ultra-pure helium gas was added to the sample. After injection of the head space gas, the samples were shaken and left to warm up to room temperature to reach equilibrium for H_2 and CH_4 between gas and water phase (Fig. 6). When equilibrium was reached, the head space was injected into a SRI 8610C gas chromatographs. The methane concentration was measured by a flame ionization detector (FID) and the hydrogen concentration by a helium-pulsed discharge detector (PDD). Each run in the gas chromatograph took 4 minutes before the results could be read as gas chromatographs on the attached computer. The results were read as the integrated area below a peak and were given in counts per second. To convert this value into concentrations a formula (gas equation) and a calibration curve were applied to the results in excel. The standards used for calibration were 1 ppm, 2 ppm, 5 ppm and 10 ppm. Hydrogen and methane have background seawater concentrations of 0.2 and 0.4 nM, respectively (e.g Baumberger, 2011).

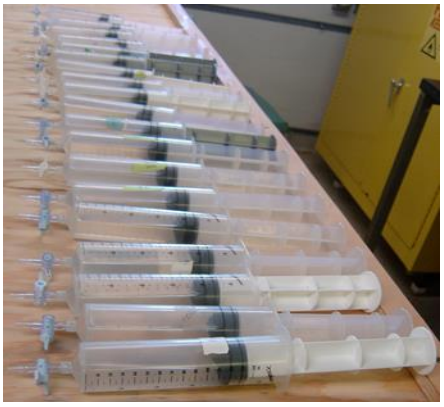

Figure 6. Water samples with He headspace gas ready for gas chromatograph analysis. Photo by Tamara Baumberger 2008.

The water samples for helium were taken by a gravity-feed technique through Tygon tubing into 24 inch copper tubes (Jenkins et al., 2010). Plastic is permeable to helium but the water stays within the plastic for a short amount of time, so this is not a problem for the measurement. The advantage of using plastic tubing is that it makes it possible to see any gas bubbles traveling in the plastic tube (Jenkins et al. 2010). It is very important to eliminate all air bubbles from the helium samples because helium has a low solubility, even a small air bubble will give a large impact on the result. The Cu tubes have duplicate half sections that

are cold-welded for later analysis of He isotopic ratios (e.g. Young and Lupton, 1983). Copper has a low permeability for helium and is therefore ideal for storing samples for a period of time without contamination (Jenkins et al., 2010). Before sampling a part of the tube is flattened to reduce the volume. When tubes with the sample have been sealed the flattened part is re-rounded to maintain a negative pressure within the sample (Jenkins et al., 2010). The sealing of the copper tubes is done by crimping the tubes to form a pressure welded seal. The samples were subsequently cleaned in freshwater to prevent salt driven corrosion. The sample tubes were sent to the NOAA-(Nation Oceanic and Atmospheric Administration) in New Port, OR, U.S.A for shore-based analysis. At NOAA, the samples were analyzed using a dual collector, 21-cm-radius mass spectrometer with 1σ precision of 0.2% in $^{3}He/^{4}He$ value and a concentration accuracy of 1% relative to a laboratory air standard.

The results of the helium isotopic ratio analysis are given in femtomolar (fM) of ^{3}He and delta ^{3}He (%). The delta ^{3}He (%) is describing the $^{3}He/^{4}He$ ratio in the seawater sample relative to the ratio in the atmosphere and is calculated using the following equation;

$100(R/Ra-1) = Del\ ^{3}He\%$

$Ra=^{3}He/^{4}He$ ratio in the atmosphere, $R=^{3}He/^{4}He$ ratio in sample.

4 Results:

4.1 The Loki`s Castle vent field

The primary goal for the cruise to the Mohns Ridge and the Knipovich Ridge in 2007 was to locate a potential hydrothermal field where the two ridge segments meet. During this cruise, 32 CTD casts with water column sampling for methane and hydrogen analysis were performed. Ten of these CTD casts were also sampled for helium isotope analyses. However, even if hydrogen and methane anomalies were detected in many of these samples, no vent field was located in 2007. Loki`s Castle was finally located towards the end of the 2008 cruise to the same region. During the 2008 cruise, dissolved CH_4 and H_2 were measured in a total of 24 CTDs (including tow-yos). Only 4 of the CTDs were sampled for helium isotope analyses. In 2009, methane and hydrogen content were measured in a total of 7 CTDs and 3 of these were also sampled for helium isotopes analyses. The results of the analyses of all samples are included in Appendix 1.

As a result of searching for a new vent field, the CTD sites in 2007 were distributed over a relatively large area but most were located east of the vent field (Fig. 7). The distribution was also relatively large in 2008, but this year most CTD cast were located west of Loki´s Castle. After locating the vent field in 2008, most CTDs were collected close to the vent field. In 2009 all CTD casts were collected almost directly above or close to the vent field.

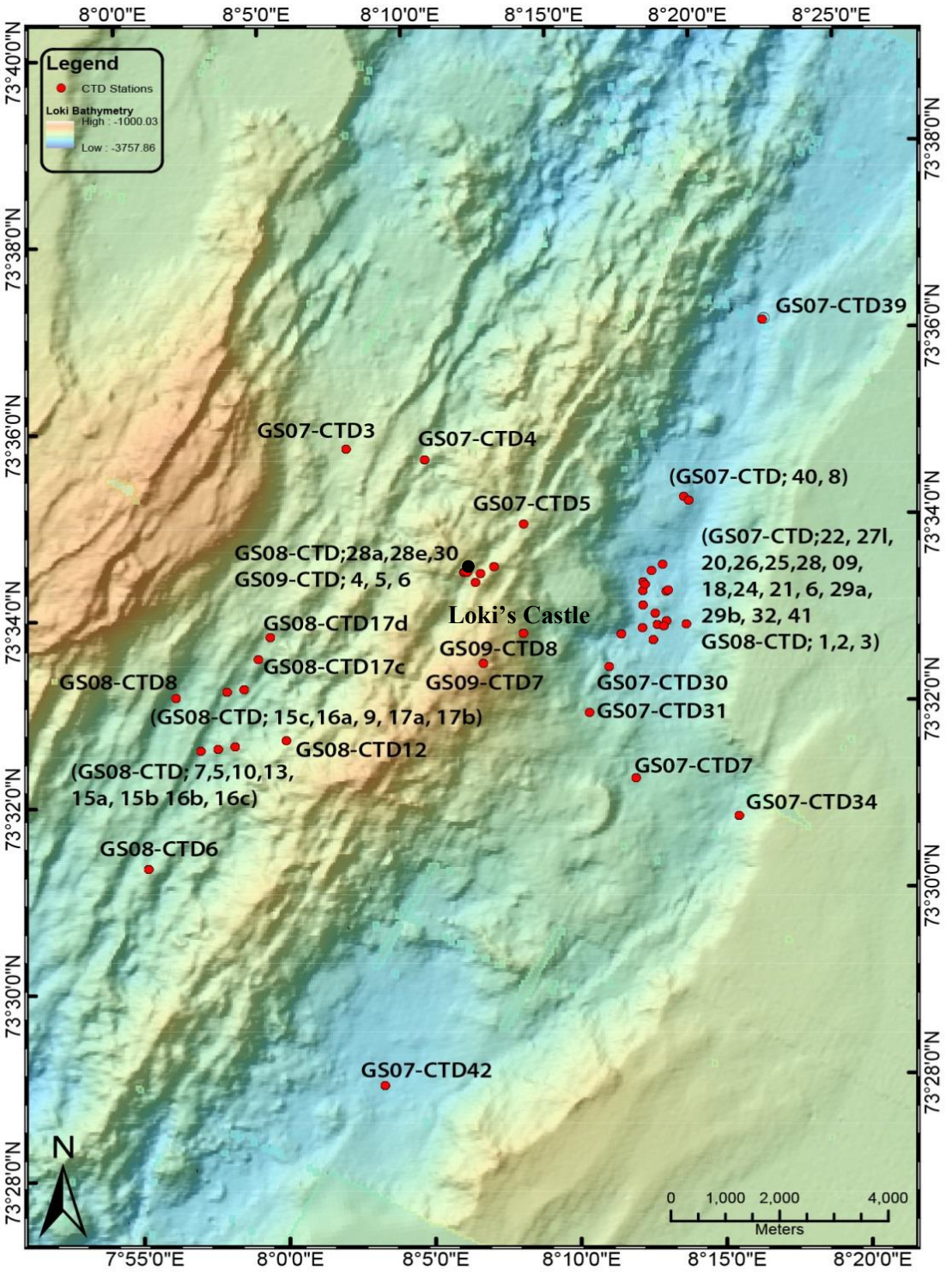

Figure 7. Bathymetric map of the Loki's Castle area showing the locations of all CTD casts collected in this area in the period 2007-2009 (red circles). The location of the vent field is indicated by a black circle. The background casts GS07-CTD; 35, 36, 37, 38 and 43 was conducted outside this region. GS07-CTD43 was located south of the rift valley and casts 35-38 further north in the rift valley of the knipovich ridge.

4.1.1 CH_4 and H_2

The methane concentrations of all the analysed samples are shown in Fig. 8A. Samples from 2007 had relative low concentrations of methane. The majority of elevated methane concentrations detected this year were located close to a depth of 2000 m. The CTD casts in 2008 had generally higher concentrations of methane compared to casts in 2007. In contrast to 2007, the peak concentrations in 2008 were found at several water depths (Fig. 8A). The maximum methane concentrations were measured in 2009, and had values that were almost 8 times higher than the highest concentration measured in the previous years. The samples with this substantial methane concentrations were from GS09-CTD6, which was located approximately 300 m SE of the vent field. The maximum methane concentration from this CTD was 8231.3 nM and was measured in the sample from 2201 m water depth.

The lowest concentrations of hydrogen were also detected in 2007 (Fig. 8B). The highest concentrations measured in 2007 were all located around a depth of 2000 m. In 2008 the highest hydrogen concentrations were also detected in samples from about 2000 m. However, elevated concentrations were also detected in samples from both below and above this depth. The highest hydrogen concentrations were detected in 2009, and multiple peaks with high concentrations were found between 2300 m and 1900 m.

In Fig. 9 the methane and hydrogen concentrations of a representative selection of CTD casts collected during 2007, 2008 and 2009 are shown. These are chosen on the basis of their concentrations as function of distance to Loki's Castle and of the depth of the anomalies.

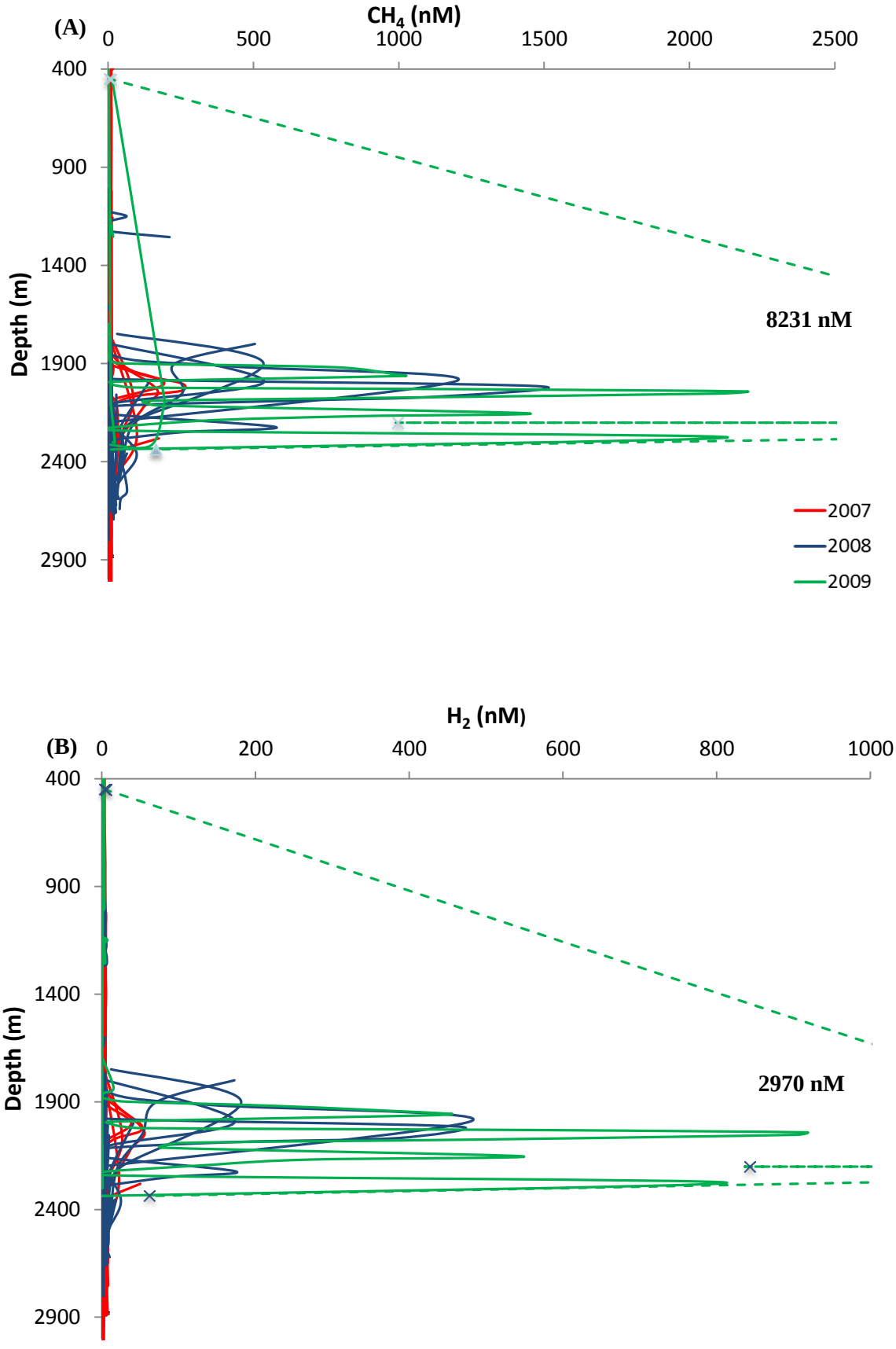

Figure 8. Methane and hydrogen concentrations as a function of depth for all CTD samples collected in the Loki's Castle area.

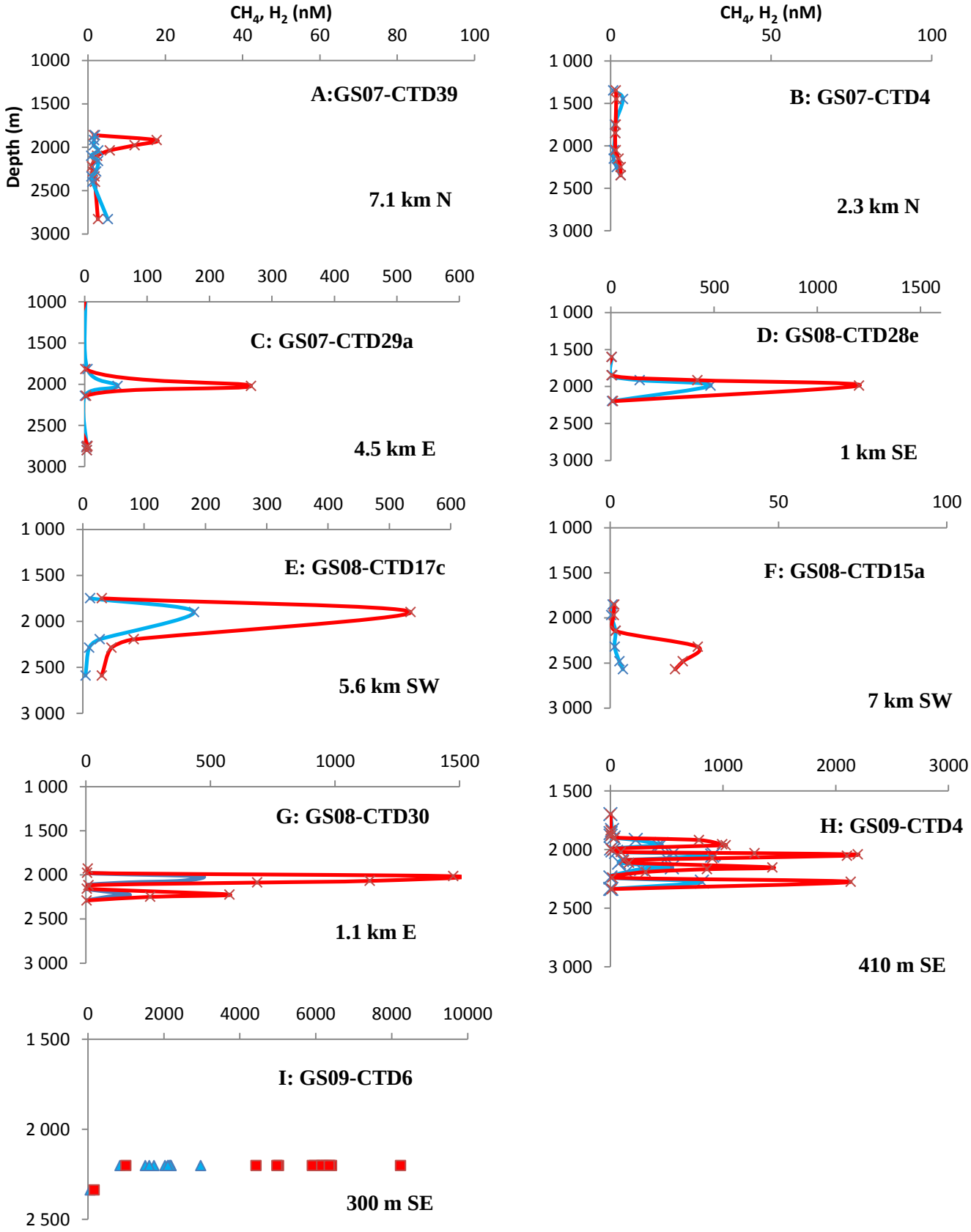

Figure 9. CH_4 and H_2 concentrations of a representative selection of CTD casts collected in 2007, 2008 and 2009.

The CTD profiles from 2007 (Fig. 9A-D) are arranged by decreasing distance to the vent field from the north (A and B) and east (C). Even though GS07-CTD39 (Fig. 9A) was obtained furthest away (7.1 km) from the vent field, this CTD showed higher concentrations of methane (17.7 nM) than GS07-CTD4, which was located much closer (2.3 km). However, hydrogen was very low in both. Similar results were also obtained from the CTD casts located between 4-6 km east of the vent field. While several of these cast had very low concentrations of both methane and hydrogen, such as GS07-CTD18 (see appendix 1), other showed strong anomalies. The highest concentrations measured in 2007 were in GS07-CTD29a (Fig. 9C), which had methane and hydrogen concentrations of 266.4 and 52.7 nM respectively. For GS08-CTD28e (Fig. 9D), which was collected in 2008 only 1 km SE of the vent field, much higher concentrations of both CH_4 (1201.1 nM) and H_2 (483.3 nM) were detected. Although the maximum concentrations for the anomalies differ between these CTDs, they all display peak concentration of both CH_4 and H_2 around 2000 m and a swift transition from peak to background values, in spite of a distance difference of 6 km.

In 2008 similar anomalies around 2000 m were also detected up to 5.5 km southwest of Loki´s Castle (GS08-CTD17c, Fig. 9E). However, for GS08-CTD15a (Fig. 9F) which was obtained 7.5 km SW of Loki's Castle, the peak concentration of methane (26 nM) was deeper (2319 m) and the hydrogen concentration (3.8 nM) was also higher close to the seafloor (2570 m) compared to the other casts. The shape of the methane profile is also different.

The GS08-CTD30 profile (Fig. 9G), which was collected 1.1 km east of Loki´s Castle, differs from the other CTDs by having two peaks of both hydrogen and methane. The upper pair of peaks were found at approximately 2000 m and had methane and hydrogen concentrations of 1474.2 and 463.8 nM, respectively. The lower peaks were located at 2223 m and had methane and hydrogen concentrations of 575.6 and 174.5 nM. In 2009 all CTD casts were obtained right over or in short distance to Loki´s Castle. GS09-CTD4 (Fig. 9H) displays concentration peaks at several depths, where the two most profound peaks are found at 2276 and 2053 m. The peak at 2276 m corresponds to methane and hydrogen concentrations of 2131.8 and 813.4 nM and the peak at 2053 m to 2099.3 and 905.3 nM, respectively. For GS09-CTD6 (Fig. 9I) fourteen bottles were released at the same depth of 2201 m. Allthough from the same depth, the concentration in each bottle varied. The maximum concentration of methane was 8231.3 nM, and of hydrogen 2970.7 nM.

4.1.2 Helium

Samples for helium isotopes analyses were collected from 17 CTDs and the results are shown in Fig. 10.

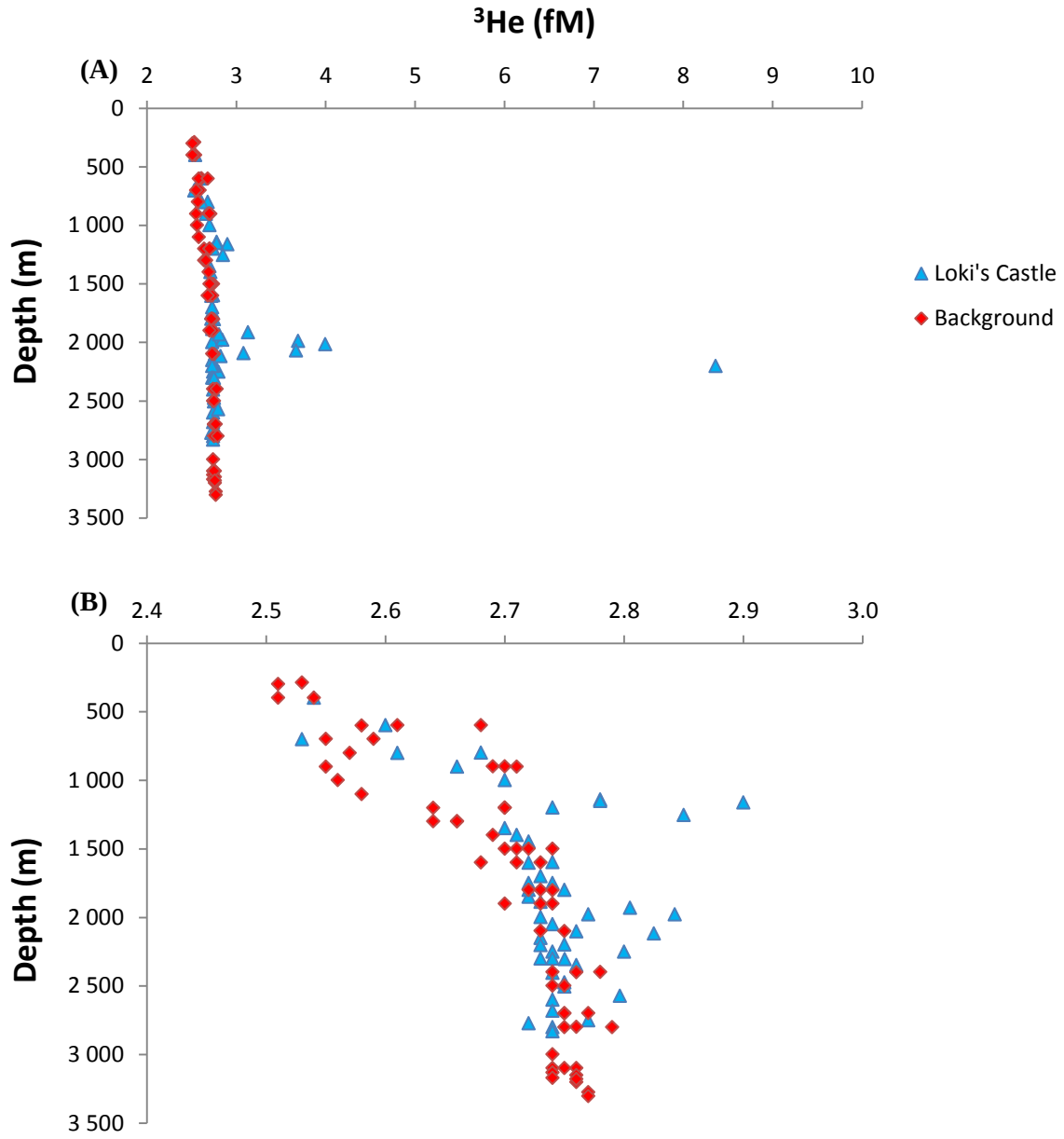

Figure 10. (A) All ^{3}He values measured from a total of 17 CTDs. (B) He scale is a close up between 2.4 and 3.

.

The background samples are from GS07-CTD35-38, 42 and 43. The results show that the background ^{3}He concentration was 2.7 -2.8 fM below 2000 m and decreased successively to 2.5 fM from 2000 m and towards the surface (Fig. 10B). The values that exceeded this

background were mostly found close to 2000 m (Fig. 10A and B), and represent the CTD casts from 2008 and 2009 that were located close to the vent field (GS08-CTD 28e, GS08-CTD30, GS09-CTD6, GS09-CTD7). The highest concentration (8.4 fM) was found in GS09-CTD6, which was collected almost directly above the vent field. In addition, the results also show an increase in ^{3}He concentrations around 1200 m in several samples (Fig. 10B).

4.2 Jan Mayen vent fields

Three cruises were carried out at the Jan Mayen vent fields between 2008 and 2012. During these cruises a total of 23 CTD casts were conducted in this region, from which water column samples were collected and analyzed for dissolved methane and hydrogen (Fig 11). The majority of the CTDs were obtained above or close to the Troll Wall vent field, and only 4 were from the Soria Moria area. Samples for helium isotopes were only collected from 4 of the CTDs, due to technical problems with the sampling equipment. The results of all the analyses are included in Appendix 2.

4.2.1 CH_4 and H_2

In 2008, only few samples were collected in the JMVF region (Fig. 11). These CTDs, which were all from above the Troll Wall vent field, had relatively high concentrations of dissolved methane (Fig. 12A). The results from 2011 display a generally lower concentration level of methane compared to 2008. The majority of all the CTDs from the JMVF region were conducted in 2012, and these show significant variations but also the highest methane concentrations. The concentration of hydrogen was low for all CTDs conducted in 2008 and 2012 (Fig. 12B). In 2011 however, hydrogen was abundant in the water column.

In Fig. 13 the methane and hydrogen concentrations of a representative selection of CTD casts collected during 2008, 2011 and 2012 are shown. These were chosen on the basis of their concentrations as function of distance to the Troll Wall or the Soria Moria vent fields and for the depth of the anomalies.

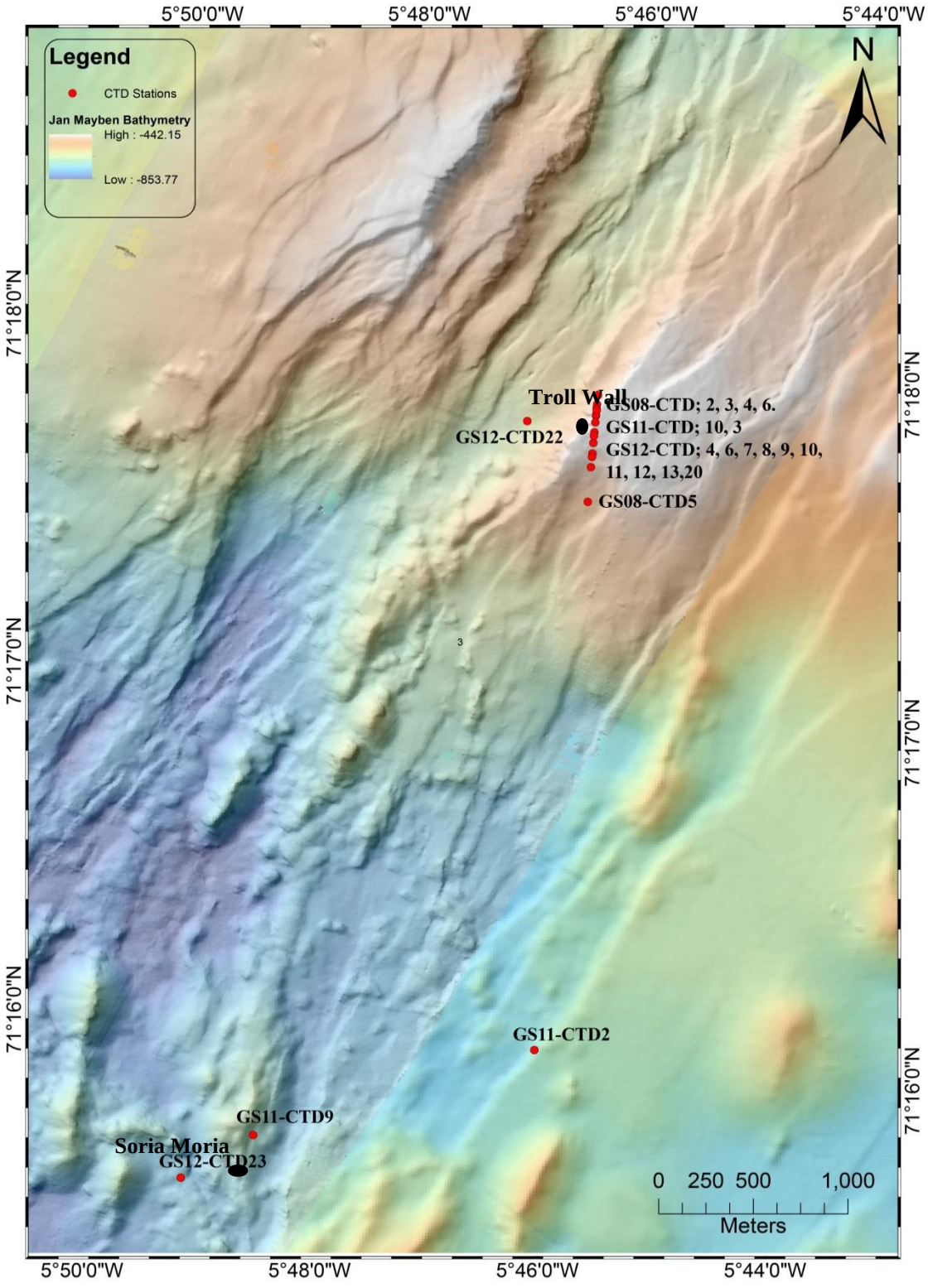

Figure 11. Bathymetric map of the JMVF area and the location of the CTD cast collected in the region. GS12-CTD25 was a background measurement in the Jan Mayen Fracture Zone and is located outside the map.

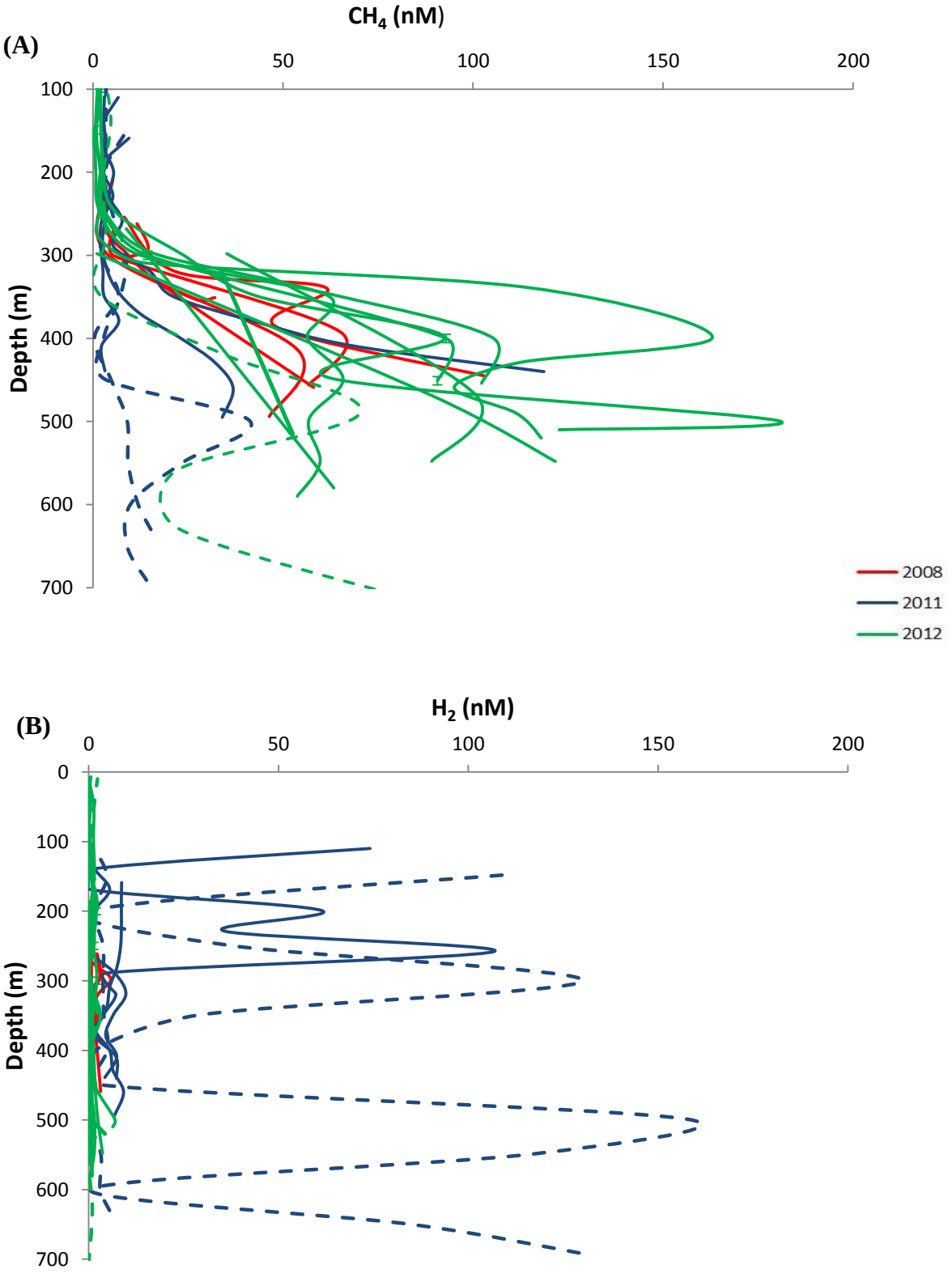

Figure 12. All CH_4 and H_2 concentrations obtained from CTD samples collected in 2008, 2011 and 2012. The stapled lines represent casts from Soria Moria and the surrounding area. All other casts were conducted above the Troll Wall vent field.

Figure 13. CH_4 and H_2 in CTDs from 2008, 2011, 2012 above the JMVF. H_2 was not analyzed for B and D.

The four CTDs from 2008 (Fig. 13 A-D) were collected close to the Troll Wall vent field. GS08-CTD6 (Fig. 13A) and GS08-CTD5 (Fig.13D) show methane profiles that were similar in shape and concentrations, with peak values around 400 m of 65 and 53.7 nM, respectively. Hydrogen was only analyzed for GS08-CTD6, where it reached a maximum value of 1.1 nM. The GS08-CTD4 methane profile (Fig.13B) is comparable to GS08-CTD6 (Fig. 13A) and GS08-CTD5 (Fig. 13D) with a peak at 350 m, however, the maximum concentration (102.9 nM) was found in the deepest sample at 445 m. This was also the case for GS08-CTD3 (Fig. 13C), where the methane gradually decreased from 58 nM at 450 m to 3 nM with decreasing depth.

The results from 2011 (Fig 13E and F) portray a very different situation compared to the results from 2008. The hydrogen concentrations for both GS11-CTD3 (Fig. 13E) and GS11-CTD2 (Fig. 13F) were significantly higher than the values obtained in 2008. GS11-CTD3 (Fig. 13E) sampled 50 m from the Troll Wall, display two distinct features: (1) the methane concentration decreased with decreasing depth from a maximum concentration of 118.6 nM in the deepest sample (440 m), and (2) three hydrogen peaks ranging from 106.8 to 61.3 nM between 258 and 199 m. GS11-CTD2 (Fig. 13F) show four hydrogen peaks at 691, 499, 300 and 148 m with concentrations ranging from 130.1 to 157.8 nM . The hydrogen peak at 499 m correlates with a much smaller methane peak. This CTD cast, however, was obtained closer to the Soria Moria (1.5 km) than the Troll Wall vent field. There was two CTD casts that were collected from the Soria Moria vent field, GS11-CTD9 and GS12-CTD23, respectively (see appendix 1). GS11-CTD9 show no anomalies in either hydrogen or methane, however, GS12-CTD23, display elevated methane (70 nM) at 489 m depth. The hydrogen concentration at the same depth was 1.1 nM.

Generally the result from 2012 (Fig. 13 G-J) were similar to the results from 2008, with low concentrations of hydrogen, and high concentrations of methane close to the seafloor. Another similarity was that several of the CTDs had high concentrations of dissolved methane close to 400 m. The CTD that differed most from the others collected in 2012 was GS12-CTD22 (Fig. 13G), where the methane profile has several distinct transitions between 590 and 349 m, with the highest concentration (65.8 nM) at 449 m water depth. GS12-CTD22 also had the highest hydrogen concentration (6.3 nM) of these four CTDs.

4.2.2 Helium isotopes JMVF

Samples for He isotopes analyses were collected from two CTDs in 2011 and two in 2012. Three of these CTDs were located close to the Troll Wall vent field, and only one CTD close to the Soria Moria vent field. No background cast for He analyses were performed in this area.

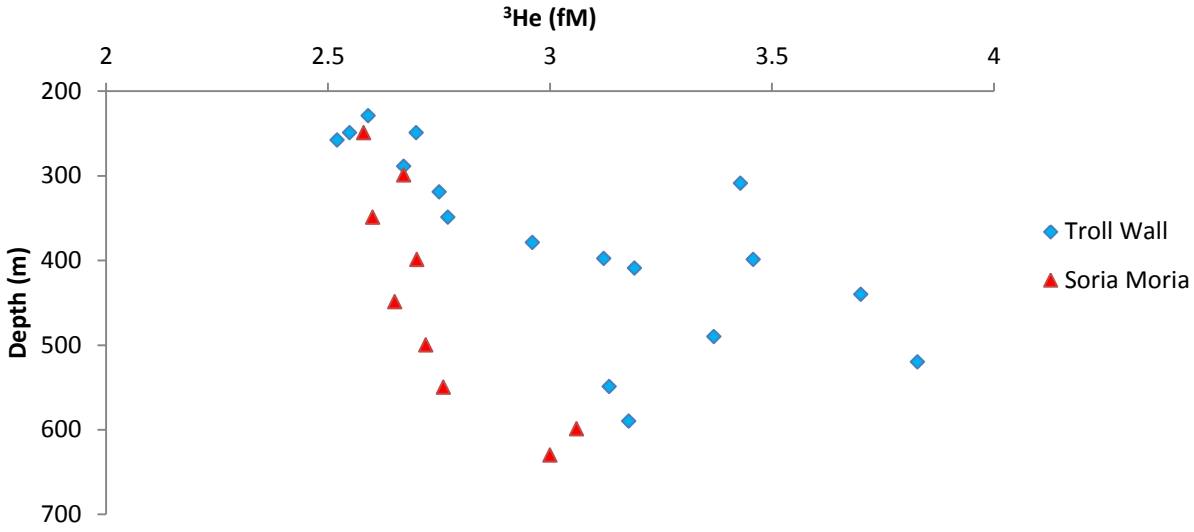

Figure 14. ^{3}He concentrations in samples from 4 CTDs collected in the JMVF area.

The highest ^{3}He concentrations (up to 3.8 fM) at the Troll Wall vent field was found between 300 and 550 m (Fig. 14). The concentration decreased gradually towards the surface to about 2.5 fM. A similar trend was observed at the Soria Moria vent field , where the ^{3}He concentrations decreased gradually from around 3 fM at 600 m towards 2.6 fM in the surface layer (Fig 14). However, this trend was only based on one CTD cast and thus does not give adequate information about the ^{3}He distribution at this site.

5 Discussion

5.1 The Loki's Castle vent field

Recent discoveries of hydrothermal vent systems show that venting at ultra-slow spreading ridges is more common than expected (German et al., 1998; Edmonds et al., 2003; Baker et al., 2004; Pedersen et al., 2010a, Pedersen et al., 2010b). One of these discoveries was the Loki´s Castle vent field at the bend of the Mohns Ridge and the Knipovich Ridge in the Norwegian–Greenland Sea (Pedersen et al., 2010).

In view of the tectonic setting of the AMOR, the volatile content observed at Loki's Castle could represent an ultra-mafic hosted system. Extreme enrichment of hydrogen together with elevated content of methane is typical for ultra-mafic hosted systems (Kelley et al., 2005). At the ultramafic influenced Rainbow hydrothermal field, Charlou et al. (2002) reported hydrogen content of 11-13 mM for the high temperature end-member fluids. The methane content in same high temperature fluid was 1.8-2.5 mM. At Loki's Castle the end-member concentration of methane (15 mM) is too high and the hydrogen concentration too low (5 mM) compared to ultra-mafic systems. The concentrations, however, are comparable to those of sediment influenced basalt hosted systems (Lilley et al., 1993; Von Damm et al., 2005; Baumberger, 2011), characterized by high thermogenic methane production (Welhan, 1988). Thus, Loki´s Castle is likely a member of the sediment-influenced class of hydrothermal systems (Pedersen et al., 2010; Baumberger, 2011).

5.1.1 General plume characteristics

The anomalies of dissolved methane and hydrogen detected in the water column around 2000 m generally show an abrupt transition to low concentrations. One typical example is GS08-CTD17c (Fig. 9E), where the methane profile shows a transition from 536.8 to 3.4 nM over a relatively short depth difference. Such concentration peaks over a limited depth difference can be interpreted as a non-buoyant plume (e.g. Jean Baptiste et al., 1998; Marbler et al., 2010). The non-buoyant plume from Loki's Castle has a distinct signature in a large area. This is

demonstrated by GS07-CTD29a (Fig. 9C) that was obtained 4.5 km east of the vent field, but still had high concentrations of methane (266 nM) and hydrogen (52 nM) at 2000 m. The plume signal can also be observed even further away (7 km), and in another direction (north) in GS07-CTD39 (Fig. 9A). However, in GS07-CTD4 (Fig. 9B), which was collected closer, the plume signal was not visible. This probably illustrates the importance of ocean currents. Loki's Castle is situated between several ocean current systems (Fig. 5), which causes the complex patterns in the fluid transportation observed in GS07-CTD29a and GS07-CTD39. The highest methane and hydrogen concentrations measured in the water column at Loki's Castle were from GS09-CTD6 from close to the vent field (300 m SE), which had values of 8231 and 2970.7 nM, respectively. However, the most common concentrations were 10-2000 nM for methane and 5-1000 nM for hydrogen. The peak hydrogen concentration was generally found at the same depth as the peak methane concentration (Fig. 9A and B). If a sample is taken at the center of the plume the concentrations will be higher than at the rim of the plume (e.g de Angelis et al., 1993). This fact combined with the complex ocean currents in the region is likely the reason for the concentration variations observed in CTD casts from Loki's Castle.

The plume at Loki's Castle rises from about 2400 to a depth of 2000 m, which gives a rise-hight close to 400 m. However, the rise-height of the plume at several vent fields located in the Atlantic Ocean is between 300 and 350 m, and about 200 m in the Pacific Ocean (e.g. Speer and Rona 1989; Rudnicki and Elderfield, 1992; Rudnicki et al., 1994; McDuff, 1995; Augustin et al., 2008). The rise-height of a plume is an individual property for a vent field. The factors determining the rise-height is the composition and temperature of the venting fluids and the depth of the vent field (e.g. Speer and Helfrich, 1995). An additional important factor, is ocean stratification, where different water layers are defined by density differences (e.g Lupton and Craig 1981; Lupton et al., 1985; de Angelis et al., 1993). Chemical plumes are dissolved gas accumulations dispersing underneath a water layer that has a lower density then the plume (e.g Lupton et al., 1985; de Angelis et al., 1993). Thus, density differences limit the rise-height of a chemical plume. The density layers will vary from ocean to ocean, mainly due to differences in salinity and temperature. This means that predicting the rise-height of the non-buoyant plume is difficult. The arctic water in the Loki's Castle region differs significantly from both the Pacific and the mid-Atlantic Oceans. The Pacific Ocean water column is characterized by increasing salinity with increasing depth (e.g. Lupton et al., 1995). This causes an increase in salinity and temperature in the water layer where neutral

buoyancy is established. In the Atlantic Ocean the salinity decreases with depth, thus showing a reverse trend to the Pacific Ocean. Speer and Rona, (1989) predicted that the reverse salinity profile in the Atlantic would cause a decrease, rather than an increase in salinity where neutral buoyancy for the plume was established. In Fig. 15 temperature, salinity and density profiles for a background CTD cast in the Loki's Castle region are shown. A bottom water temperature here of -1 °C is extremely low compared to about 2.5 °C at the TAG vent field in the mid-Atlantic Ocean and to 1.8 °C in the Pacific Ocean (Rudnicki and Elderfield. 1992; Lupton, 1995). The temperature and salinity of the deep water in the Norwegian-Greenland Sea also display stable, nearly vertical profiles resulting in only a minor decrease in density by decreasing depth (Fig. 15) (e.g. Quadfasal and Meincke, 1987).

In the water column above Loki's Castle a significant increase in temperature (from -0.8 to -0.6 °C) and a decrease in salinity and density can be observed close to 2000 m depth, demonstrating where the hydrothermal plume is entrained (Fig. 16A and B). This rise-height of 400 m at Loki´s Castle is 50-100 m higher than at other vent fields in the Atlantic, and almost 200 m higher than plumes in the northern Pacific (e.g. Speer and Rona, 1989; Rudnicki and Elderfield, 1992; Rudnicki et al., 1994; Mcduff, 1995; Augustin et al., 2008). A likely explanation for this is the smaller changes of temperature and salinity throughout the water column in the Norwegian-Greenland Sea, which allow the plume to rise higher before non-buoyancy is reached.

GS09-CTD4 (Fig. 16) differed from the general structure by displaying several plume layers in the water column (Fig. 9H). Similary, a double plume layer can be seen in GS08-CTD30, which was collected 1.1 km from the vent field. This suggests that the dissolved gas has accumulated in two different density layers. The upper plume layer in GS08-CTD30 is located approximately at the same depth as in most cases at Loki's Castle, around 2000 m, but the second plume layer was deeper than the general trend in the area. Such a feature has also been reported at the Rainbow hydrothermal site where it was concluded that this could be a result of a discrete venting from several vents (Jean-Baptiste et al., 2004). However, the 4 known chimneys at Loki's Castle have similar composition and temperature, and are situated at similar depths (Pedersen et al., 2010b). The existence of additional vents at or in the vicinity of Loki's Caste can, however, not be excluded. Another possibility is that the rise-height could be affected by tidal cycles (Rudnicki et al., 1994; Jean-Baptiste et al., 2004).

If the double plume structure in GS08-CTD30 was caused by a vent different from the known chimneys at Loki's Castle, the profile in GS09-CTD4 could be explained by several different unknown vents. GS09-CTD4 was obtained 400 m from the vent field. It is therefore more likely that this profile reflected samples collected within the buoyant plume, therefore contained several concentration layers due to turbulent mixing. The temperature, salinity and density plot (Fig. 16) for GS09-CTD4 therefore reflects a buoyant plume rather than a non-buoyant. Thus, a similar plot for a non-buoyant plume would probably show a weaker signal for all 3 parameters due to higher dilution (see section 5.1.3).

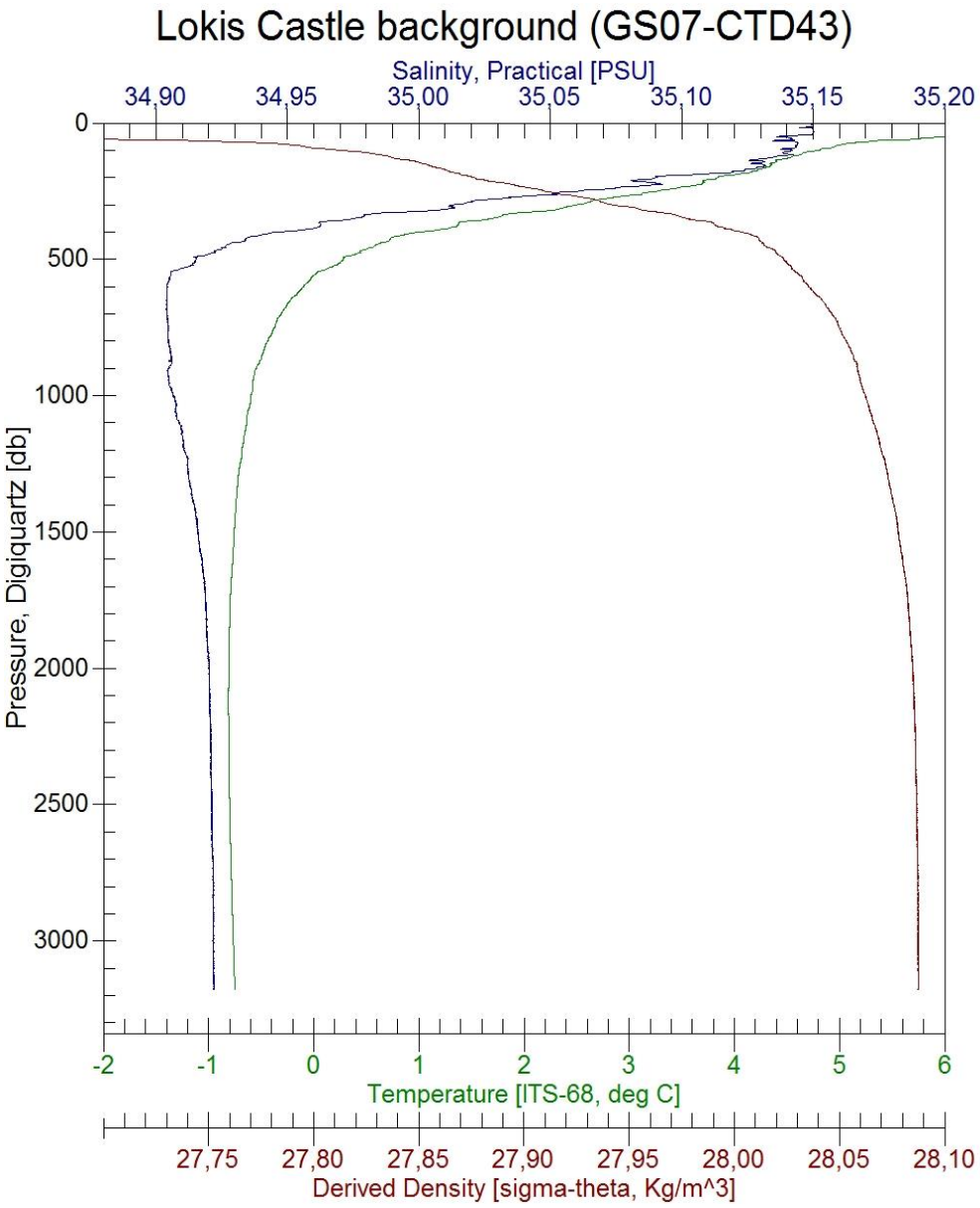

Figure 15. Temperature, salinity and density profiles from the background cast GS07-CTD43, which was located outside the rift valley, 21 km south of Loki's Castle.

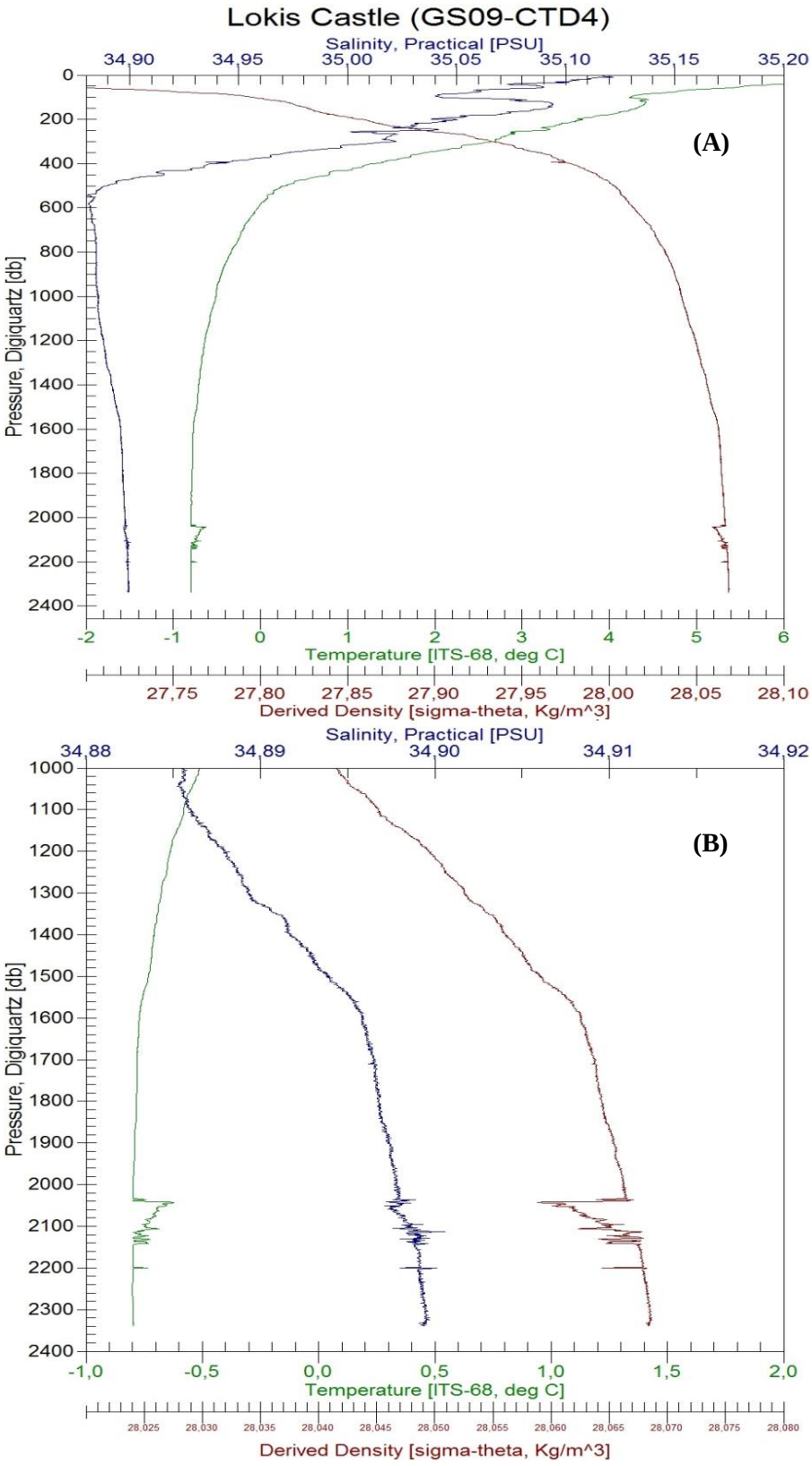

Figure 16. (A) Temperature, salinity and density profiles for GS09-CTD4, which likely reflects the buoyant plume. (B) a close up of the plume signal in the profiles.

5.1.2 Additional vent field

The elevated hydrogen and methane concentrations detected in GS08-CTD15a (Fig. 9F) were located at a considerably deeper level (2300 m) than the general trend (about 2000 m). This CTD was collected 7 km southwest of Loki´s Castle, where the seafloor has a depth of 2600 m. Thus, the depth of the anomalies at this site indicates that they may represent a non-buoyant plume from a deeper vent field than Loki´s Castle. As the water column is separated in several layers defined by density differences (e.g Lupton et al., 1985; de Angelis et al., 1993), a non-buoyant plume cannot move into a deeper layer in the water column. Thus, even if the plume signal at 2000 m in GS08-CTD17c indicates transport of dissolved gases from the Loki´s Castle to southwest, this could not explain the anomalies at 2300 m.

GS08-CTD15a is also different from the other CTDs due to elevated hydrogen concentrations (4 nM) close to the seafloor, at 2570 m depth. Hydrogen is consumed quickly in the water column (Amend et al., 2011; Petersen et al., 2011), and the elevated hydrogen signal could therefore indicate that there is an active vent in close proximity.

Elevated hydrogen concentrations in this region were not limited to GS08-CTD15a. In GS08-CTD16c (Appendix 1) the peak hydrogen concentration of 10.2 nM was measured in a sample from 2621m depth, approximately 10m above the seafloor. The GS08-CTD16c cast was located 400 m from GS08-CTD15a, and both CTDs indicated therefore the same regional setting. Hydrogen close to the seafloor in two CTDs this close to each other and so far from the Loki's Castle vent field increases the possibility of an additional vent field in this region. However, hydrogen oxidation at hydrothermal vent fields is not well documented (see further discussion in section 5.1.3).

Additional verification of this possibility comes from the bathymetry and geology data. The Loki's Castle vent field is situated on the crest of a volcanic ridge segment (Fig. 7) (Pedersen et al., 2010a, 2010b). The bathymetry data show that further southwest there are several half-grabens and fault zones. Following this down faulted western area southwards, the seafloor depth increases. GS08-CTD15a and GS08-CTD16c were obtained in this southwestern part of the area, close to a half-graben. Hydrothermal fields are associated with tectonic active settings. The southwestern segment in the area may therefore be an ideal location for an additional vent field. Thus, both geological information and the dissolved gas anomalies suggest that there may be an additional field in this region.

5.1.3 Mixing and CH_4 and H_2 consumption

It is generally assumed that the fast consumption of hydrogen is a result of hydrogen being a favorable electron donor for micro organisms feeding of the dissolved species (Petersen et al., 2011). The reason for this is the high energy yield from aerobic hydrogen oxidation;

Aerobic hydrogen oxidation $2H_2+O_2 \rightarrow 2H_2O$

Laboratory experiments on biological samples from the Logatchev vent field, suggested that the energy yield from this process could provide up to 7 times more energy per kg of water compared to methane oxidation at the Logatchev vent field (Petersen et al., 2011).

Due to the conservative nature of ^{3}He, helium isotope analysis can be used to determine the age of plume sampled and to determine dilution and consumption of methane and hydrogen in the water column (e.g. Lilley et al. 1995; Lupton, 1995; Kelley et al., 1998, 2002).

In Fig. 17 the correlation between ^{3}He and CH_4 (Fig. 17A), and ^{3}He and H_2 (Fig. 17B) in the plume depth interval (1900-2000 m) for GS08-CTD28e and GS08-CTD30 is shown. These two casts were located 1 and 1.1 km from the Loki's Castle, respectively. A linear correlation both with methane and hydrogen in both CTD casts indicates that oxidation had not yet started for either of these compounds. This suggests that the plume sampled in GS08-CTD28e and GS08-CTD30 is very young. Thus, even though hydrogen is commonly assumed to oxidize within hours to days in the hydrothermal plume, there is no indication of this process over a distance within 1.1 km from the Loki's castle vent field (defined here as the proximal region to the vent field). This is also illustrated by high correlation between CH_4 and H_2 in proximal samples (Fig. 18A), suggesting CH_4/H_2 ratios close to the end-member fluids of Loki's Castle. With end-member concentrations of methane and hydrogen for the Loki's Castle vent fluids of 15 and 5 mM, respectively (Pedersen et al., 2010a), the end-member CH4/H2 ratio is 3.

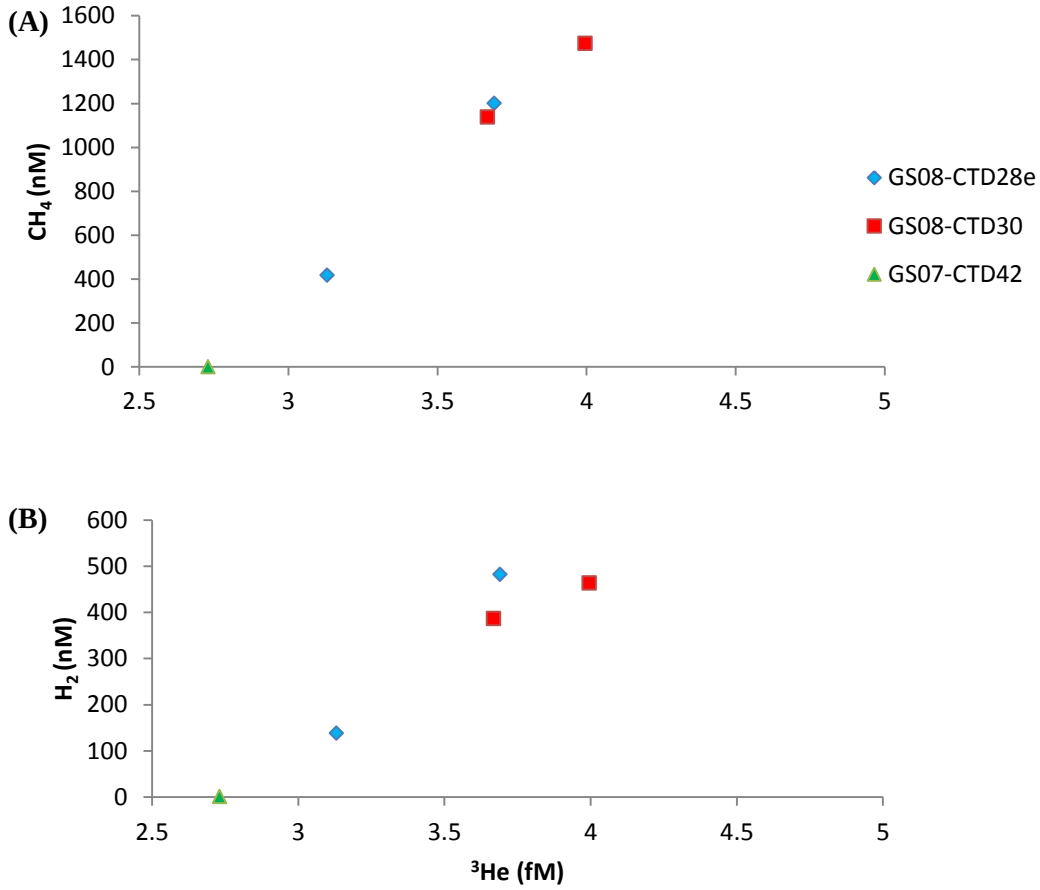

Figure 17. Correlation in the plume layer (1900-2200 m) between ^{3}He and (A) CH_4 and (B) H_2 for three CTD casts. Two casts, GS08-CTD28e and GS08-CTD30 represent the plume, whereas cast GS07-CTD42 was collected as background.

In Fig. 18A some of the proximal samples, however, plot below the end-member ratio line, indicating an enrichment of hydrogen relative to methane. As hydrogen is assumed to oxidize faster than methane (e.g. de Angelis et al., 1993; Amend et al., 2011), oxidation processes in the water column is unlikely to result in an enrichment of hydrogen. Furthermore, analyses of black smoker fluids in 2007, 2008 and 2009 indicate that the end-member composition is stable and similar for all chimneys (Pedersen et al. 2010b). Thus, the H_2 enrichment has to be either a result of mixing with water masses that had a higher hydrogen content, or possibly be caused by an error in the analytical methods. The samples of high concentrations with low CH_4/H_2 ratio are generally sampled in the buoyant plume.

Some samples with clear anomalies in the plume depth interval from different distances from the vent field show elevated CH_4/H_2 ratios, which is consistent with preferential oxidation of hydrogen (Fig. 18B). However, samples with low concentrations within the Loki's Castle area

show mostly lower CH_4/H_2 ratio than the end-member fluids (Fig. 18B). Similarly, the background samples also have lower ratios (0.3 and 1). The hydrogen enrichments observed in the plume relative to the end-member composition may therefore indicate extensive mixing between hydrothermal fluids and ambient seawater. This may be caused by ocean currents that rapidly transport the plume away from the venting area in different directions. This is also indicated by the wide distribution of the plume signal (Fig. 9) that changes in strength with time. Elevated hydrogen values in the background may be contradicting to the assumption that hydrogen is oxidized within hours to a day (e.g. Petersen et al., 2011). To understand why hydrogen is detected in concentrations higher than normal background level of 0.2 nM further work is needed. An extensive mixing and transport of hydrothermal fluids rich in nutrients and energy sources may be important for microbial life in the artic water.

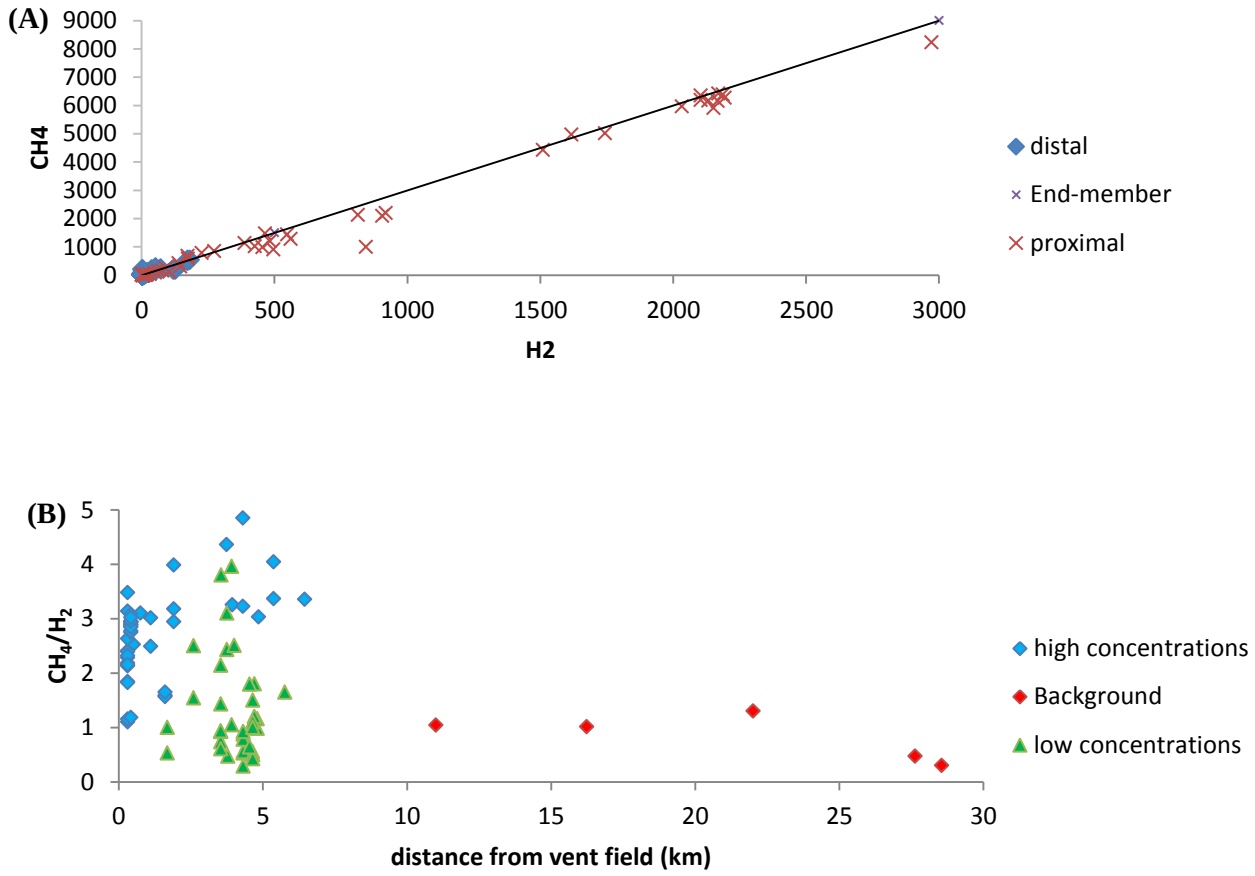

Figure 18. (A) H_2 and CH_4 concentrations in end-member fluids and in all CTD samples collected in 2007-2009 except those indicating an additional vent field. The line indicate a CH_4/H_2 ratio of 3. (B) CH_4/H_2 ratio of samples fromthe plume layer depth interval (1900-2200 m) with high concentrations (>10 nM), low concentrations (<10 nM), and from background casts.

As ^{3}He is not consumed or oxidized in the seawater, the concentration is only reduced by dilution. The end-member ^{3}He concentration at the Loki's Castle vent field has been measured to 9800 fM (personal communication M. D. Lilley), and the background concentration between 2.5 and 2.8 fM. The water column samples for helium isotope analyses that were collected closest to the vent field (300 m) were from GS09-CTD6, where all samples were from one depth (2201 m) (Fig. 9I). This was also the CTD where maximum methane and hydrogen concentrations were detected (Fig. 9I). The ^{3}He concentration measured in this CTD was 8.4 fM, which also is the highest concentration measured in the water column at the Loki's Castle vent field. The plume measured in GS09-CTD6 had therefore a ^{3}He enhancement of 5.8 fM compared to background, which indicates a minimum dilution factor in the plume of 1700. A theoretical value for dilution of plumes in the Pacific Ocean has been calculated to be between 8000 and 10000 (Speer and Rona, 1989; McDuff, 1995; Field and Sherrell, 1999). Thus, the dilution factor at Loki's Castle (1700) is much less than what is estimated for the Pacific. The ratios calculated for the Pacific Oceans are estimated from the attainment of neutral buoyancy. However, the low dilution factor at Loki's Castle suggests that the sample from which the dilution factor was calculated represented the buoyant plume. This is also indicated by the changing methane and hydrogen concentrations in samples from the same depth (Fig. 9I). The methane and hydrogen profiles for the GS08-CTD30 cast, which was collected 1.1 km from the vent field, display the non-buoyant plume (Fig. 9G). The maximum ^{3}He concentration measured in the plume in this CTD was 1.1 fM above the background, indicating a dilution factor of 8900. This value is consistent with the theoretical value estimated for the Pacific Ocean.

5.1.4 Comparing ^{3}He at Loki's Castle to other MAR vent fields

The Rainbow hydrothermal vent field is situated on the Mid-Atlantic Ridge (36°14'N) (Jean-Baptiste et al., 2004). Venting from this ultramafic influenced field occurs at a depth between 2270 and 2330 m (e.g. Charlou et al., 2002; Douville et al., 2002; Jean-Baptiste et al., 2004), and the buoyant plume rises to between 2000 and 2100 m (e.g. German et al., 1996). This is the same depth as the general plume at Loki's Castle is observed. However, the difference in rise height between Rainbow and Loki's Castle is 50-100 m. The Lucky Strike vent field is also situated on the MAR (37°17'N). Venting occurs at a depth between 1600 m and 1730 m (Von Damm et al., 1998), and the buoyant plume rises to between 1350 and 1400 m (Wilson et al., 1996).

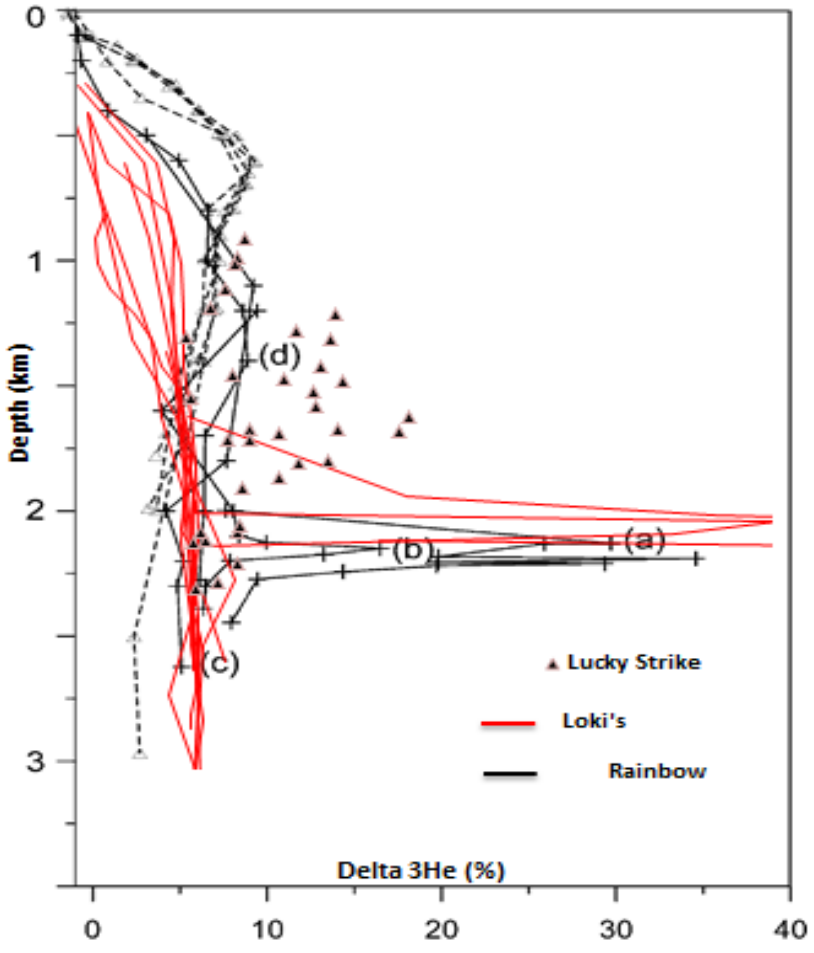

Figure 19. Delta ^{3}He % as a function of depth for all CTD cast where He was sampled at the Loki's Castle vent field, compared to the Lucky Strike vent field (Jean Baptiste et al., 1998) and the Rainbow vent field (Jean-Baptiste et al., 2004).

Elevated delta ^{3}He (%) values were detected below 2000 m at both the Rainbow and the Loki's Castle vent field (Fig. 19), and the maximum delta ^{3}He in the plume at both vent fields was about 40 %. Delta ^{3}He (%) data from the Lucky Strike vent field (Jean Baptiste et al., 1998) display elevated values at a shallower depth than Rainbow and Loki's Castle (Fig. 19). However, the plume at the Lucky Strike vent field is located at 1350-1400 m water depth. Through this comparison it becomes evident that the Rainbow and the Loki's Castle vent fields have similarities in amount of ^{3}He released as well as the depth to which the plume rises. Based on ^{3}He concentrations and heat, Jean Baptiste et al., 2004 calculated an annual thermal output of 1320 ± 600 MW for the Rainbow vent field. The maximum delta ^{3}He (%) value for Loki's Castle is so similar to that reported from the Rainbow hydrothermal field that the thermal output from Rainbow could be an analog to the Loki's Castle vent field.

5.1.5 The general background

When searching for a new vent field in 2007 several CTD casts were performed outside a 10 km range from the Loki's Castle (see appendix 1). All these background casts except GS07-CTD43 and GS07-CTD35 was located in the rift valley. The data obtained from these CTD casts (appendix 1) provide information about the general background seawater composition, which is useful for estimating the magnitude of the total hydrothermal activity and how high a signal has to be in order to indicate a new vent field.

Delta ^{3}He (%) describes the ^{3}He/^{4}He ratio in the water column in reference to the ratio in the atmosphere. In the deep water layer in the Atlantic Ocean the background signal is 5 %. In this region of the Norwegian-Greenland Sea, however, the background signal in the deep water is about 2 % higher than the general background (Fig. 20A). The delta ^{3}He background in Norwegian Sea display low values in the deep water (e.g. 2-3 % in the Lofoten Basin) (Heinze et al., 1990). However, further north in the Fram Strait, delta ^{3}He in the deep water is between 5 and 7 % (Heinze et al., 1990). Heinze et al., (1990) suggested that the elevated ^{3}He in the deep water originates from hydrothermal activity in the region. The elevated concentrations in the background seawater from the Mohns and Knipovich ridge may therefore originate from either deep water transport from further north, or hydrothermal input from the ridge below.

The samples collected close to the Loki's Castle vent field show a clear hydrothermal signature with elevated ^{3}He concentrations compared to the background samples (Fig. 20B). The background samples display stable concentrations in the plume layer depth interval with increasing distance from the vent field. However, all these samples were obtained in the rift valley north and south of the vent field. The enrichment of ^{3}He in the background water (Fig. 20A) may therefore indicate that ^{3}He is added to the water column by hydrothermal processes along the spreading ridge in this region. It has been suggested that the ^{3}He input is proportional to the scale of tectonic activity (e.g. Lupton, 1995). The background samples from the Loki's Castle region are all collected at the ultraslow spreading AMOR, with spreading rates >20 mm/y. The East Pacific rise is one of the world's fastest spreading ridges, with spreading rates of 150 mm/y (e.g. Lupton and Craig, 1981), which is 7.5 times more than at the AMOR. The background delta ^{3}He value at the East Pacific Rise is about 40 % (Lupton and Craig, 1981; Lupton, 1995), which is about 6 times more than the background values for the Loki's Castle area. This indicates that there is a correlation between spreading rates and helium input.

Another depth with elevated ^{3}He concentrations was identified close to 1200 m (Fig. 10B). The helium anomaly in the upper water layer is found in all oceans. This feature has its origin from test-bombing during in the cold war. All tritium in nature today is found as water molecules due to atmospheric testing of thermonuclear bombs (Östlund, 1982). ^{3}He is produces by radioactive decay of tritium produces by this bomb-testing. The anomaly observed in this study matches elevated ^{3}He concentrations in the upper water layer at the Rainbow hydrothermal field (Fig. 19) (Jean Baptiste et al., 2004). The results from Rainbow however, display a larger anomaly than what is reported in this thesis (Fig. 19).

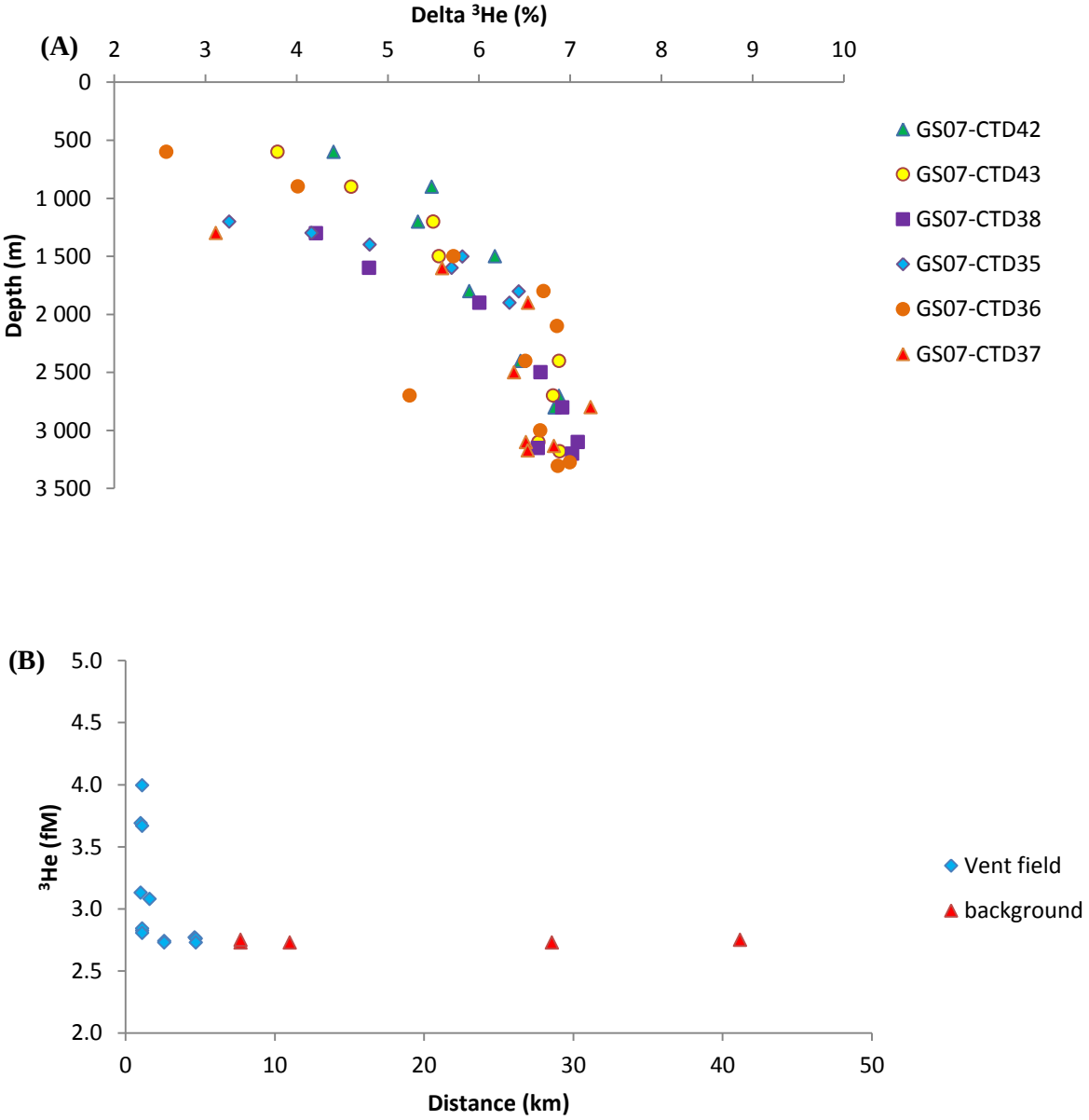

Figure 20. (A) Delta ^{3}He (%) with depth in casts GS07-CTD-35, 36, 37, 38, 42 and 43, which were collected 28, 41, 27, 16, 11 and 22 km from Loki's Castle, respectively. All casts, with exception of GS07-CTD42 and 43, were collected in the rift valley of the Knipovich ridge north of Loki's Castle. GS07-CTD43 and GS07-CTD35 were cast outside the rift valley, south and northwest of Loki's Castle. (B) ^{3}He concentrations in samples obtained in the plume layer (1900- 2200 m) as a function of distance from Loki's Castle.

Based on dissolution of, and equilibrium with the atmospheric gases the general background concentrations for CH_4 and H_2 should be 0.4 and 0.2, respectively (e.g. Baumberger, 2011). However, the background signal detected in this study is much higher (Fig. 21). A background level of H_2 between 0 and 4 nM (Fig. 21A) indicates that hydrogen must have concentrations above 5 nM to indicate hydrothermal influence. Methane has a more complex background signal in these samples (Fig. 21B). The background in the upper water layers has

a concentration between 1 and 3 nM, while the deeper water layers have concentrations between 1.5 and 6 nM. The highest concentrations, which were detected in the deepest samples from a sediment filled basin in the rift vally of the Knipovich Ridge (GS07-CTD37 and GS07-CTD38), probably originating from the decay of organic material in the sediments. The methane concentrations in the background samples indicate that methane must have a concentration higher than 7 nM to indicate hydrothermal influence.

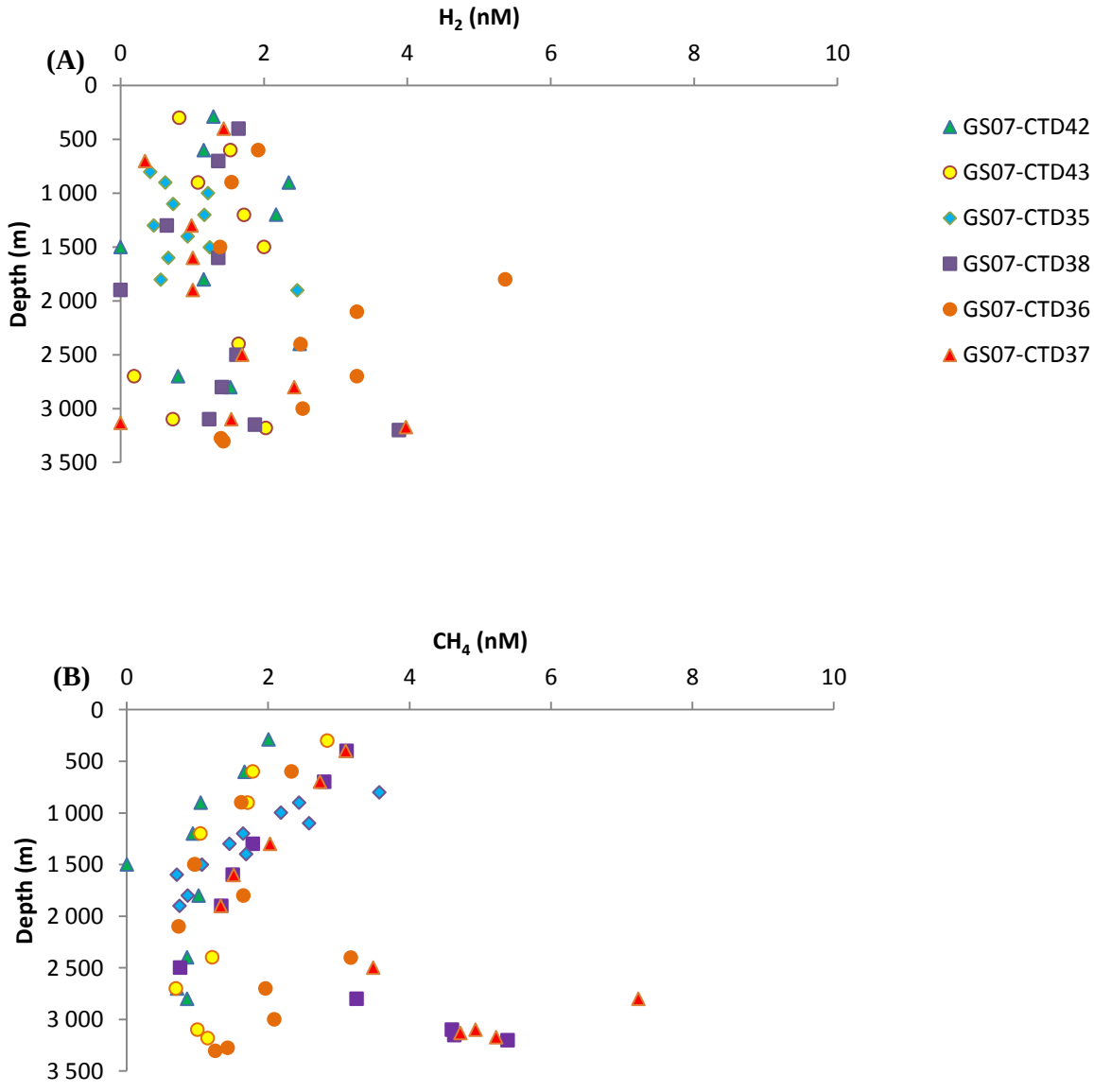

Figure 21. (A) H_2 and (B) CH_4 as function of depth in casts GS07- CTD- 35, 36, 37, 38, 42 and 43, which were collected 28, 41, 27, 16, 11 and 22 km from Loki's Castle, respectively. All casts, with exception of GS07-CTD42 and 43, were collected in the rift valley of the Knipovich ridge north of Loki's Castle. GS07-CTD43 and GS07-CTD35 were cast outside the rift valley, south and northwest of Loki's Castle.

5.2 The Jan Mayen vent fields

5.2.1 General plume characteristics

Both the Troll Wall and the Soria Moria vent fields are basalt-hosted, and include several venting areas. The vent fluids emitted from both vent sites have a temperature of 270°C, and are characterized by high CO_2 concentrations and moderate to low content of methane and hydrogen (Pedersen et al., 2010a, Baumberger, 2011). This composition is also reflected by the amount of methane and hydrogen in the non-buoyant plume.

The moderate methane peaks detected between 300 and 400 m at the Troll Wall vent field (Fig. 13A-C, H, J) document where the non-buoyant plume was entrained. The methane values in the plume rarely exceeded concentrations of 150 nM and hydrogen was found in small quantities in both 2008 and 2012. Of the two casts (GS11-CTD9 and GS12-CTD23) obtained at Soria Moria, only GS12-CTD23 displayed a plume signal. In GS12-CTD23 the non-buoyant plume was characterized by low hydrogen and moderate methane concentrations close to 500 m. The concentrations were therefore similar to that of the Troll Wall vent field. The CTD casts sampled in 2011 displayed different properties compared to 2008 and 2012, and will therefore be discussed separately.

As venting at the Troll Wall occurs at 550 m, and the non-buoyant plume is located at 300-400 m, the rise-height of the hydrothermal fluids is 150-250 m. At Soria Moria, where the venting occurs at 700 m and the plume was observed at about 500 m, the hydrothermal fluids have a rise-height of 200 m (Fig. 12).

The background water column in the Jan Mayen region (Fig. 22) showed steep salinity and temperature profiles similar to those at Loki's Castle (Fig. 15). The plume at the Troll wall vent field is detected by an increase in density and temperature (0.1 °C) and a decrease in salinity (Fig. 23). None of the parameters are however, affected as much as observed in GS09-CTD4 from the Loki's Castle.

The CTD obtained closest to the Troll Wall vent field (50 m) was GS12-CTD4 (Fig. 13J), which had the highest ^{3}He concentration (3.8 fM) of any year, measured at a depth of 520 m. The background ^{3}He concentration at the Troll Wall was estimated to be 2.6 fM by averaging values in CTD casts where a plume signal was not detected. The ^{3}He concentration in GS12-

CTD4 was therefore 1.2 fM enhanced above the background value. The end-member concentration of ^{3}He were measured to be 11.4 pM at the Troll Wall (personal correspondence with M. D. Lilley). This indicates a minimum dilution factor of 9500 for the Troll Wall vent field. This is also consistent with the theoretical value for dilution at the attainment of neutral buoyancy in the Pacific Ocean, which was estimated to be between 8000 and 10000 (Speer and Rona, 1989; McDuff, 1995; Field and Sherrell, 1999). There are too few samples from Soria Moria to make an estimate of the dilution factor for this plume at Soria Moria, but based on similar properties of the plume one can assume that also the dilution factor is similar.

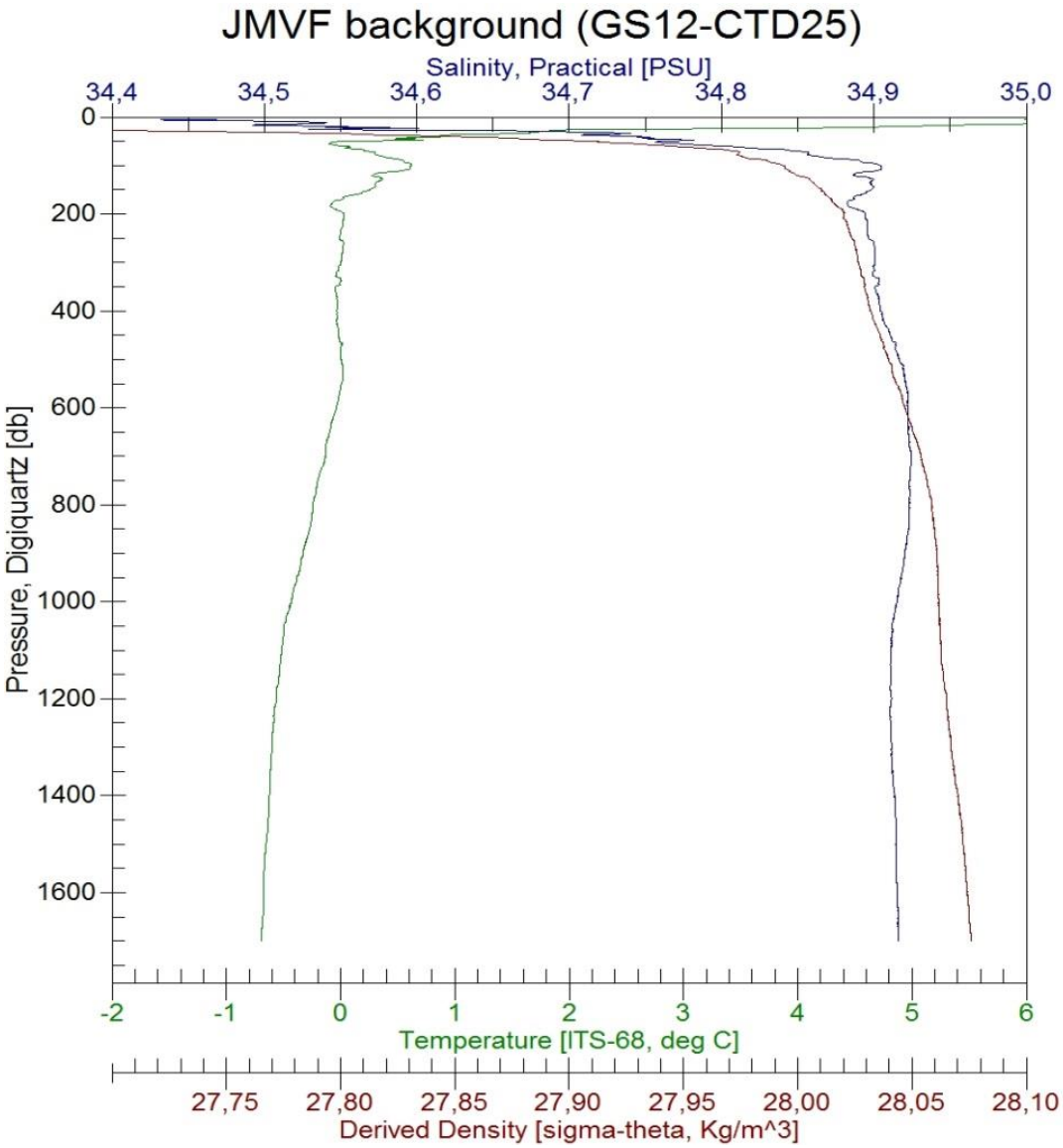

Figure 22. Background cast from the Jan Mayen fracture zone (GS12-CTD25)

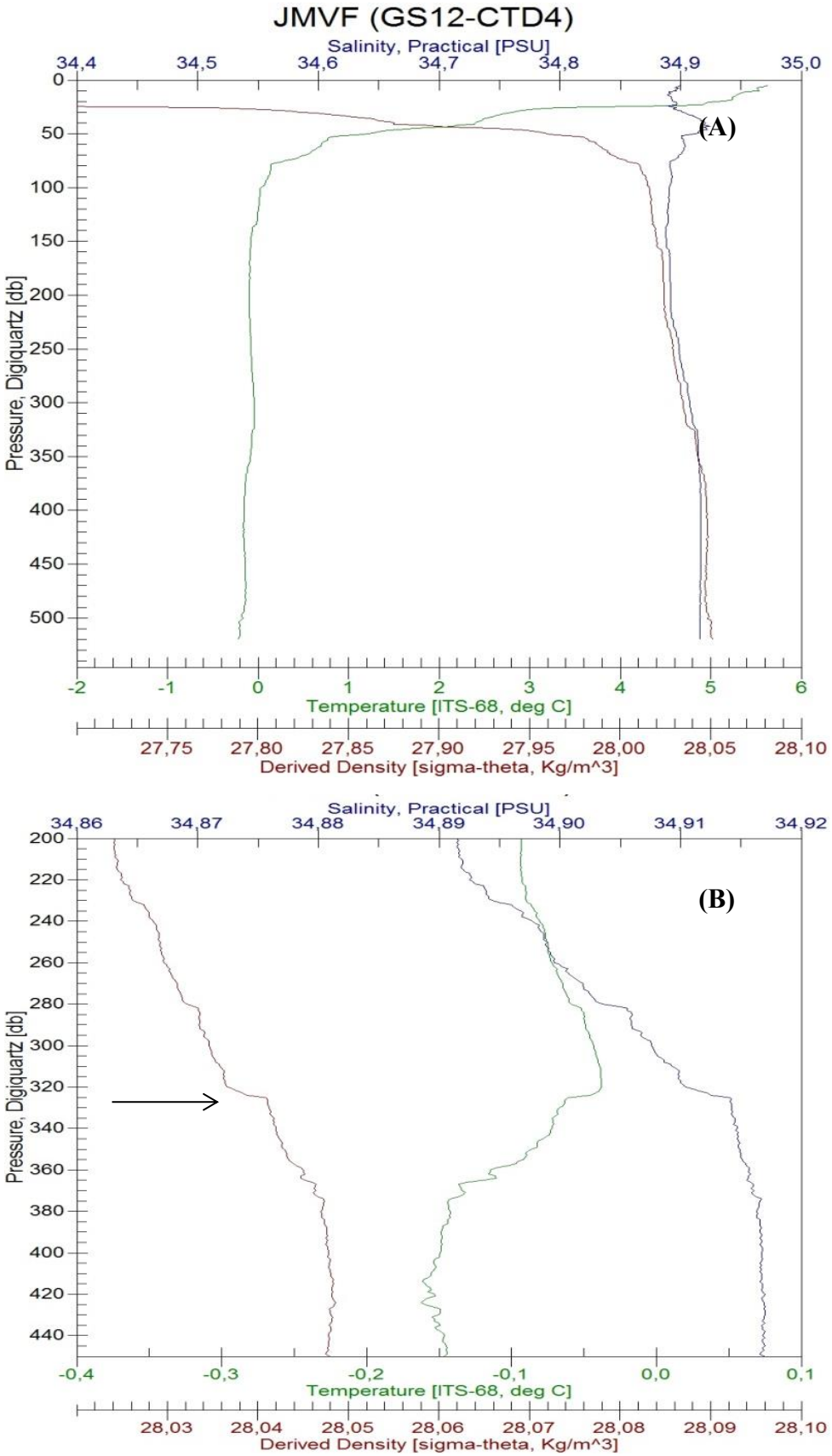

Figure 23. Temperature, salinity and density profiles from (A) GS12-CTD4, and (B) enlarged to emphasize the plume signal.

Several CTD casts from the Troll Wall display high concentrations of methane close to the seafloor (e.g. Fig 13, B-E, H, I), which likely reflect the extensive diffuse venting observed in this region (Pedersen et al., 2010a). Diffuse venting occurs when reduced hydrothermal fluids mix with oxygen-saturated seawater in the crust in close vicinity to active vents (Von Damm and Lilley, 2004). The diffuse venting at the Troll Wall vent field is characterized by moderate methane concentration and very low hydrogen concentration, similar to the non-buoyant plume from the focused venting (Fig. 13). Von Damm and Lilley, (2004) reported loss of H_2, H_2S and CO_2 combined with a gain in methane in diffuse vent fluids at the East Pacific Rise. This is consistent with the observations at the diffuse vents at the Troll Wall vent field and may be a result of biological activity. Microbes consuming hydrogen and carbon dioxide may produce methane through the following reaction (e.g. Von Damm and Lilley, 2004):

$$CO_2+4H_2 = CH_4+2H_2O$$

Methanogenesis could be a plausible explanation for the high methane concentration diffusing from the Troll Wall vent field. However, the white microbial mats at the Troll Wall were dominated by sulfur-oxidizing bacteria (Lanzen et al., 2011; Urich et al., 2013). Methanogenic microorganisms may, however, be more abundant in the subseafloor environment.

In the past, diffuse venting has not been abundantly sampled compared to focused black and white smoker vents (e.g. Von Damm and Lilley, 2004), thus, the dataset for diffuse vents is not as extensive as for focused venting. However, the results from the JMVF display several examples of diffuse venting (e.g. Fig. 13C, Fig. 13H) suggesting that diffuse venting is playing an important role in this environment, and should be extensively investigated. A particularly good example of diffuse venting is demonstrated by GS11-CTD3 (Fig. 13E), where methane has high concentrations close to seafloor and diffuses in the water column towards the surface. In GS11-CTD3 the decrease in concentration with decreasing depth is prominent. The results from the Soria Moria vent field do not show any signs of diffuse venting. This is consistent with more bacterial mats at the Troll Wall vent field compared to the Soria Moria vent field (Pedersen et al. 2010a). This difference in diffuse venting may be linked to the geology at the two fields. The Troll Wall vent field is situated on a talus located at the hanging wall of the Troll Wall enscarpment, while the hydrothermal deposits at Soria

Moria are directly situated on ancient lava flows (Pedersen et al., 2010a). This difference may explain the more extensive diffuse venting at the Troll Wall.

5.2.2 Additional vent field

The water column data collected at the JMVF between 2008 and 2012 do not give any indication of an additional vent field. However, this does not mean that an additional vent could not exist in the region. If the plume of an additional vent field where at the same depth, and had similar chemical signature as the JMVF its identification would be difficult. During a CGB cruise to the JMVF in 2013 a new vent field was discovered 2 km NE of the Troll Wall vent field (G.O. Sars scientific party, unpublished data). The new vent field was discovered by randomly sampling the water column with CTDs. In 2007, the year before the discovery of the Loki's Castle vent field, the plume was detected 7.1 km away from the vent field. At the Jan Mayen vent fields the dissolved gases in the water column was already linked to the vent fields below. This indicates why the new vent field was not discovered before.

5.2.3 The hydrogen anomaly of 2011

Measurements of hydrogen had low concentrations in both 2008 and 2012. However, in 2011, hydrogen was elevated in every cast. The end-member composition in 2011 was 0.7 mM methane and 0.02 mM hydrogen for the Troll Wall vent field, and 0.3-0.6 mM methane and 0.1-0.3 mM hydrogen for the Soria Moria vent field, which is similar to the end-member composition in 2008 and 2012 (personal communication M. D Lilley). Most CTD samples collected above the JMVF display values consistent with the end-member ratios (Fig. 24). However, 12 samples show the opposite trend with high hydrogen and low methane concentrations. All these samples were obtained in 2011 by the casts, GS11-CTD2 (Fig. 13F) and GS11-CTD3 (Fig. 13F), which display multiple hydrogen peaks but low methane content. As GS11-CTD2 was obtained 1.5 km NE from the Soria Moria vent field, these anomalies could indicate an additional vent field in this region. However, GS11-CTD3 was obtained only 90 m from the Troll Wall vent field. In addition the hydrogen peak were found higher up in the water column than the focused plume at the Troll Wall was located.

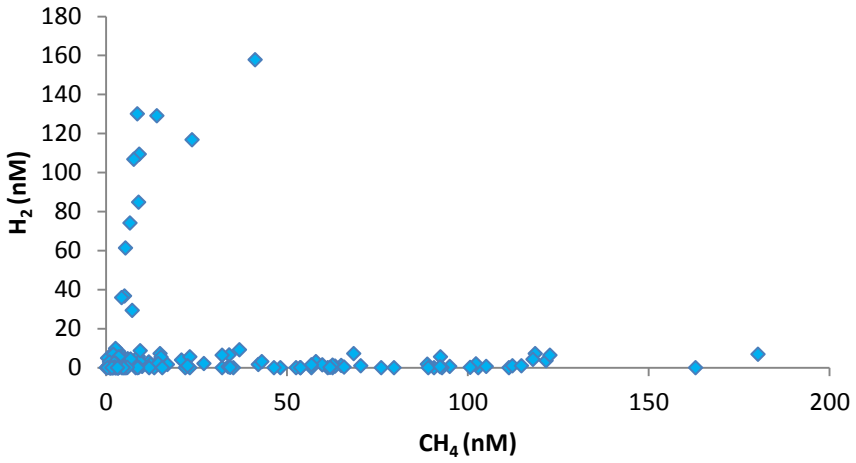

Figure 24. H_2 in relation with CH_4 in the samples from the JMVF.

In 2011, samples for ^{3}He analysis were collected from two casts, GS11-CTD3 at the Troll Wall vent field and GS11-CTD9 at the Soria Moria vent field. However, only GS11-CTD3 showed a hydrogen anomaly. A possible explanation for this is that the GS11-CTD9 was sampled 4 days after GS11-CTD3, thus giving an indication of the time range of the hydrogen anomaly in 2011. However, the lack of excess hydrogen in this CTD may also reflect that ocean currents transported material in a different direction. As ^{3}He is associated with water in contact with magma, the correlation between hydrogen and helium can be used to determine the origin of the hydrogen (Fig. 25).

The correlation between CH_4 and ^{3}He in GS11-CTD3 (Fig. 25A) is nearly linear (R^2= 0.98), indicating that consumption of methane has not yet started and that the water column is only diluted. The absence of consumption may indicate that this plume was young when sampled.

The correlation between H_2 and ^{3}He show two different trends (Fig. 25B); (1) Low concentrations of hydrogen and elevated concentrations of ^{3}He, and (2) where the ^{3}He concentration is low the hydrogen concentration is high. The first trend is consistent with the end-member composition of the venting fluids, having relatively low concentrations of hydrogen. The second trend however, is not consistent with the end-member fluids.

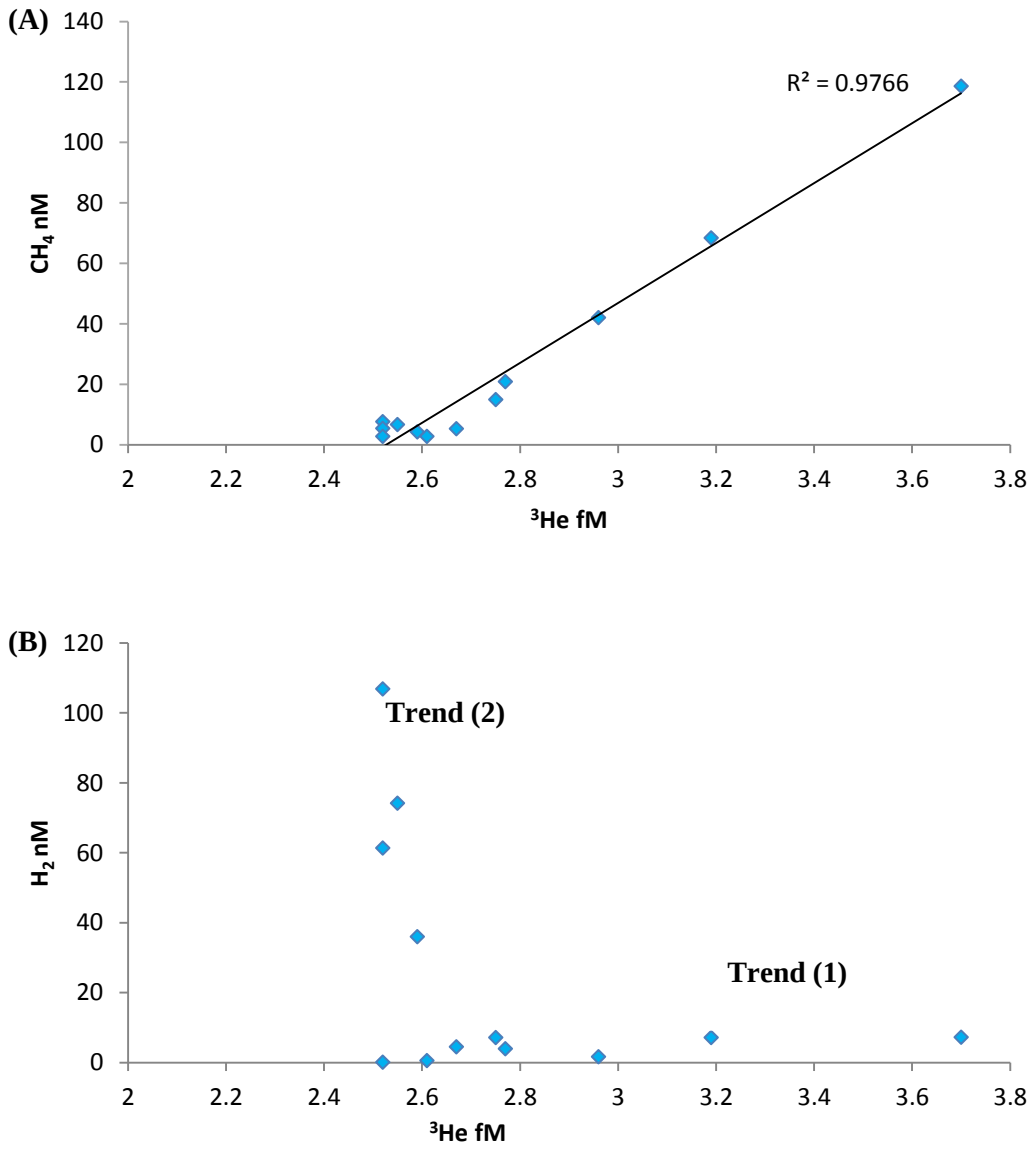

Figure 25. Correlation of ^{3}He with (A) CH_4 and (B) H_2 in GS11-CTD3. The R^2 indicates the linearity of the trendline, R^2=1 means perfect linearity.

Because the hydrogen so clearly did not originate from the vent fields, a possibility of an event plume as the source for this anomaly arises. Three models for occurrence of event plumes have been proposed; (1) crustal rupture causes a sudden release of volatiles (e.g. Baker et al., 1989; Baker and Lupton, 1990; Lupton et al., 1999a; 2000), (2) dike intrusion causes a release of heat and volatiles (e.g. Lowell and Germanovich, 1995), (3) volatiles produced by either lava flow or pillow lava formation (e.g. Butterfield et al., 1997; Palmer and Ernst, 1998). The first evidence of event plumes where reported by Baker et al., (1987) at the Juan de Fuca Ridge. These first reports provided evidence that submarine eruptive events

are associated with high release of hydrothermal fluids. (Baker et., 1987; 1989, 1995; Lupton et al., 1989; Lupton, 1995; Kelley 1998).

Event plumes are rarely sampled during the eruption, and thus the concentrations of volatiles may change before samples are taken. One study of an event plume where CH_4, H_2 and ^3He were sampled, was at the Gorda Ridge event plume in 1996 (Kelley et al., 1998). At the Gorda Ridge event the highest H_2 concentration detected was 47 nM (Kelley et al., 1998). However, the measurements were performed after the eruptive event had occurred.

One eruptive event has been reported where the results were obtained during and shortly after the eruption. In 2008 a cruise was sampling the water column above the Northeast Lau Spreading Center (NELSC) when high hydrogen concentrations were detected (Baker et al., 2011; Baumberger, 2011). This event plume at NELSC had a maximum hydrogen concentration of 9000 nM (Baker et al., 2011), which is significantly higher than the maximum hydrogen concentrations (157 nM) detected at the JMVF in 2011. However, the maximum concentrations measured in 2008 and 2012 were only 5.8 and 6.9 nM, respectively. The maximum hydrogen concentration in 2011 was therefore almost 26 times higher than the highest result from other years.

Methane measured at the NELSC did not show any enrichment above background (Baumberger, 2011), which is similar to the results from the JMVF. Another similarity is the low ^3He concentrations observed at the JMVF and at the NELSC. Low ^3He concentrations can be explained by the extruding/intruding lava has not cooled enough when the eruptive event releases hydrogen. Sampling after an eruptive event has suggested that ^3He degasses when the basalt has cooled enough to crack (Baker et al., 1995; Lupton et al., 1999b; Baker et al., 2011).

The event plume at the NELSC was a result of a lava flow at the seafloor, which was sampled in 2009 and dated to November 2008 (the year of the event plume).

The event plume at NELSC shares several properties with the results from the JMVF. This could therefore indicate that the hydrogen anomaly in 2011 was a product of a lava flow reacting with seawater.

6 Summary

The Loki's Castle vent field emits hydrothermal fluids with high concentrations of methane and moderate to high concentrations of hydrogen. The buoyant plume rises 400 m, from about 2400 to about 2000 m, where neutral buoyancy is established. This is about 50 m higher than most plumes in the Atlantic and about 200 m higher than plumes in the Pacific Ocean. The plume signal vary significantly, from clear methane peaks at 2000 m up to 7.1 km from the vent field, to not detectable methane anomalies at a distance of only 2.3 km. This is probably a result of the complex ocean currents in the region, which cause extensive mixing and transportation of the plume. Deviations of the CH_4/H_2 ratio in the plume relative to the end-member ratio is likely a result of such mixing between the hydrothermal fluids and ambient seawater, in addition to oxidation processes The background seawater is enriched in hydrogen relative to methane. This is not only the opposite of the end-member composition, it is also conflicting with the current understanding of hydrogen oxidation in seawater. The extensive mixing and transport of hydrothermal fluids rich in nutrients and energy sources may be important for microbial life and activity in the artic water.

The minimum dilution factor for the buoyant and the non-buoyant plume is estimated to 1700 and 8900, respectively. The dilution factor for the non-buoyant plume is consistent with theoretical estimates for hydrothermal plumes in the Pacific Ocean. The Loki's Castle vent field have a similar delta ^{3}He profile as the Rainbow hydrothermal field, situated on the MAR. Due to this similarity thermal output can be estimated to be 1320 ± 600 MW. The ambient deep water in the rift valley of the Mohns and Knipovich ridges show an increase in deep water delta ^{3}He (%) of about 2% compared to the Atlantic Ocean and of 5 % relative to the Norwegian Sea. This could either be due to deep water transportation from the Artic, with similar delta ^{3}He in the deep water, or helium input from the ridge segments below. A comparison with deep water at the East Pacific Rise reveal a possible correlation between spreading rates and ^{3}He input. Background data also indicates that concentrations of H_2 and CH_4 should be higher than 5 and 7 nM, respectively, to indicate a hydrothermal vent field. Anomalies at 2319 m southwest of the Loki's Castle vent field indicate another deeper vent field in this region.

Summary

The non-buoyant plume at the JMVF rises 100-150 m above the Troll Wall and 200 m above the Soria Moria vent field, and is characterized by moderate CH_4 and low H_2 concentrations. The diffuse flow, found mostly at the Troll Wall vent field is detected as white bacterial mats at the seafloor, and is also dominated by methane relative to hydrogen. The methane produced here may be of biogenic origin, produced by methanogenesis at or below the seafloor. The dilution factor at the Troll Wall is estimated to be at least 9500, which is consistent with estimates for the non-buoyant plume in the Pacific Ocean. The dilution factor at Soria Moria could not be calculated due to the lack of data. In 2011 the hydrogen content in the water column was 26 times higher than in any other year at the JMVF. This excess hydrogen did not correlate to the end-member fluid composition, and was thus not originating from the vent fields. However, the methane and ^3He concentrations from the same year did not show any deviations from the general pattern. Through comparisons with an eruptive event study from the NELSC, the hydrogen anomaly at JMVF is interpreted as an eruptive event plume originating from an eruption at the seafloor.

7 Future work

This study generated several questions that needs further investigation. Generally more detailed search is needed to locate a potential new vent field southwest of Loki's Castle. Further investigation is also needed to understand the hydrogen oxidation in the plume and the surrounding seawater. The background seawater in the Loki's Castle region showed elevated in hydrogen compared to methane, which is contradicting the present theories on hydrogen oxidation. More ^{3}He data for the deep water at the Mohns and Knipovich ridges could increase the understanding of the relationship between spreading rates and ^{3}He input. This study illustrates extensive transportation of the plume due to ocean currents. When searching for hydrothermal vent fields in the future, the effects of ocean currents transport should be taken into account.

Diffuse venting is less known than focused venting, thus further investigations of the diffuse flow at the JMVF could increase the data set on this type of venting. The water column data do not show any evidence for diffuse venting at the Soria Moria vent field. However, more samples are needed to confirm this. Another interesting aspect is to locate the eruptive lava, which produced the hydrogen anomaly in 2011.

8 References:

Alt, J. 1995. Subseafloor processes in mid-ocean ridge hydrothermal systems. Pp. 85–114 in *Seafloor Hydrothermal Systems: Physical, Chemical, Biological, and Geological Interactions*. S.E. Humphris, R.A.

Augustin, N., Lackschewitz, K.S., Kuhn, T., Devey, C.W., 2008. Mineralogical and chemical mass changes in mafic and ultramafic rocks from the Logatchev hydrothermal field (MAR 15°N). Marine Geology 256, 18‑29.

Baker, E.German C.R, and Elderfield H. 1995.Hydrothermal plumes over spreading-center axes: Global distributions and geological inferences. Pp. 47–71 in *Seafloor Hydrothermal Systems: Physical, Chemical, Biological, and Geological Interactions*. S.E. Humphris, R.A. Zierenberg, L.S. Mullineaux, and R.E. Thomson, eds, AGU Monograph Series, No. 91, American Geophysical Union, Washington, DC.

Baker E.T, Edmonds H. N, Micheal P. J, Bach H, Dick H. J. B, Snow J. E, Walker S. L, Banerjee N. R and Langmuir C. H. 2004. Hydrothermal venting in magma deserts: The ultraslow-spreading Gakkel and Southwest Indian Ridges, Geochemistry Geophysics Geosystems, 5.

Baker, E. T., Lavelle J. W, Feely R.A, Massoth G.J, Walker S.L, and Lupton J.E. 1989-Episodic venting of hydrothermal fluids from the Juan de Fuca Ridge, J. Geophys.Res., 94, 9237–9250, doi:10.1029/JB094iB07p09237.

Baker E.T, Lupton J.E, Resing J.A, Baumberger T, Lilley M.D, Walker S.L and Rubin K.H. 2011. Unique event plumes from a 2008 eruption on the Northeast Lau Spreading Center. Geochem. Geophys. Geosyst., 12, Q0AF02, doi:10.1029/2011GC003725.

Baker E.T and Lupton J.E. 1990. Changes in Submarine Hydrothermal He-3/heat Ratios as an Indicator of Magmatic Tectonic Activity, Nature, 346 (6284), 556-558.

Baker, E.T., Massoth, G.J., Feeley, R.A., 1987. Cataclysmic hydrothermal venting on the Juan de Fuca Ridge. Nature 329, 149-151.

Baumberger T. 2011.Volatiles in Marine Hydrothermal Systems. Diss. ETH No. 20061

Bischoff J. L and Seyfried. 1978. Hydrothermal chemistry of seawater from 25 to 350 °C. Am. J. Sci. 278, 838-860.

Blindheim J and Rey F. 2004. Water mass formation and distribution in the Nordic Seas during the 1990s. ICES journal of marine science. 61: 846-863

References

Blindheim J and Østerhus S, 2005 The Nordic Seas, Main Oceanographic Features

Bradley A.S, Summons R.E. 2010. Multiple origins of methane at the Lost City Hydrothermal Field. Earth and Planetary Science Letters 297, 34–41.

Butterfield D. A, Jonasson I.R, Massoth G.J, Feely R.A, Roe, K. K, Embley R.E, Holden J.F, McDuff R.E, Lilley M.D and Delaney J.R. 1997.Seafloor eruptions and evolution of hydrothermal chemistry. Philosophical Transactions of the Royal Society of London Series a-Mathematical Physical and Engineering Sciences. 355 (1723), 369-386.

Charlou J.L, Donval J. P, Fouquet Y, Jean-Baptist P and Holm N. 2002. Geochemistry of high H_2 and CH_4 vent fluids issuing from ultramafic rocks at the Rainbow hydrothermal field. Chemical Geology 191(4),345-359.

Connelly, D. P., C. R. German, M. Asada, K. Okino, A. Egorov, T. Naganuma, N. Pimenov, G. Cherkashev, and K. Tamaki (2007), Hydrothermal activity on the ultra-slow spreading southern Knipovich Ridge, *Geochem. Geophys. Geosyst.*, *8*, Q08013,doi:10.1029/2007GC001652.

Corliss, J. B., et al. (1979), Submarine thermal springs on the Galapagos Rift, Science, 203, 1073–1083.

De Angelis M. A, Lilley M.D, Olson E.J and Baross J.A. 1993. Methane oxidation in deep-sea hydrothermal plumes at the Endeavour segment of the Juan de Fuca Ridge. Deep sea research, 40, 1169-1189

Dick H.J.B, Lin J and Schouten H. 2003. An ultraslow-spreading class of ocean ridge, Nature, 426(6965), 405-412.

Douville E, Charlou J.L, Oelkers E.H, Bienvenu P, Jove Colon C.F, Donval J.P, Fouquet Y, Prieur D, Appriou P. 2002. The Rainbow vent fluids (36°14`N, MAR): the influence of ultramafic rocks and phase separation on trace mineral content in Mid-Atlantic Ridge hydrothermal fluids. Chem. Geol. 184, 37-48.

Edmonds H. N, Michael P.J, Baker E.T, Connelly D.P, Snow J.E, and Langmuir C.H. 2003, Discovery of abundant hydrothermal venting on the ultraslow-spreading Gakkel ridge in the Arctic Ocean, *Nature, 421*, 252–256.

Field P.M, Sherrell R.M. 1999. Dissolved and particulate Fe in a hydrothermal plume at 9°45'N, East Pacific Rise: Slow Fe (II) oxidation kinetics in Pacific plumes.

German C.R, Baker E.T, Mevel C, Tamaki K, and the FUJI science team. 1998. Hydrothermal activity along the southwest Indian ridge, Nature, 395, 490–493.

German C.R, Bowen A, Coleman M.L, Honig D.L, Huber J.A, Jakuba M.V[e], Kinsey J.C, Kurz M.D, Leroy S, McDermott J.M, Mercier de Lépinay B, Nakamura K, Seewald J.S.. Smith J.L[d], Sylva S.P, Van Dover C.L, Whitcomb L.L and Yoerger D.R. 2010. Diverse styles of submarine venting on the ultraslow spreading Mid-Cayman Rise. 14020–14025. PNAS. vol. 107. no. 32.

References

German C.R, Klinkhammer G.P and Rudnicki M.D. 1996. The Rainbow hydrothermal plume, 36°15'N, MAR. GEOPHYSICAL RESEARCH LETTERS, VOL. 23, NO. 21, PAGES 2979-2982.

Hannington, M., P. Herzig, P. Stoffers, J. Scholten, D. Garbe-Schönberg,I. R. Jonasson, and W. Roest (2001), First observations of high-temperature submarine vents and massive anhydrite deposits off the north coast of Iceland, *Mar. Geol.*, *177*, 199–220

Heinze C. H, Schlosser P, Koltermann K. P and Meincke J. 1990. A tracer study of the deep water renewal in the European polar seas. Deep-sea research. Vol 37. No 9, pp 1425-1453.

Horita, J., Berndt, M.E., 1999. Abiogenic methane formation and isotopic fractionation under hydrothermal conditions. Science 285, 1055–1057

James R.H, Elderfield H,.Rudnicki M.D, German C.R, Palmer M.R and 8 others. 1995 Hydrothermal plumes at Broken Spur,29°N Mid-Atlantic Ridge: Chemical and physical characteristics, in Hydrothermal Vents and Processes edited by L.M.Parson,C.L.Walker and D.R.Dixon, pp97-110, Geol. Soc. (London) Spec. Publ. 87

Jean-Baptiste P, Bougault H, Vangriesheim A, Charlou J.L, Radford-Knoery J, Fouquet Y, Needham D, German C. 1998. Mantle ^{3}He in hydrothermal vents and plume of the lucky strike site (MAR 37°17'N) and associated geothermal heat flux. Earth and planetary letters 157. 69-77.

Jean-Baptiste P, Fourrè E, Charlou J.L, German C.R, Radford-Knoery J. 2004. Helium isotopes at the Rainbow hydrothermal site (Mid-Atlantic Ridge, 36°14`N). Earth and Planetary Science Letters 221, 325-335.

Jenkins W.J , Lott D.E, Cahill K, Curtice J, Landry P**. 2010.** SAMPLING AND MEASURING HELIUM ISOTOPES AND TRITIUM IN SEAWATER. IOCCP report No. 14, ICPO publication series No.134, Version 1. 2010

Jutterström S and Jeansson E. 2008. Anthropogenic carbon in the East Greenland Current. Progress in Oceanography 78. 29–36

Johannesen O.M. 1986. Brief overview of the physical oceanography. Edited by Hurdle B.G. The Nordic Seas. 103-127.

Kelley D.S, Baross J.A, Delaney J.R. 2002. Volcanoes, fluids, and life at mid-ocean ridge spreading centers. Earth Planet. Sci 30:385-491

Kelley D. S and Delaney J. R. 1987. Two-phase separation and fracturing in mid-ocean gabbros at temperatures greater than 700 °C. Earth Planet. Sci. Lett., 83, 53-66.

Kelley D.S, Lilley M.D, Lupton J.E and Olson E.J 1998. Enriched H_2, CH_4 and ^{3}He concentrations in hydrothermal plumes associated with the 1996 Gorda Ridge eruptive event. Deep-Sea Research II 45 2665-2682.

References

Kelley D. S. ; Karson J.A, Früh-green G.L. ; Yoerger D.R. ; Shank T.M. ; Butterfield D.A. ; Hayes J.M. ; Schrenk M.O. ; Olson E.J. ; Proskurowski G ; Jakuba M ; Bradley A ; Larson B ; Ludwig K ; Glickson D ; Buckman K ; Bradley A S. ; Brazelton W.J. ; Roe K ; Elend M.J ; Delacour A ; Bernasconi S.M. ; Lilley M.D. ; Baross J.A ; Summons R.E. ; Sylva S.P. 2005. A Serpentinite-Hosted Ecosystem: The Lost City Hydrothermal Field. Science [0036-8075]. vol:307 iss:5714 pg:1428 -1434

Lanzen A, Jørgensen S. L, Bengtsson M. M, Jonassen I, Øverås L and Urich T. 2011. Exploring the composition and diversity of microbial communities at the Jan Mayen hydrothermal vent field using RNA and DNA. FEMS Microbiol. Ecol. 77, 577-589.

Lilley M. D, Butterfield D.A, Olson E.J, Lupton J.E, Macko S.A and McDuff R.E. 1993. Anomalous CH_4 and NH_4^+ Concentrations at an unsedimented Mid-Ocean-Ridge hydrothermal system, edited by Humphris S. E et al., pp369-391. Geophysical Monograph. American geophysical union.

Lilley MD, Landsteiner MC, McLaughlin EA, Parker CB, Cherkaoui ASM, et al. 1995.Real-time mapping of hydrothermal plumes on the Endeavour Segment of the Juan de Fuca. *Eos Trans. Am. Geophys. Union* 76:420

List E. J. 1982. Turbulent jets and plumes, Annu. Rev. Fluid Mech.14, 189-212.

Lowell R. P and Germanovich L. N. 1995. Dike Injections and the Formation of Megaplumes at Ocean Ridges. Science, 267(5205), 1804-1807.

Lupton JE. 1995. Hydrothermal plumes: near and far field. See Humphris et al. 1995, pp.317–46.

Lupton, J. E., Baker E, Embley R, Greene R, and Evans L. 1999b. Anomalous helium and heat signatures associated with the 1998 Axial Volcano event, Juan de Fuca Ridge, Geophys. Res. Let t. , 26, 3449–3452, doi:10.1029/1999GL002330.

Lupton, J. E., Baker E.T, and Massoth G.J .1989. Variable 3He/heat ratios in submarine hydrothermal systems: Evidence from two plumes over the Juan de Fuca Ridge, Nature, 337, 161–164, doi:10.1038/337161a0.

Lupton J.E, Baker E. T and Massoth G. J. 1999a. Helium, Heat, and the generation of hydrothermal event plumes at mid-ocean ridges. Earth and Planetary Science letters, 180(1-2), 219-222.

Lupton J.E, Baker E. T and Massoth G. J. 2000. Reply to comment on "Helium, Heat, and the generation of hydrothermal event plumes at mid-ocean ridges" by Lupton J. E, Baker E. T and Massoth G. J. Earth and Planetary Science letters, 180(1-2), 219-222.

Lupton J.E and Craig H.1981. A major helium-3 source at 15°S on the East Pacific Rise. Science, 214, 13-18.

References

Lupton J.E, Delaney J.R, Johnson H.P and Tivey M.K.1985. Entrainment and vertical transport of deep-ocean water by buoyant hydrothermal plumes. Nature, 316,621-623

Malmberg, S-Aa. 1983. Hydrographic investigations in the Iceland and Greenland Seas in late winter 1971 - ‘‘Deep Water project’’. Jökull, 33: 133-140.

Malmberg, S-Aa., and Jönsson, S. 1997. Timing of deep convection in the Greenland and Iceland Seas. ICES Journal of Marine Science, 54: 300-309.

Marbler H, Koschinsky A, Pape T, Seifert R, Weber S, Baker E. T, de Carvalho L. M, Schmidt K. 2010. Geochemical and physical structure of the hydrothermal plume at the ultramafic-hosted Logatchev hydrothermalfield at 14°45′N on the Mid-Atlantic Ridge. Marine Geology 271. 187–197

Marcaillou C , Muñoz M, Vidal O , Parra T, Harfouche M. 2011. Mineralogical evidence for H2 degassing during serpentinization at 300 °C/300 bar. Earth and Planetary Science Letters 303 281–290

Massoth GJ, Baker ET, Feely RA, Lupton JE, Collier RW, et al. 1998. Manganese and iron in hydrothermal plumes resulting from the 1996 Gorda Ridge Event. *Deep-Sea Res. II* 45:2683–712

McCollom, T.M. and Seewald, J.S., 2007. Abiotic Synthesis of Organic Compounds in DeepSea Hydrothermal Environments. Chem. Rev. (Washington, DC, United States) 107,382–401.

McDuff R. E. 1995. Physical dynamics of deep-sea hydrothermal plumes. In Seafloor hydrothermal Systems: Physical, chemical, biological and geological interactions (e.d S.E Humphris et al.) 99. 357-368. Am. Geophys. Union.

McLaughlin EA. 1998. *Microbial hydrogen oxidation in hydrothermal systems*. PhD thesis.Univ. Washington. 125 pp

Meincke, J., and Rudels, B. 1995. The Arctic Ocean Nordic Seas thermohaline system. ICES C.M. 1995, Mini:2. 16 pp.

Micheal P. J, Langmuir C. H, Dick H. J. B, Snow J. E, Goldstein S. L, Graham D. W, Lehnert K, Kurras G, Jokat W, Muhe R and Edmonds H.N. 2003. Magmatic and amagmatic seafloor generation at the ultraslow-spreading Gakkel ridge, Arctic Ocean, Nature, 423(6943), 956-U951.

Nygaard, T. E., T. Bjerkgaard, D. Kelley, I. Thorseth, and R. B. Pedersen (2003), Hydrothermal chimneys and sulphide mineralized breccias from the Kolbeinsey and the Mohns Ridge, *Geophys. Res. Abstr.*, *5*, Abstract 11863.

Olafsson, J., K. Thors, U. Stefansson, S. P. Jakobsson, W. J. Jenkins, G. Thompson, S. Honjo, F. T. Manheim, R. F. Commeau, and R. R. Jones (1990), Geochemical observations of a boiling hydrothermal site on the Kolbeinsey Ridge, *Eos Trans. AGU*, *71*,1650

References

Palmer M. R and Ernst G. G. J. 1998. Generation of hydrothermal megaplumes by cooling of pillow basalts at mid-ocean ridges. Nature, 393(6686), 643-647.

Pedersen, R. B, Thorseth I.H, Hellevang B, Schultz A, Taylor P, Knudsen H.P, and Steinsbu B.O (2005), Two vent fields discovered at the ultraslow spreading Arctic Ridge System, *Eos Trans. AGU*, *86*(52), Fall Meet. Suppl., Abstract OS21C-01.

Pedersen R.B, Thorseth I.H, Nygård T.E, Lilley M.D and Kelley D.S. 2010a. Hydrothermal Activity at the Arctic Mid-Ocean Ridges. Diversity of Hydrothermal Systems on Slow Spreading Ocean Ridges Geophysical Monograph Series 188 Copyright 2010 by the American Geophysical Union. 10.1029/2008GM000783

Pedersen.R.B, Rapp H.T, Thorseth I.H, Lilley M.D, Barriga F.J.A.S, Baumberger T, Flesland K, Fonseca R, Früh-Green G.L, Jorgensen S.L.2010b. Discovery of a black smoker vent field and vent fauna at the Arctic Mid-Ocean Ridge. Nature communication: DOI: 10.1038/ncomms1124

Petersen J.M, Zielinski F.U, Pape T, Seifert R, Moraru C, Amann R, Hourdez S, Girguis P.R, Wankel S.D, Barbe V, Pelletier E, Fink D, Borowski C, Bach W and Dublilie N. 2011. Hydrogen is an energy source for hydrothermal vent symbioses. NATURE VOL 476.

Proskurowski G, Lilley M.D, Seewald J.S, Früh-Green G.L, Olson E.J, Lupton J.E, Sylva S.P, Kelley D.S. 2008. Abiogenic Hydrocarbon Production at Lost City Hydrothermal Field. Science Vol. 319 no. 5863 pp. 604-607 DOI: 10.1126/science.1151194.

Quadfasal D and Meincke J .1987. Note on the thermal structure of the Greenland Sea gyres. Deep-Sea Research, Vol. 34, No. 11, ppr 1883—188

Resing J.R, Lupton J.E, Feeley R.A, Lilley M.D. 2004. CO2 and ^{3}He in hydrothermal plumes: implications for mid-ocean ridge CO2 flux. Earth and Planetary Science Letters 226 (2004) 449 – 464

Rudnicki M.D and Elderfield H.1992. A chemical model of the buoyant and neutrally buoyant plume above the TAG vent field, 26 degrees N, Mid-Atlantic Ridge. Geochimica et Cosmochimica Acta Vol. 57, pp. 2939-2957

Rudnicki M.D, James R.H, Elderfield H.1994. Near-field variability of the TAG non-buoyant plume, 26N Mid-Atlantic Ridge. Earth Planet. Sci. Lett. 127 I-IO.

Snow, J., W. Jokat, E. Hellebrand, R. Mühe, and Shipboard Scientific Party (2001), Magmatic and hydrothermal activity in Lena Trough, Arctic Ocean, *Eos Trans. AGU*, *82*(17), 193–197.

References

Speer K.G and Helfrich K.R. 1995. Hydrothermal plumes: a review of flow and fluxes. From PARSON, L. M., WALKER, C. L. & DIXON, D. R. (eds), 1995, Hydrotherrnal Vents and Processes, Geological Society Soecial Publication No. 87, 37.3--385.

Speer K.G and Rona P.A. 1989. A model of an Atlantic and Pacific Hydrothermal plume. GeophysR.es. 94, 6213-6220.

Stein C. A and Stein S. 1994. Constraints on Hydrothermal Heat flux through the Oceanic Lithosphere from Global Heat Flow. Journal of Geophysical research, Vol. 99, no.B2, pages 3081-3095.

Swith J.H. 1986. The Arctic Waters. Edited by Hurdle B.G. The Nordic Seas. 129-153.

Tivey M. K. 2007. Generation of seafloor hydrothermal vent fluids and associated mineral deposits. Oceanography, Volume 20, Number 1.

Urich T, Lanzen A, Stokke R, Pedersen R. B, Bayer C, Thorseth I. H, Schleper C, Steen I. H, Overas L. 2013. Integrated meta-omics reveals controlling factors of microbial community structure and functioning in deep-sea sediments associated with diffuse hydrothermal venting. Environ. Microbiol. (in press).

Von Damm K. L, Parker C. M, Zierenberg R. A, Lilley M.D. 2005. The Escabana Trough, Gorda Ridge hydrothermal system: Temporal stability and subseafloor complexity. Geochemica Et Cosmochimica Acta, 69(21), 4971-4984.

Von Damm K.L, Bray A.M, Buttermore L.G, Oosting S.E. 1998. The geochemical controls on vent fluids from the Lucky Strike vent field, Mid-Atlantic Ridge. Earth and Planetary Science Letters 160, 521–536.

Von Damm K.L and Lilley M.D. 2004. Diffuse flow hydrothermal fluids from 9°50'N East Pacific Rise: Origin, Evolution and Biogeochemical Controls.

Wilson C, Charlou J.L, Ludford E, Klinkhammer G, Chin C, Bougault H, German C, Speer K, Palmer M. 1996. Hydrothermal anomalies in the Lucky Strike segment on the Mid-Atlantic Ridge (37'17'N). Earth and Planetary Science Letters 142, 467-477

Welhan J.A. 1988. Origins of methane in hydrothermal systems. Chemical Geology, 71, 183-198

Young, C. and Lupton, J.E. 1983. An ultra-tight fluid sampling system using cold-welded copper tubing. EOS, American geophysical union Transactions, 64, 735.

Östlund H. G. 1982. The Residence Time of the Freshwater Component in the Arctic Ocean. JOURNAL OF GEOPHYSICAL RESEARCH, VOL. 87, NO. C3, PAGES 2035-2043.

References

9 Appendix

9.1 Appendix 1- The Loki's Castle Vent Field

All CTD casts from the Loki's Castle area in the period 2007-2009. The year, sample, coordinates, depth, concentration of H_2, CH_4 and ^3He are given for each cast.

year	site	CTD- btl	coordinates	depth	H_2 (nM)	CH_4 (nM)	^3He (fM)	Delta ^3He (%)
2007	Loki`s Castle	GS07-CTD02-1	71°17.811'N,5°46.384'W	393	5.9	6.0		
2007	Loki`s Castle	GS07-CTD02-2	71°17.811'N, 5°46.384'W	393	6.3	8.2		
2007	Loki`s Castle	GS07-CTD02-3	71°17.811'N, 5°46.384'W	361	3.8	5.8		
2007	Loki`s Castle	GS07-CTD02-4	71°17.811'N, 5°46.384'W	361	6.3	8.7		
2007	Loki`s Castle	GS07-CTD02-5	71°17.811'N, 5°46.384'W	310	5.3	6.0		
2007	Loki`s Castle	GS07-CTD02-6	71°17.811'N, 5°46.384'W	310	3.0	6.2		
2007	Loki`s Castle	GS07-CTD02-7	71°17.811'N, 5°46.384'W	220	3.9	5.0		
2007	Loki`s Castle	GS07-CTD02-8	71°17.811'N, 5°46.384'W	220	1.8	6.0		
2007	Loki`s Castle	GS07-CTD03-3	73°35.45'N, 8°05.950'E	2271	0.6	3.3		
2007	Loki`s Castle	GS07-CTD03-4	73°35.45'N, 8°05.950'E	2170	0.7	3.8		
2007	Loki`s Castle	GS07-CTD03-5	73°35.45'N, 8°05.950'E	2070	0.8	3.2		
2007	Loki`s Castle	GS07-CTD03-6	73°35.45'N, 8°05.950'E	1870	0.5	1.4		
2007	Loki`s Castle	GS07-CTD03-10	73°35.45'N, 8°05.950'E	1570	0.4	1.6		
2007	Loki`s Castle	GS07-CTD03-11	73°35.45'N, 8°05.950'E	1470	0.8	1.6		
2007	Loki`s Castle	GS07-CTD04-11	73°35.23'N, 8°08.62'E	1 348	0.83	1.63	2.70	5.02
2007	Loki`s Castle	GS07-CTD04-10	73°35.23'N, 8°08.62'E	1 448	3.85	1.77	2.72	5.45
2007	Loki`s Castle	GS07-CTD04-8	73°35.23'N, 8°08.62'E	1 750	1.27	1.57	2.74	6.48
2007	Loki`s Castle	GS07-CTD04-7	73°35.23'N, 8°08.62'E	1 850	1.47	1.44	2.72	6.42
2007	Loki`s Castle	GS07-CTD04-6	73°35.23'N, 8°08.62'E	2 050	1.02	1.57	2.74	5.87
2007	Loki`s Castle	GS07-CTD04-5	73°35.23'N, 8°08.62'E	2 150	0.98	2.45	2.73	6.70
2007	Loki`s Castle	GS07-CTD04-2	73°35.23'N, 8°08.62'E	2 249	1.88	3.10	2.74	6.54
2007	Loki`s Castle	GS07-CTD04-1	73°35.23'N, 8°08.62'E	2 348	3.10	3.13	2.76	6.67
2007	Loki`s Castle	GS07-CTD05-1	73°34.41'N, 8°11.71'E	2340	2.9	4.1		
2007	Loki`s Castle	GS07-CTD05-3	73°34.41'N, 8°11.71'E	2140	0.1	3.5		
2007	Loki`s Castle	GS07-CTD05-4	73°34.41'N, 8°11.71'E	2040	0.8	0.8		
2007	Loki`s Castle	GS07-CTD05-5	73°34.41'N, 8°11.71'E	1940	2.1	1.1		

Appendix

year	site	CTD- btl	coordinates	depth	H_2 (nM)	CH_4 (nM)	^3He (fM)	Delta ^3He (%)
2007	Loki`s Castle	GS07-CTD06-8	73°33.50'N, 8°16.30'E	1 750	0.99	1.63	2.72	5.89
2007	Loki`s Castle	GS07-CTD06-5	73°33.50'N, 8°16.30'E	2 250	22.40	99.08	2.8	8.97
2007	Loki`s Castle	GS07-CTD06-3	73°33.50'N, 8°16.30'E	2 505	5.27	18.87	2.75	7.13
2007	Loki`s Castle	GS07-CTD06-1	73°33.50'N, 8°16.30'E	2 800	4.16	4.06	2.74	6.86
2007	Loki`s Castle	GS07-CTD07-3	73°31.54'N, 8°14.29'E	2249	2.4	2.9		
2007	Loki`s Castle	GS07-CTD07-4	73°31.54'N, 8°14.29'E	2650	4.2	2.2		
2007	Loki`s Castle	GS07-CTD07-5	73°31.54'N, 8°14.29'E	2240	4.7	2.5		
2007	Loki`s Castle	GS07-CTD07-6	73°31.54'N, 8°14.29'E	2199	1.8	3.0		
2007	Loki`s Castle	GS07-CTD08-1	73°34.49'N, 8°17.40'E	2780	1.1	2.7		
2007	Loki`s Castle	GS07-CTD08-3	73°34.49'N, 8°17.40'E	2498	1.6	2.1		
2007	Loki`s Castle	GS07-CTD08-5	73°34.49'N, 8°17.40'E	2181	2.4	2.4		
2007	Loki`s Castle	GS07-CTD08-7	73°34.49'N, 8°17.40'E	1995	1.0	1.1		
2007	Loki`s Castle	GS07-CTD09-1	73°33.18'N, 8°16.15'E	2799	3.0	5.5		
2007	Loki`s Castle	GS07-CTD09-3	73°33.18'N, 8°16.15'E	2513	2.6	9.7		
2007	Loki`s Castle	GS07-CTD09-4	73°33.18'N, 8°16.15'E	2506	2.4	5.9		
2007	Loki`s Castle	GS07-CTD09-5	73°33.18'N, 8°16.15'E	2369	2.5	5.6		
2007	Loki`s Castle	GS07-CTD09-6	73°33.18'N, 8°16.15'E	2352	1.9	10.4		
2007	Loki`s Castle	GS07-CTD09-7	73°33.18'N, 8°16.15'E	2281	50.0	174.7		
2007	Loki`s Castle	GS07-CTD18-13	73°33.12'N, 8°16.82'E	1 700	1.09	1.15	2.73	6.31
2007	Loki`s Castle	GS07-CTD18-11	73°33.12'N, 8°16.82'E	1 800	1.50	1.93	2.75	6.46
2007	Loki`s Castle	GS07-CTD18-9	73°33.12'N, 8°16.82'E	1 886	1.75	0.94	2.73	5.80
2007	Loki`s Castle	GS07-CTD18-7	73°33.12'N, 8°16.82'E	1 979	1.96	1.10	2.77	6.55
2007	Loki`s Castle	GS07-CTD18-5	73°33.12'N, 8°16.82'E	2 300	0.53	0.82	2.74	6.37
2007	Loki`s Castle	GS07-CTD18-3	73°33.12'N, 8°16.82'E	2 404	1.48	1.06	2.74	6.08
2007	Loki`s Castle	GS07-CTD18-1	73°33.12'N, 8°16.82'E	2 750	4.73	1.10	2.77	6.65
2007	Loki`s Castle	GS07-CTD20-1	73°33.51'N, 8°16.37'E	2800	0.4	3.1		
2007	Loki`s Castle	GS07-CTD20-2	73°33.51'N, 8°16.37'E	2500	2.5	16.0		
2007	Loki`s Castle	GS07-CTD20-3	73°33.51'N, 8°16.37'E	2200	0.3	1.1		
2007	Loki`s Castle	GS07-CTD20-4	73°33.51'N, 8°16.37'E	1900	0.7	0.6		
2007	Loki`s Castle	GS07-CTD21-1	73°33.63'N, 8°15.54'E	2831	5.3	3.5		
2007	Loki`s Castle	GS07-CTD21-2	73°33.63'N, 8°15.54'E	2396	2.1	4.8		
2007	Loki`s Castle	GS07-CTD21-3	73°33.63'N, 8°15.54'E	2130	36.1	117.8		
2007	Loki`s Castle	GS07-CTD21-4	73°33.63'N, 8°15.54'E	2033	54.7	168.3		
2007	Loki`s Castle	GS07-CTD21-5	73°33.63'N, 8°15.54'E	1876	1.0	1.3		
2007	Loki`s Castle	GS07-CTD22-1	73°33.79'N, 8°16.31'E	2881	4.1	3.7		

Appendix

year	site	CTD- btl	coordinates	depth	H_2 (nM)	CH_4 (nM)	^3He (fM)	Delta ^3He (%)
2007	Loki`s Castle	GS07-CTD22-2	73°33.79'N, 8°16.31'E	2384	0.7	1.2		
2007	Loki`s Castle	GS07-CTD22-3	73°33.79'N, 8°16.31'E	1162	0.8	2.4		
2007	Loki`s Castle	GS07-CTD24-1	73°33.14'N, 8°15.29'E	2750	1.5	2.1		
2007	Loki`s Castle	GS07-CTD24-3	73°33.14'N, 8°15.29'E	2312	4.9	35.8		
2007	Loki`s Castle	GS07-CTD24-5	73°33.14'N, 8°15.29'E	2066	26.6	86.4		
2007	Loki`s Castle	GS07-CTD24-7	73°33.14'N, 8°15.29'E	1735	0.7	1.2		
2007	Loki`s Castle	GS07-CTD25-1	73°33.38'N, 8°15.42'E	2770	3.6	4.2		
2007	Loki`s Castle	GS07-CTD25-2	73°33.38'N, 8°15.42'E	2401	4.7	30.4		
2007	Loki`s Castle	GS07-CTD25-3	73°33.38'N, 8°15.42'E	2130	7.1	31.0		
2007	Loki`s Castle	GS07-CTD25-4	73°33.38'N, 8°15.42'E	2030	0.6	1.1		
2007	Loki`s Castle	GS07-CTD25-5	73°33.38'N, 8°15.42'E	1875	0.4	0.8		
2007	Loki`s Castle	GS07-CTD26-1	73°33.54'N, 8°15.49'E	2819	0.7	1.4		
2007	Loki`s Castle	GS07-CTD26-2	73°33.54'N, 8°15.49'E	2398	2.2	1.0		
2007	Loki`s Castle	GS07-CTD26-3	73°33.54'N, 8°15.49'E	2128	0.3	0.7		
2007	Loki`s Castle	GS07-CTD26-4	73°33.54'N, 8°15.49'E	2028	0.2	0.7		
2007	Loki`s Castle	GS07-CTD26-5	73°33.54'N, 8°15.49'E	1874	0.7	0.8		
2007	Loki`s Castle	GS07-CTD26-?	73°33.54'N, 8°15.49'E		4.2	36.3		
2007	Loki`s Castle	GS07-CTD27l	73°33.74'N, 8°15.89'E	2300	4.5	37.0		
2007	Loki`s Castle	GS07-CTD27l	73°33.74'N, 8°15.89'E	2080	1.2	1.2		
2007	Loki`s Castle	GS07-CTD27l	73°33.74'N, 8°15.89'E	2030	2.4	1.0		
2007	Loki`s Castle	GS07-CTD28-1	73°33.28'N, 8°15.80'E	2770	1.2	6.0		
2007	Loki`s Castle	GS07-CTD28-2	73°33.28'N, 8°15.80'E	2438	0.2	3.1		
2007	Loki`s Castle	GS07-CTD28-3	73°33.28'N, 8°15.80'E	2263	0.9	5.9		
2007	Loki`s Castle	GS07-CTD28-5	73°33.28'N, 8°15.80'E	1906	0.5	1.2		
2007	Loki`s Castle	GS07-CTD29a-1	73°33.152'N, 8°15.82'E	2798	3.2	3.5		
2007	Loki`s Castle	GS07-CTD29a-2	73°33.152'N, 8°15.82'E	2761	2.6	3.4		
2007	Loki`s Castle	GS07-CTD29a-3	73°33.152'N, 8°15.82'E	2748	3.5	4.3		
2007	Loki`s Castle	GS07-CTD29a-4	73°33.152'N, 8°15.82'E	2140	0.5	2.3		
2007	Loki`s Castle	GS07-CTD29a-5	73°33.152'N, 8°15.82'E	2020	52.7	266.4		
2007	Loki`s Castle	GS07-CTD29a-6	73°33.152'N, 8°15.82'E	1815	4.5	1.3		
2007	Loki`s Castle	GS07-CTD29a-7	73°33.152'N, 8°15.82'E	871	1.2	2.5		
2007	Loki`s Castle	GS07-CTD29b-1	73°33.152'N, 8°15.82'E	2831	4.4	5.9		
2007	Loki`s Castle	GS07-CTD29b-2	73°33.152'N, 8°15.82'E	2712	0.6	2.4		
2007	Loki`s Castle	GS07-CTD29b-3	73°33.152'N, 8°15.82'E	2599	0.8	1.8		
2007	Loki`s Castle	GS07-CTD29b-5	73°33.152'N, 8°15.82'E	2400	1.5	2.0		

Appendix

year	site	CTD- btl	coordinates	depth	H_2 (nM)	CH_4 (nM)	^3He (fM)	Delta ^3He (%)
2007	Loki`s Castle	GS07-CTD29b-6	73°33.152'N, 8°15.82'E	2298	2.0	32.1		
2007	Loki`s Castle	GS07-CTD29b-7	73°33.152'N, 8°15.82'E	2193	1.9	2.0		
2007	Loki`s Castle	GS07-CTD29b-8	73°33.152'N, 8°15.82'E	2094	0.6	1.5		
2007	Loki`s Castle	GS07-CTD29b-9	73°33.152'N, 8°15.82'E	2000	38.2	192.9		
2007	Loki`s Castle	GS07-CTD29b-10	73°33.152'N, 8°15.82'E	1899	0.9	1.4		
2007	Loki`s Castle	GS07-CTD29b-11	73°33.152'N, 8°15.82'E	1799	0.8	1.7		
2007	Loki`s Castle	GS07-CTD29b	73°33.152'N, 8°15.82'E	1699.0	1.1	1.0		
2007	Loki`s Castle	GS07-CTD30-1	73°32.77'N, 8°13.93'E	2680	1.3	1.3		
2007	Loki`s Castle	GS07-CTD30-8	73°32.77'N, 8°13.93'E	1978	1.4	0.6		
2007	Loki`s Castle	GS07-CTD30-12	73°32.77'N, 8°13.93'E	1020	1.7	1.9		
2007	Loki`s Castle	GS07-CTD30-6	73°32.77'N, 8°13.93'E	2179	0.6	4.0		
2007	Loki`s Castle	GS07-CTD31-1	73°32.30'N, 8°13.02'E	2600	1.1	1.5		
2007	Loki`s Castle	GS07-CTD31-2	73°32.30'N, 8°13.02'E	2200	0.3	1.3		
2007	Loki`s Castle	GS07-CTD31-3	73°32.30'N, 8°13.02'E	2000	0.7	0.8		
2007	Loki`s Castle	GS07-CTD32-1	73°33.10'N, 8°14.52'E	2880	1.7	1.9		
2007	Loki`s Castle	GS07-CTD32-2	73°33.10'N, 8°14.52'E	2649	3.7	1.9		
2007	Loki`s Castle	GS07-CTD32-3	73°33.10'N, 8°14.52'E	2449	0.2	0.7		
2007	Loki`s Castle	GS07-CTD32-4	73°33.10'N, 8°14.52'E	2248	0.2	1.6		
2007	Loki`s Castle	GS07-CTD32-5	73°33.10'N, 8°14.52'E	2198	0.9	0.8		
2007	Loki`s Castle	GS07-CTD32-6	73°33.10'N, 8°14.52'E	2098	1.3	0.9		
2007	Loki`s Castle	GS07-CTD32-7	73°33.10'N, 8°14.52'E	2049	0.9	1.3		
2007	Loki`s Castle	GS07-CTD32-8	73°33.10'N, 8°14.52'E	1990	1.5	0.9		
2007	Loki`s Castle	GS07-CTD32-9	73°33.10'N, 8°14.52'E	1948	0.9	1.9		
2007	Loki`s Castle	GS07-CTD32-10	73°33.10'N, 8°14.52'E	1899	0.9	0.8		
2007	Loki`s Castle	GS07-CTD32-11	73°33.10'N, 8°14.52'E	1798	0.6	1.4		
2007	Loki`s Castle	GS07-CTD32-12	73°33.10'N, 8°14.52'E	1498	1.2	1.2		

2007	Loki`s Castle	GS07-CTD34-12	73°31.00'N, 8°17.65'E	399	0.18	1.89	2.54	0.49
2007	Loki`s Castle	GS07-CTD34-11	73°31.00'N, 8°17.65'E	599	0.20	1.55	2.6	1.64
2007	Loki`s Castle	GS07-CTD34-10	73°31.00'N, 8°17.65'E	798	1.08	1.76	2.68	5.19
2007	Loki`s Castle	GS07-CTD34-9	73°31.00'N, 8°17.65'E	999	0.68	1.22	2.7	5.94
2007	Loki`s Castle	GS07-CTD34-8	73°31.00'N, 8°17.65'E	1 199	0.19	1.07	2.74	6.02
2007	Loki`s Castle	GS07-CTD34-7	73°31.00'N, 8°17.65'E	1 399	1.92	1.02	2.71	6.09
2007	Loki`s Castle	GS07-CTD34-6	73°31.00'N, 8°17.65'E	1 598	0.18	0.66	2.74	6.44
2007	Loki`s Castle	GS07-CTD34-5	73°31.00'N, 8°17.65'E	1 799	0.96	0.99	2.72	6.67
2007	Loki`s Castle	GS07-CTD34-4	73°31.00'N, 8°17.65'E	1 998	0.18	1.59	2.73	6.43
2007	Loki`s Castle	GS07-CTD34-3	73°31.00'N, 8°17.65'E	2 198	0.00	1.32	2.75	6.57
2007	Loki`s Castle	GS07-CTD34-1	73°31.00'N, 8°17.65'E	2 600	3.36	0.97	2.74	6.59

Appendix

year	site	CTD- btl	coordinates	depth	H_2 (nM)	CH_4 (nM)	^3He (fM)	Delta ^3He (%)
2007	Loki`s Castle	GS07-CTD35-12	73°47.79'N, 7°43.85'E	800	0.41	3.57	2.57	1.47
2007	Loki`s Castle	GS07-CTD35-11	73°47.79'N, 7°43.85'E	900	0.63	2.44	2.55	0.91
2007	Loki`s Castle	GS07-CTD35-10	73°47.79'N, 7°43.85'E	998	1.22	2.18	2.56	1.09
2007	Loki`s Castle	GS07-CTD35-9	73°47.79'N, 7°43.85'E	1 100	0.73	2.58	2.58	1.80
2007	Loki`s Castle	GS07-CTD35-8	73°47.79'N, 7°43.85'E	1 200	1.17	1.64	2.64	3.26
2007	Loki`s Castle	GS07-CTD35-7	73°47.79'N, 7°43.85'E	1 299	0.46	1.45	2.66	4.16
2007	Loki`s Castle	GS07-CTD35-6	73°47.79'N, 7°43.85'E	1 399	0.94	1.69	2.69	4.80
2007	Loki`s Castle	GS07-CTD35-5	73°47.79'N, 7°43.85'E	1 500	1.24	1.06	2.74	5.82
2007	Loki`s Castle	GS07-CTD35-4	73°47.79'N, 7°43.85'E	1 599	0.66	0.71	2.71	5.70
2007	Loki`s Castle	GS07-CTD35-2	73°47.79'N, 7°43.85'E	1 801	0.56	0.86	2.74	6.44
2007	Loki`s Castle	GS07-CTD35-1	73°47.79'N, 7°43.85'E	1 900	2.46	0.75	2.73	6.33
2007	Loki`s Castle	GS07-CTD36-12	73°54.27'N, 8°38.16'E	598	1.92	2.33	2.61	2.57
2007	Loki`s Castle	GS07-CTD36-11	73°54.27'N, 8°38.16'E	898	1.55	1.62	2.69	4.01
2007	Loki`s Castle	GS07-CTD36-9	73°54.27'N, 8°38.16'E	1 499	1.39	0.96	2.71	5.72
2007	Loki`s Castle	GS07-CTD36-8	73°54.27'N, 8°38.16'E	1 799	5.36	1.65	2.73	6.71
2007	Loki`s Castle	GS07-CTD36-7	73°54.27'N, 8°38.16'E	2 099	3.30	0.73	2.75	6.85
2007	Loki`s Castle	GS07-CTD36-6	73°54.27'N, 8°38.16'E	2 400	2.51	3.17	2.76	6.51
2007	Loki`s Castle	GS07-CTD36-5	73°54.27'N, 8°38.16'E	2 699	3.30	1.96	2.75	5.24
2007	Loki`s Castle	GS07-CTD36-4	73°54.27'N, 8°38.16'E	2 999	2.54	2.08	2.74	6.67
2007	Loki`s Castle	GS07-CTD36-3	73°54.27'N, 8°38.16'E	3 198	3.02	1.66	bad	bad
2007	Loki`s Castle	GS07-CTD36-2	73°54.27'N, 8°38.16'E	3 274	1.40	1.43	2.77	6.99
2007	Loki`s Castle	GS07-CTD36-1	73°54.27'N, 8°38.16'E	3 304	1.43	1.25	2.77	6.86
2007	Loki`s Castle	GS07-CTD37-12	73°47.38'N, 8°31.52'E	398	1.44	3.10	2.54	-0.41
2007	Loki`s Castle	GS07-CTD37-11	73°47.38'N, 8°31.52'E	699	0.34	2.73	2.59	1.09
2007	Loki`s Castle	GS07-CTD37-9	73°47.38'N, 8°31.52'E	1 299	0.99	2.02	2.64	3.11
2007	Loki`s Castle	GS07-CTD37-8	73°47.38'N, 8°31.52'E	1 600	1.01	1.51	2.73	5.60
2007	Loki`s Castle	GS07-CTD37-7	73°47.38'N, 8°31.52'E	1 899	1.01	1.33	2.74	6.54
2007	Loki`s Castle	GS07-CTD37-6	73°47.38'N, 8°31.52'E	2 201	2.01	0.94	bad	bad
2007	Loki`s Castle	GS07-CTD37-5	73°47.38'N, 8°31.52'E	2 499	1.70	3.48	2.74	6.38
2007	Loki`s Castle	GS07-CTD37-4	73°47.38'N, 8°31.52'E	2 799	2.42	7.23	2.76	7.22
2007	Loki`s Castle	GS07-CTD37-3	73°47.38'N, 8°31.52'E	3 099	1.54	4.93	2.74	6.51
2007	Loki`s Castle	GS07-CTD37-2	73°47.38'N, 8°31.52'E	3 132	0.00	4.72	2.74	6.82
2007	Loki`s Castle	GS07-CTD37-1	73°47.38'N, 8°31.52'E	3 171	3.98	5.22	2.74	6.53
2007	Loki`s Castle	GS07-CTD38-12	73°42.24'N, 8°21.57'E	399	1.64	3.11	2.51	0.58
2007	Loki`s Castle	GS07-CTD38-11	73°42.24'N, 8°21.57'E	699	1.36	2.79	2.55	1.05
2007	Loki`s Castle	GS07-CTD38-9	73°42.24'N, 8°21.57'E	1 300	0.64	1.78	2.66	4.21
2007	Loki`s Castle	GS07-CTD38-8	73°42.24'N, 8°21.57'E	1 599	1.36	1.50	2.68	4.79
2007	Loki`s Castle	GS07-CTD38-7	73°42.24'N, 8°21.57'E	1 899	0.00	1.34	2.7	6.00
2007	Loki`s Castle	GS07-CTD38-6	73°42.24'N, 8°21.57'E	2 199	0.97	0.98		bad

Appendix

year	site	CTD- btl	coordinates	depth	H_2 (nM)	CH_4 (nM)	^3He (fM)	Delta ^3He (%)
2007	Loki`s Castle	GS07-CTD38-5	73°42.24'N, 8°21.57'E	2 499	1.61	0.76	2.75	6.67
2007	Loki`s Castle	GS07-CTD38-4	73°42.24'N, 8°21.57'E	2 800	1.41	3.25	2.75	6.91
2007	Loki`s Castle	GS07-CTD38-3	73°42.24'N, 8°21.57'E	3 099	1.24	4.60	2.76	7.08
2007	Loki`s Castle	GS07-CTD38-2	73°42.24'N, 8°21.57'E	3 150	1.87	4.63	2.76	6.65
2007	Loki`s Castle	GS07-CTD38-1	73°42.24'N, 8°21.57'E	3 200	3.88	5.38	2.76	7.02
2007	Loki`s Castle	GS07-CTD39.-1	73°36.28'N, 8°21.04'E	2830	5.1	2.6		
2007	Loki`s Castle	GS07-CTD39.-3	73°36.28'N, 8°21.04'E	2399	1.2	1.8		
2007	Loki`s Castle	GS07-CTD39.-4	73°36.28'N, 8°21.04'E	2338	0.9	1.7		
2007	Loki`s Castle	GS07-CTD39.-5	73°36.28'N, 8°21.04'E	2279	2.1	1.2		
2007	Loki`s Castle	GS07-CTD39.-6	73°36.28'N, 8°21.04'E	2220		1.0		
2007	Loki`s Castle	GS07-CTD39.-7	73°36.28'N, 8°21.04'E	2159	2.6	1.6		
2007	Loki`s Castle	GS07-CTD39.-8	73°36.28'N, 8°21.04'E	2099	0.8	2.3		
2007	Loki`s Castle	GS07-CTD39.-9	73°36.28'N, 8°21.04'E	2038	2.7	5.6		
2007	Loki`s Castle	GS07-CTD39.-10	73°36.28'N, 8°21.04'E	1978	1.5	12.0		
2007	Loki`s Castle	GS07-CTD39.-11	73°36.28'N, 8°21.04'E	1919	1.5	17.7		
2007	Loki`s Castle	GS07-CTD39.-12	73°36.28'N, 8°21.04'E	1860	1.8	1.5		
2007	Loki`s Castle	GS07-CTD40.-1	73°34.44'N, 8°17.54'E	2800	1.6	1.3		
2007	Loki`s Castle	GS07-CTD40.-2	73°34.44'N, 8°17.54'E	2599	3.2	1.7		
2007	Loki`s Castle	GS07-CTD40.-3	73°34.44'N, 8°17.54'E	2399	1.4	1.0		
2007	Loki`s Castle	GS07-CTD40.-4	73°34.44'N, 8°17.54'E	2339	0.9	1.0		
2007	Loki`s Castle	GS07-CTD40.-5	73°34.44'N, 8°17.54'E	2279	0.7	0.9		
2007	Loki`s Castle	GS07-CTD40.-6	73°34.44'N, 8°17.54'E	2219	0.7	0.8		
2007	Loki`s Castle	GS07-CTD40.-7	73°34.44'N, 8°17.54'E	2159	1.0	0.9		
2007	Loki`s Castle	GS07-CTD40.-8	73°34.44'N, 8°17.54'E	2099	0.8	0.4		
2007	Loki`s Castle	GS07-CTD40.-9	73°34.44'N, 8°17.54'E	2018	2.2	0.6		
2007	Loki`s Castle	GS07-CTD40.-10	73°34.44'N, 8°17.54'E	1979	0.9	0.5		
2007	Loki`s Castle	GS07-CTD40.-11	73°34.44'N, 8°17.54'E	1918	0.9	0.7		
2007	Loki`s Castle	GS07-CTD40.-12	73°34.44'N, 8°17.54'E	1859	0.9	0.8		
2007	Loki`s Castle	GS07-CTD41.-1	73°33.13'N, 8°16.03'E	2801	1.1	3.9		
2007	Loki`s Castle	GS07-CTD41.-2	73°33.13'N, 8°16.03'E	2699	1.2	3.6		
2007	Loki`s Castle	GS07-CTD41.-3	73°33.13'N, 8°16.03'E	2599	1.2	1.9		
2007	Loki`s Castle	GS07-CTD41.-4	73°33.13'N, 8°16.03'E	2539	1.6	2.5		
2007	Loki`s Castle	GS07-CTD41.-5	73°33.13'N, 8°16.03'E	2399	1.5	1.7		
2007	Loki`s Castle	GS07-CTD41.-6	73°33.13'N, 8°16.03'E	2292	1.4	0.8		
2007	Loki`s Castle	GS07-CTD41.7	73°33.13'N, 8°16.03'E	2199	1.8	1.6		
2007	Loki`s Castle	GS07-CTD41.-8	73°33.13'N, 8°16.03'E	2099	1.0	0.8		
2007	Loki`s Castle	GS07-CTD41.-9	73°33.13'N, 8°16.03'E	1999	1.2	0.9		
2007	Loki`s Castle	GS07-CTD41.-10	73°33.13'N, 8°16.03'E	1899	1.2	1.0		
2007	Loki`s Castle	GS07-CTD41.-11	73°33.13'N, 8°16.03'E	1800	1.0	10.4		

Appendix

year	site	CTD- btl	coordinates	depth	H_2 (nM)	CH_4 (nM)	^{3}He (fM)	Delta ^{3}He (%)
2007	Loki`s Castle	GS07-CTD41.-12	73°33.13'N, 8°16.03'E	1699	0.8	1.2		
2007	Loki`s Castle	GS07-CTD42-10	73°28.58'N, 8°4.06'E	288	1.3	2.0	2.5	0.4
2007	Loki`s Castle	GS07-CTD42-9	73°28.58'N, 8°4.06'E	600	1.2	1.7	2.6	4.4
2007	Loki`s Castle	GS07-CTD42-8	73°28.58'N, 8°4.06'E	900	2.3	1.0	2.7	5.5
2007	Loki`s Castle	GS07-CTD42-7	73°28.58'N, 8°4.06'E	1 199	2.2	0.9	2.7	5.3
2007	Loki`s Castle	GS07-CTD42-6	73°28.58'N, 8°4.06'E	1 499	0.0	0.0	2.7	5.9
2007	Loki`s Castle	GS07-CTD42-5	73°28.58'N, 8°4.06'E	1 799	1.2	1.0	2.7	6.2
2007	Loki`s Castle	GS07-CTD42-4	73°28.58'N, 8°4.06'E	2 098	1.1	1.1	2.7	5.9
2007	Loki`s Castle	GS07-CTD42-3	73°28.58'N, 8°4.06'E	2 399	2.5	0.9	2.7	6.5
2007	Loki`s Castle	GS07-CTD42-2	73°28.58'N, 8°4.06'E	2 700	0.8	0.7	2.8	6.9
2007	Loki`s Castle	GS07-CTD42-1	73°28.58'N, 8°4.06'E	2 800	1.5	0.9	2.8	6.8
2007	Loki`s Castle	GS07-CTD43-12	73°25.29'N, 7°44.06'E	298	0.8	2.8	2.5	-0.1
2007	Loki`s Castle	GS07-CTD43-11	73°25.29'N, 7°44.06'E	599	1.5	1.8	2.7	3.8
2007	Loki`s Castle	GS07-CTD43-10	73°25.29'N, 7°44.06'E	899	1.1	1.7	2.7	4.6
2007	Loki`s Castle	GS07-CTD43-9	73°25.29'N, 7°44.06'E	1 200	1.7	1.0	2.7	5.5
2007	Loki`s Castle	GS07-CTD43-8	73°25.29'N, 7°44.06'E	1 499	2.0	1.0	2.7	5.6
2007	Loki`s Castle	GS07-CTD43-7	73°25.29'N, 7°44.06'E	1 799	1.9	1.3		6.0
2007	Loki`s Castle	GS07-CTD43-6	73°25.29'N, 7°44.06'E	2 099	2.3	3.0		bad
2007	Loki`s Castle	GS07-CTD43-5	73°25.29'N, 7°44.06'E	2 399	1.6	1.2	2.8	6.9
2007	Loki`s Castle	GS07-CTD43-4	73°25.29'N, 7°44.06'E	2 699	0.2	0.7	2.8	6.8
2007	Loki`s Castle	GS07-CTD43-3	73°25.29'N, 7°44.06'E	2 999	0.7	1.1		7.0
2007	Loki`s Castle	GS07-CTD43-2	73°25.29'N, 7°44.06'E	3 099	0.7	1.0	2.8	6.7
2007	Loki`s Castle	GS07-CTD43-1	73°25.29'N, 7°44.06'E	3 180	2.0	1.1	2.8	6.9
2008	Loki`s Castle	GS08A-CTD1-11	73°33.116'N,8°15.837'E	1 849	1.5	1.5		
2008	Loki`s Castle	GS08A-CTD1-10	73°33.116'N 8°15.837'E	2 031	1.5	1.8		
2008	Loki`s Castle	GS08A-CTD1-9	73°33.116'N 8°15.837'E	2 103	1.0	1.8	2.8	6.8
2008	Loki`s Castle	GS08A-CTD1-8	73°33.116'N,8°15.837'E	2 202			2.7	6.5
2008	Loki`s Castle	GS08A-CTD1-7	73°33.116'N,8°15.837'E	2 301	0.9	1.8	2.7	6.3
2008	Loki`s Castle	GS08A-CTD1-6	73°33.116'N,8°15.837'E	2 385	2.6	1.4		
2008	Loki`s Castle	GS08A-CTD1-5	73°33.116'N,8°15.837'E	2 474	1.0	0.9	2.8	7.1
2008	Loki`s Castle	GS08A-CTD1-4	73°33.116'N,8°15.837'E	2 583	2.2	1.3		
2008	Loki`s Castle	GS08A-CTD1-3	73°33.116'N,8°15.837'E	2 682	4.5	1.3	2.7	6.7
2008	Loki`s Castle	GS08A-CTD1-2	73°33.116'N,8°15.837'E	2 772	1.6	1.5	2.7	6.5
2008	Loki`s Castle	GS08A-CTD1-1	73°33.116'N,8°15.837'E	2 831	1.5	1.5	2.7	6.4
2008	Loki`s Castle	GS08A-CTD2-12	73°33.280'N, 8°15.828'	1 957	2.0	1.0		
2008	Loki`s Castle	GS08A-CTD2-11	73°33.280'N,8°15.828'E	2 040	1.0	1.1		
2008	Loki`s Castle	GS08A-CTD2-10	73°33.280'N,8°15.828'E	2 155	1.2	1.8		
2008	Loki`s Castle	GS08A-CTD2-9	73°33.280'N,8°15.828'E	2 180				

Appendix

year	site	CTD- btl	coordinates	depth	H_2 (nM)	CH_4 (nM)	^3He (fM)	Delta ^3He (%)
2008	Loki`s Castle	GS08A-CTD2-8	73°33.280'N,8°15.828'E	2 215	3.3	1.4		
2008	Loki`s Castle	GS08A-CTD2-7	73°33.280'N,8°15.828'E	2 268	1.1	1.1		
2008	Loki`s Castle	GS08A-CTD2-6	73°33.280'N,8°15.828'E	2 310	1.1	1.4		
2008	Loki`s Castle	GS08A-CTD2-5	73°33.280'N,8°15.828'E	2 364	1.9	1.2		
2008	Loki`s Castle	GS08A-CTD2-4	73°33.280'N,8°15.828'E	2 434	1.3	3.5		
2008	Loki`s Castle	GS08A-CTD2-3	73°33.280'N,8°15.828'E	2 500	1.3	2.0		
2008	Loki`s Castle	GS08A-CTD2-2	73°33.280'N,8°15.828'E	2 700	1.9	1.4		
2008	Loki`s Castle	GS08A-CTD2-1	73°33.280'N,8°15.828'E	2 801	1.8	1.6		
2008	Loki`s Castle	GS08A-CTD3-9	73°33.461'N,8°15.889'E	2 105	0.8	0.5		
2008	Loki`s Castle	GS08A-CTD3-8	73°33.461'N,8°15.889'E	2 225	0.6	1.1		
2008	Loki`s Castle	GS08A-CTD3-7	73°33.461'N,8°15.889'E	2 342	1.0	1.0		
2008	Loki`s Castle	GS08A-CTD3-6	73°33.461'N,8°15.889'E	2 476	2.0	1.3		
2008	Loki`s Castle	GS08A-CTD3-5	73°33.461'N,8°15.889'E	2 506	0.8	0.9		
2008	Loki`s Castle	GS08A-CTD3-4	73°33.461'N,8°15.889'E	2 578	1.6	1.2		
2008	Loki`s Castle	GS08A-CTD3-3	73°33.461'N,8°15.889'E	2 641	1.4	1.7		
2008	Loki`s Castle	GS08A-CTD3-2	73°33.461'N,8°15.889'E	2 711	1.1	1.3		
2008	Loki`s Castle	GS08A-CTD3-1	73°33.461'N,8°15.889'E	2 800	2.1	1.1		
2008	Loki`s Castle	GS08A-CTD5-5	73°32.526'N,8°00.563'E	2 004	0.8	1.3		
2008	Loki`s Castle	GS08A-CTD5-4	73°32.526'N,8°00.563'E	2 183		bad		
2008	Loki`s Castle	GS08A-CTD5-3	73°32.526'N,8°00.563'E	2 358	17.2	64.5		
2008	Loki`s Castle	GS08A-CTD5-2	73°32.526'N,8°00.563'E	2 522	6.0	18.7		
2008	Loki`s Castle	GS08A-CTD5-1	73°32.526'N,8°00.563'E	2 522	3.7	17.5		
2008	Loki`s Castle	GS08-CTD6	73°31.182'N,7°56.784'E	2 304	0.6	6.1	2.8	7.1
2008	Loki`s Castle	GS08-CTD6	73°31.182'N,7°56.784'E	2 572	1.2	5.8	2.8	8.5
2008	Loki`s Castle	GS08-CTD6	73°31.182'N,7°56.784'E					6.7
2008	Loki`s Castle	GS08-CTD6	73°31.182'N,7°56.784'E				2.7	7.2
2008	Loki`s Castle	GS08-CTD6	73°31.182'N,7°56.784'E				2.7	6.7
2008	Loki`s Castle	GS08-CTD6	73°31.182'N,7°56.784'E				2.8	6.9
2008	Loki`s Castle	GS08-CTD6	73°31.182'N,7°56.784'E				2.7	7.4
2008	Loki`s Castle	GS08-CTD6	73°31.182'N,7°56.784'E				2.7	6.6
2008	Loki`s Castle	GS08-CTD6	73°31.182'N,7°56.784'E				2.8	6.8
2008	Loki`s Castle	GS08-CTD6	73°31.182'N,7°56.784'E				2.7	6.7
2008	Loki`s Castle	GS08-CTD6	73°31.182'N,7°56.784'E				2.7	5.9
2008	Loki`s Castle	GS08A-CTD7-11	73°32.575'N,8°00.070'E	1 774	2.1	1.2		
2008	Loki`s Castle	GS08A-CTD7-10	73°32.575'N,8°00.070'E	1 842	0.8	0.9		
2008	Loki`s Castle	GS08A-CTD7-9	73°32.575'N,8°00.070'E	1 951	1.5	1.0		
2008	Loki`s Castle	GS08A-CTD7-8	73°32.575'N,8°00.070'E	1 996	1.1	1.0		
2008	Loki`s Castle	GS08A-CTD7-7	73°32.575'N,8°00.070'E	2 012	0.8	0.9		

Appendix

year	site	CTD- btl	coordinates	depth	H_2 (nM)	CH_4 (nM)	^3He (fM)	Delta ^3He (%)
2008	Loki`s Castle	GS08A-CTD7-6	73°32.575'N,8°00.070'E	2 092	1.0	1.5		
2008	Loki`s Castle	GS08A-CTD7-5	73°32.575'N,8°00.070'E	2 151	1.0	1.7		
2008	Loki`s Castle	GS08A-CTD7-4	73°32.575'N,8°00.070'E	2 196	1.4	1.8		
2008	Loki`s Castle	GS08A-CTD7-3	73°32.575'N,8°00.070'E	2 353	24.8	97.4		
2008	Loki`s Castle	GS08A-CTD7-2	73°32.575'N,8°00.070'E	2 482	10.2	48.1		
2008	Loki`s Castle	GS08A-CTD7-1	73°32.575'N,8°00.070'E	2 551	3.0	10.5		
2008	Loki`s Castle	GS08A-CTD8-4	73°32.805'N,7°58.575'E	2 064	0.0	0.6		
2008	Loki`s Castle	GS08A-CTD8-3	73°32.805'N,7°58.575'E		0.0			
2008	Loki`s Castle	GS08A-CTD8-2	73°32.805'N,7°58.575'E	2 349	0.0	1.9		
2008	Loki`s Castle	GS08A-CTD8-1	73°32.805'N,7°58.575'E	2 632	0.0	2.6		
2008	Loki`s Castle	GS08A-CTD9-4	73°32.784'N,8°00.313'E	2 027	0.0	1.1		
2008	Loki`s Castle	GS08A-CTD9-2	73°32.784'N,8°00.313'E	2 348	0.0	5.8		
2008	Loki`s Castle	GS08A-CTD9-1	73°32.784'N,8°00.313'E	2 619	0.0	16.6		
2008	Loki`s Castle	GS08A-CTD10-5	73°32.46N, 7°59.69E	1 940	0.4	0.9		
2008	Loki`s Castle	GS08A-CTD10-4	73°32.46N, 7°59.69E	2 038	0.0	0.8		
2008	Loki`s Castle	GS08A-CTD10-2	73°32.46N, 7°59.69E	2 483	0.0	6.2		
2008	Loki`s Castle	GS08A-CTD10-1	73°32.46N, 7°59.69E	2 581	1.0	11.0		
2008	Loki`s Castle	GS08A-CTD11-6	73°32.58N, 7°59.96E	1 840	0.2	0.6		
2008	Loki`s Castle	GS08A-CTD11-5	73°32.58N, 7°59.96E	2 037	0.3	1.1		
2008	Loki`s Castle	GS08A-CTD11-4	73°32.58N, 7°59.96E	2 262	1.1	2.9		
2008	Loki`s Castle	GS08A-CTD11-2	73°32.58N, 7°59.96E	2 400	1.5	16.2		
2008	Loki`s Castle	GS08A-CTD11-1	73°32.58N, 7°59.96E	2 661	0.0	12.3		
2008	Loki`s Castle	GS08A-CTD12	73°32.252'N,8°02.559E	UNKN	2.0	3.0		
2008	Loki`s Castle	GS08A-CTD12-5	73°32.252'N,8°02.559E	1 777	1.0	0.7		
2008	Loki`s Castle	GS08A-CTD12-4	73°32.252'N,8°02.559E	2 142	0.9	0.9		
2008	Loki`s Castle	GS08A-CTD12-2	73°32.252'N,8°02.559E	2 232	1.2	1.3		
2008	Loki`s Castle	GS08A-CTD12-1	73°32.252'N,8°02.559E	2 299	2.9	18.5		
2008	Loki`s Castle	GS08A-CTD13-6	73°32.58'N, 8°00.05'E	1 699	1.0	1.0		
2008	Loki`s Castle	GS08A-CTD13-5	73°32.58'N, 8°00.05'E	1 967	1.1	0.8		
2008	Loki`s Castle	GS08A-CTD13-4	73°32.58'N, 8°00.05'E	2 141	1.2	1.0		
2008	Loki`s Castle	GS08A-CTD13-2	73°32.58'N, 8°00.05'E	2 380	0.7	4.0		
2008	Loki`s Castle	GS08A-CTD13-1	73°32.58'N, 8°00.05'E	2 541	1.2	12.9		
2008	Loki`s Castle	GS08A-CTD15a-1	73°32.56'N, 8°00.21'E	2 570	3.8	19.3		
2008	Loki`s Castle	GS08A-CTD15a-2	73°32.56'N, 8°00.21'E	2 482	2.7	21.6		
2008	Loki`s Castle	GS08A-CTD15a-3	73°32.56'N, 8°00.21'E	2 319	1.3	26.0		

Appendix

year	site	CTD- btl	coordinates	depth	H_2 (nM)	CH_4 (nM)	^3He (fM)	Delta ^3He (%)
2008	Loki`s Castle	GS08A-CTD15a-4	73°32.56'N, 8°00.21'E	2 144	1.6	1.6		
2008	Loki`s Castle	GS08A-CTD15a-5	73°32.56'N, 8°00.21'E	1 970	0.3	1.1		
2008	Loki`s Castle	GS08A-CTD15a-6	73°32.56'N, 8°00.21'E	1 853	0.7	1.2		
2008	Loki`s Castle	GS08A-CTD15b-7	73°32.544'N,7°59.804'E	2 611	2.2	0.0		
2008	Loki`s Castle	GS08A-CTD15b-9	73°32.544'N,7°59.804'E	2 320	1.7	15.8		
2008	Loki`s Castle	GS08A-CTD15b-10	73°32.544'N,7°59.804'E	2 139	1.0	1.3		
2008	Loki`s Castle	GS08A-CTD15b-11	73°32.544'N,7°59.804'E	1 849	2.7	1.3		
2008	Loki`s Castle	GS08A-CTD15c-12	73°32.535'N,7°59.166'E	2 624	1.3	19.6		
2008	Loki`s Castle	GS08A-CTD15c-13	73°32.535'N,7°59.166'E	2 348	3.6	13.6		
2008	Loki`s Castle	GS08A-CTD15c-14	73°32.535'N,7°59.166'E	2 147	3.7	0.0		
2008	Loki`s Castle	GS08A-CTD15c-15	73°32.535'N,7°59.166'E	2 125	1.7	1.0		
2008	Loki`s Castle	GS08A-CTD15c-16	73°32.535'N,7°59.166'E	1 857	1.4	1.0		
2008	Loki`s Castle	GS08A-CTD15d-17	73°32.523'N,7°58.584'E	2 661	1.8	20.5		
2008	Loki`s Castle	GS08A-CTD15d-18	73°32.523'N,7°58.584'E	2 510	2.3	21.1		
2008	Loki`s Castle	GS08A-CTD15d-19	73°32.523'N,7°58.584'E	2 158	0.9	1.6		
2008	Loki`s Castle	GS08A-CTD15d-20	73°32.523'N,7°58.584'E	1 862	0.8	1.5		
2008	Loki`s Castle	GS08A-CTD15e-21	73°32.521'N,7°58.008'E	2 694	1.2	18.8		
2008	Loki`s Castle	GS08A-CTD15e-22	73°32.521'N,7°58.008'E	2 338	1.8	11.4		
2008	Loki`s Castle	GS08A-CTD15e-23	73°32.521'N,7°58.008'E	2 178	2.5	1.4		
2008	Loki`s Castle	GS08A-CTD15e-24	73°32.521'N,7°58.008'E	1 862	2.6	1.2		
2008	Loki`s Castle	GS08A-CTD16a-1	73°32.750'N,8°00.585'E	2 641	2.9	39.5		
2008	Loki`s Castle	GS08A-CTD16a-2	73°32.750'N,8°00.585'E	2 588	3.0	43.8		
2008	Loki`s Castle	GS08A-CTD16a-3	73°32.750'N,8°00.585'E	2 552	5.3	64.6		
2008	Loki`s Castle	GS08A-CTD16a-4	73°32.750'N,8°00.585'E	2 462	5.6	56.5		
2008	Loki`s Castle	GS08A-CTD16a-5	73°32.750'N,8°00.585'E	2 400	10.0	45.3		
2008	Loki`s Castle	GS08A-CTD16a-6	73°32.750'N,8°00.585'E	2 350	8.8	47.7		
2008	Loki`s Castle	GS08A-CTD16b-9	73°32.516'N,8°00.585'E	2 590	3.6	37.5		
2008	Loki`s Castle	GS08A-CTD16b-10	73°32.516'N,8°00.585'E	2 501	6.9	16.3		
2008	Loki`s Castle	GS08A-CTD16b-11	73°32.516'N,8°00.585'E	2 351	3.4	12.2		
2008	Loki`s Castle	GS08A-CTD16b-12	73°32.516'N,8°00.585'E	2 227	6.0	26.7		
2008	Loki`s Castle	GS08A-CTD16b-13	73°32.516'N,8°00.585'E	2 058	8.4	28.2		
2008	Loki`s Castle	GS08A-CTD16c-14	73°32.325'N,7°59.796'E	2 621	10.2	27.6		
2008	Loki`s Castle	GS08A-CTD16c-15	73°32.325'N,7°59.796'E	2 557	4.4	19.7		
2008	Loki`s Castle	GS08A-CTD16c-16	73°32.325'N,7°59.796'E	2 465	7.0	8.0		
2008	Loki`s Castle	GS08A-CTD16c-17	73°32.325'N,7°59.796'E	2 350	2.3	8.1		

Appendix

year	site	CTD- btl	coordinates	depth	H_2 (nM)	CH_4 (nM)	^3He (fM)	Delta ^3He (%)
2008	Loki`s Castle	GS08A-CTD16c-18	73°32.325'N,7°59.796'E	2 232	8.1	10.6		
2008	Loki`s Castle	GS08A-CTD17a-1	73°32.935'N,8°00.951'E	2 641	3.8	7.5		
2008	Loki`s Castle	GS08A-CTD17a-2	73°32.935'N,8°00.951'E	2 550	3.0	5.0		
2008	Loki`s Castle	GS08A-CTD17a-3	73°32.935'N,8°00.951'E	2 459	3.8	3.5		
2008	Loki`s Castle	GS08A-CTD17a-4	73°32.935'N,8°00.951'E	2 350	3.7	4.2		
2008	Loki`s Castle	GS08A-CTD17a-5	73°32.935'N,8°00.951'E	2 129	7.0	1.8		
2008	Loki`s Castle	GS08A-CTD17a-6	73°32.935'N,8°00.951'E	2 074	5.1	2.1		
2008	Loki`s Castle	GS08A-CTD17b-7	73°33.111'N,8°01.373'E	2 659	6.8	26.9		
2008	Loki`s Castle	GS08A-CTD17b-9	73°33.111'N,8°01.373'E	2 581	3.7	25.7		
2008	Loki`s Castle	GS08A-CTD17b-10	73°33.111'N,8°01.373'E	2 449	7.5	44.9		
2008	Loki`s Castle	GS08A-CTD17b-11	73°33.111'N,8°01.373'E	2 388	7.5	45.6		
2008	Loki`s Castle	GS08A-CTD17b-12	73°33.111'N,8°01.373'E	2 301	10.2	51.2		
2008	Loki`s Castle	GS08A-CTD17b-13	73°33.111'N,8°01.373'E	2 218	10.9	44.0		
2008	Loki`s Castle	GS08A-CTD17b-14	73°33.111'N,8°01.373'E	2 000	41.1	138.3		
2008	Loki`s Castle	GS08A-CTD17c-15	73°33.308'N,8°01.840'E	2 589	4.4	31.0		
2008	Loki`s Castle	GS08A-CTD17c-16	73°33.308'N,8°01.840'E	2 287	10.4	46.7		
2008	Loki`s Castle	GS08A-CTD17c-17	73°33.308'N,8°01.840'E	2 196	27.4	83.0		
2008	Loki`s Castle	GS08A-CTD17c-18	73°33.308'N,8°01.840'E	1 899	181.3	534.4		
2008	Loki`s Castle	GS08A-CTD17c-19	73°33.308'N,8°01.840'E	1 749	11.9	30.9		
2008	Loki`s Castle	GS08A-CTD17d-20	73°33.529'N,8°02.371'E	2 440	11.1	48.4		
2008	Loki`s Castle	GS08A-CTD17d-21	73°33.529'N,8°02.371'E	2 209	20.0	86.9		
2008	Loki`s Castle	GS08A-CTD17d-22	73°33.529'N,8°02.371'E	2 050	52.7	255.2		
2008	Loki`s Castle	GS08A-CTD17d-23	73°33.529'N,8°02.371'E	1 901	71.0	228.8		
2008	Loki`s Castle	GS08A-CTD17d-24	73°33.529'N,8°02.371'E	1 800	172.5	505.0		
2008	Loki`s Castle	GS08A-CTD28a-1	73°33.939'N,8°09.964'E	2 200	4.6	11.6		
2008	Loki`s Castle	GS08A-CTD28a-2	73°33.939'N,8°09.964'E	2 000	7.6	0.0		
2008	Loki`s Castle	GS08A-CTD28b-4	73°33.939'N,8°09.964'E	2 200	4.4	5.8		
2008	Loki`s Castle	GS08A-CTD28b-6	73°33.939'N,8°09.964'E	2 107	5.9	2.8		
2008	Loki`s Castle	GS08A-CTD28b-7	73°33.939'N,8°09.964'E	1 991	173.0	536.8		
2008	Loki`s Castle	GS08A-CTD28b-9	73°33.939'N,8°09.964'E	1 799	4.8	3.4		
2008	Loki`s Castle	GS08A-CTD28e-16	73°33.848'N,8°09.745'E	2 198	5.0	8.9		
2008	Loki`s Castle	GS08A-CTD28e-17	73°33.848'N,8°09.745'E	1 987	482.3	1201.1	3.7	36.6
2008	Loki`s Castle	GS08A-CTD28e-18	73°33.848'N,8°09.745'E	1 914	138.7	418.3	3.1	18.9
2008	Loki`s Castle	GS08A-CTD28e-19	73°33.848'N,8°09.745'E	1 849	5.4	1.9		
2008	Loki`s Castle	GS08A-CTD28e-20	73°33.848'N,8°09.745'E	1 601	3.7	2.7	2.7	6.3

Appendix

year	site	CTD- btl	coordinates	depth	H_2 (nM)	CH_4 (nM)	^3He (fM)	Delta ^3He (%)
2008	Loki`s Castle	GS08A-CTD30-1	73°33.99'N, 8°10.47'E	2 290	2.5	2.1		
2008	Loki`s Castle	GS08A-CTD30-2	73°33.99'N, 8°10.47'E	2 249	90.1	257.5		
2008	Loki`s Castle	GS08A-CTD30-3	73°33.99'N, 8°10.47'E	2 223	174.1	575.6		
2008	Loki`s Castle	GS08A-CTD30-5	73°33.99'N, 8°10.47'E	2 157	1.4	3.2		
2008	Loki`s Castle	GS08A-CTD30-6	73°33.99'N, 8°10.47'E	2 117	1.5	10.1	2.8	6.5
2008	Loki`s Castle	GS08A-CTD30-7	73°33.99'N, 8°10.47'E	2 087	172.2	686.4		
2008	Loki`s Castle	GS08A-CTD30-9	73°33.99'N, 8°10.47'E	2 068	386.7	1138.8	3.7	34.3
2008	Loki`s Castle	GS08A-CTD30-10	73°33.99'N, 8°10.47'E	2 015	463.8	1474.2	4.0	40.4
2008	Loki`s Castle	GS08A-CTD30-11	73°33.99'N, 8°10.47'E	1 978	2.7	3.9	2.8	6.7
2008	Loki`s Castle	GS08A-CTD30-12	73°33.99'N, 8°10.47'E	1 930	2.2	6.7	2.8	6.7
2009	Loki`s Castle	GS09-CTD4-24	73°33.97'N, 08°09.40'E	1 699	1.0	2.1		
2009	Loki`s Castle	GS09-CTD4-23	73°33.97'N, 08°09.40'E	1 835	15.2	3.9		
2009	Loki`s Castle	GS09-CTD4-22	73°33.97'N, 08°09.40'E	1 860	2.4	2.2		
2009	Loki`s Castle	GS09-CTD4-21	73°33.97'N, 08°09.40'E	1 883	2.4	3.4		
2009	Loki`s Castle	GS09-CTD4-20	73°33.97'N, 08°09.40'E	1 899	30.4	38.9		
2009	Loki`s Castle	GS09-CTD4-19	73°33.97'N, 08°09.40'E	1 919	225.5	784.9		
2009	Loki`s Castle	GS09-CTD4-18	73°33.97'N, 08°09.40'E	1 956	454.9	992.4		
2009	Loki`s Castle	GS09-CTD4-17	73°33.97'N, 08°09.40'E	1 963	424.9	1022.7		
2009	Loki`s Castle	GS09-CTD4-16	73°33.97'N, 08°09.40'E	1 993	6.6	5.8		
2009	Loki`s Castle	GS09-CTD4—15	73°33.97'N, 08°09.40'E	2 010	18.8	20.7		
2009	Loki`s Castle	GS09-CTD4-14	73°33.97'N, 08°09.40'E	2 022	50.0	92.0		
2009	Loki`s Castle	GS09-CTD4-13	73°33.97'N, 08°09.40'E	2 031	560.2	1278.5		
2009	Loki`s Castle	GS09-CTD4-12	73°33.97'N, 08°09.40'E	2 042	917.6	2195.3		
2009	Loki`s Castle	GS09-CTD4-11	73°33.97'N, 08°09.40'E	2 053	905.3	2099.3		
2009	Loki`s Castle	GS09-CTD4-10	73°33.97'N, 08°09.40'E	2 075	495.6	905.0		
2009	Loki`s Castle	GS09-CTD4-9	73°33.97'N, 08°09.40'E	2 091	103.5	119.7		
2009	Loki`s Castle	GS09-CTD4-8	73°33.97'N, 08°09.40'E	2 113	77.9	165.9		
2009	Loki`s Castle	GS09-CTD4-7	73°33.97'N, 08°09.40'E	2 153	546.8	1437.1		
2009	Loki`s Castle	GS09-CTD4-6	73°33.97'N, 08°09.40'E	2 168	273.0	856.9		
2009	Loki`s Castle	GS09-CTD4-5	73°33.97'N, 08°09.40'E	2 192	145.3	313.1		
2009	Loki`s Castle	GS09-CTD4-4	73°33.97'N, 08°09.40'E	2 240	1.9	16.2		
2009	Loki`s Castle	GS09-CTD4-3	73°33.97'N, 08°09.40'E	2 276	813.4	2131.8		
2009	Loki`s Castle	GS09-CTD4-2	73°33.97'N, 08°09.40'E	2 337	0.0	14.0		
2009	Loki`s Castle	GS09-CTD4-1	73°33.97'N, 08°09.40'E	2 338	8.6	9.5		
2009	Loki`s Castle	GS09-CTD5-1	73°33.97'N, 08°09.43'E	50	0.0	4.4		
2009	Loki`s Castle	GS09-CTD5-3	73°33.97'N, 08°09.43'E	100	0.0	2.6		
2009	Loki`s Castle	GS09-CTD5-5	73°33.97'N, 08°09.43'E	1 000	0.0	1.4		

Appendix

year	site	CTD- btl	coordinates	depth	H_2 (nM)	CH_4 (nM)	^3He (fM)	Delta ^3He (%)
2009	Loki`s Castle	GS09-CTD6-21	73°33.97'N, 08°09.51'E	451	5.7	10.7		
2009	Loki`s Castle	GS09-CTD6-20	73°33.97'N, 08°09.51'E	450	4	4.2		
2009	Loki`s Castle	GS09-CTD6-19	73°33.97'N, 08°09.51'E	2 201	1509	4427.8		
2009	Loki`s Castle	GS09-CTD6-18	73°33.97'N, 08°09.51'E	2 201	1742.5	5020.2		
2009	Loki`s Castle	GS09-CTD6-17	73°33.97'N, 08°09.51'E	2 201	1616.9	4974.6		
2009	Loki`s Castle	GS09-CTD6-16	73°33.97'N, 08°09.51'E	2 201	842.9	997.4		
2009	Loki`s Castle	GS09-CTD6-15	73°33.97'N, 08°09.51'E	2 201	2103.5	6192.1		
2009	Loki`s Castle	GS09-CTD6-14	73°33.97'N, 08°09.51'E	2 201	2192.9	6271.4		
2009	Loki`s Castle	GS09-CTD6-13	73°33.97'N, 08°09.51'E	2 201	2032.1	5965.3		
2009	Loki`s Castle	GS09-CTD6-12	73°33.97'N, 08°09.51'E	2 201	2132.1	6166.5		
2009	Loki`s Castle	GS09-CTD6-11	73°33.97'N, 08°09.51'E	2 201	2186	6381.0		
2009	Loki`s Castle	GS09-CTD6-10	73°33.97'N, 08°09.51'E	2 201	2151.2	5907.7		
2009	Loki`s Castle	GS09-CTD6-9	73°33.97'N, 08°09.51'E	2 201	2970.7	8231.3		
2009	Loki`s Castle	GS09-CTD6-8	73°33.97'N, 08°09.51'E	2 201	2166.8	6155.0		
2009	Loki`s Castle	GS09-CTD6-7	73°33.97'N, 08°09.51'E	2 201	2169.6	6416.1		
2009	Loki`s Castle	GS09-CTD6-6	73°33.97'N, 08°09.51'E	2 201	2103	6352.2	8.4	154.4
2009	Loki`s Castle	GS09-CTD6-1	73°33.97'N, 08°09.51'E	2 337	61.8	164.4		
2009	Loki`s Castle	GS09-CTD7-	73°32.97'N, 08°09.60'E	451	3.3	1.2		
2009	Loki`s Castle	GS09-CTD7	73°32.97'N, 08°09.60'E	451	2.8	13.1		
2009	Loki`s Castle	GS09-CTD7	73°32.97'N, 08°09.60'E	2 091	122.6	194.5		
2009	Loki`s Castle	GS09-CTD7	73°32.97'N, 08°09.60'E	2 091	127.2	199.0	3.1	17.3
2009	Loki`s Castle	GS09-CTD7	73°32.97'N, 08°09.60'E	2 091	118.0	194.6		
2009	Loki`s Castle	GS09-CTD7	73°32.97'N, 08°09.60'E	2 314	5.1	150.2		
2009	Loki`s Castle	GS09-CTD7	73°32.97'N, 08°09.60'E	2 314	2.7	7.8		
2009	Loki`s Castle	GS09-CTD8-20	73°33.24'N, 08°11.14'E	450	0.3	4.7		
2009	Loki`s Castle	GS09-CTD8-19	73°33.24'N, 08°11.14'E	450	1.1	2.5		
2009	Loki`s Castle	GS09-CTD8-7	73°33.24'N, 08°11.14'E	2 100	0.0	9.2		
2009	Loki`s Castle	GS09-CTD8-6	73°33.24'N, 08°11.14'E	2 100	0.4	8.4		
2009	Loki`s Castle	GS09-CTD8-2	73°33.24'N, 08°11.14'E	2 300	0.7	23.0		
2009	Loki`s Castle	GS09-CTD8-1	73°33.24'N, 08°11.14'E	2 300	0.0	16.1		

Appendix

9.2 Appendix 2- The Jan Mayen Vent Fields

All CTD casts from the JMVF area in the period 2008, 2009 and 2012. The year, sample, coordinates, depth, concentration of H_2, CH_4 and ^3He are given for each cast.

Year	Location	CTD-btl	Coordinates	Depth(m)	H_2 (nM)	CH_4 (nM)	^3He (fM)	Delta ^3He (%)
2008	JMVF	GS08B-CTD2-2	71°17.78N, 5°46.32W	351	0.0	32.1		
2008	JMVF	GS08B-CTD2-3	71°17.78N, 5°46.32W	353	2.1	27.0		
2008	JMVF	GS08B-CTD2-4	71°17.78N, 5°46.32W	310	1.7	8.3		
2008	JMVF	GS08B-CTD2-5	71°17.78N, 5°46.32W	293	3.1	14.5		
2008	JMVF	GS08B-CTD2-6	71°17.78N, 5°46.32W	262	2.1	11.6		
2008	JMVF	GS08B-CTD3-1	71°17.75N, 5°46.18W	459	3.1	58.0		
2008	JMVF	GS08B-CTD3-2	71°17.75N, 5°46.18W	332	1.7	17.0		
2008	JMVF	GS08B-CTD3-3	71°17.75N, 5°46.18W	298	5.8	8.9		
2008	JMVF	GS08B-CTD3-4	71°17.75N, 5°46.18W	266	0.0	3.3		
2008	JMVF	GS08B-CTD3-5	71°17.75N, 5°46.18W	208	0.0	5.2		
2008	JMVF	GS08B-CTD4-1	71°17.74N, 5°46.02W	445	nm*	102.9		
2008	JMVF	GS08B-CTD4-2	71°17.74N, 5°46.02W	386	nm*	48.2		
2008	JMVF	GS08B-CTD4-3	71°17.74N, 5°46.02W	339	nm*	61.3		
2008	JMVF	GS08B-CTD4-4	71°17.74N, 5°46.02W	320	nm*	21.9		
2008	JMVF	GS08B-CTD4-5	71°17.74N, 5°46.02W	254	nm*	8.2		
2008	JMVF	GS08B-CTD5-1	71°17.61N, 5°46.06W	494	0.0	46.4		
2008	JMVF	GS08B-CTD5-2	71°17.61N, 5°46.06W	413	0.0	53.7		
2008	JMVF	GS08B-CTD5-3	71°17.61N, 5°46.06W	301	0.0	4.3		
2008	JMVF	GS08B-CTD5-4	71°17.61N, 5°46.06W	217	0.0	3.4		
2008	JMVF	GS08B-CTD6-1	71°17.71N, 5°46.04W	456	0.0	56.7		
2008	JMVF	GS08B-CTD6-2	71°17.71N, 5°46.04W	392	1.1	65.0		
2008	JMVF	GS08B-CTD6-3	71°17.71N, 5°46.04W	301	0.0	5.7		
2008	JMVF	GS08B-CTD6-4	71°17.71N, 5°46.04W	271	0.0	5.3		
2011	JMVF	GS11A-CTD2-1	71°16.02`N, 5°46.49`W	691	129.2	14.1		
2011	JMVF	GS11A-CTD2-2	71°16.02`N, 5°46.49`W	650	84.9	9.0		
2011	JMVF	GS11A-CTD2-3	71°16.02`N, 5°46.49`W	599	0.7	10.0		
2011	JMVF	GS11A-CTD2-4	71°16.02`N, 5°46.49`W	549	116.8	23.7		
2011	JMVF	GS11A-CTD2-5	71°16.02`N, 5°46.49`W	499	157.8	41.2		
2011	JMVF	GS11A-CTD2-6	71°16.02`N, 5°46.49`W	449	2.2	3.1		

Appendix

Year	Location	CTD-btl	Coordinates	Depth(m)	H_2 (nM)	CH_4 (nM)	^{3}He (fM)	Delta ^{3}He (%)
2011	JMVF	GS11A-CTD2-7	71°16.02`N, 5°46.49`W	399	2.0	2.8		
2011	JMVF	GS11A-CTD2-8	71°16.02`N, 5°46.49`W	349	29.4	7.2		
2011	JMVF	GS11A-CTD2-9	71°16.02`N, 5°46.49`W	300	130.1	8.7		
2011	JMVF	GS11A-CTD2-10	71°16.02`N, 5°46.49`W	249	36.8	5.1		
2011	JMVF	GS11A-CTD2-11	71°16.02`N, 5°46.49`W	199	0.6	3.1		
2011	JMVF	GS11A-CTD2-12	71°16.02`N, 5°46.49`W	148	109.5	9.2		
2011	JMVF	GS11A-CTD3-1	71°17.86`N, 5°46.30`W	440	7.3	118.7	3.7	38.6
2011	JMVF	GS11A-CTD3-2	71°17.86`N, 5°46.30`W	409	7.2	68.4	3.2	20.5
2011	JMVF	GS11A-CTD3-3	71°17.86`N, 5°46.30`W	379	1.7	42.0	3.0	10.5
2011	JMVF	GS11A-CTD3-4	71°17.86`N, 5°46.30`W	349	3.9	20.8	2.8	7.3
2011	JMVF	GS11A-CTD3-5	71°17.86`N, 5°46.30`W	319	7.2	14.9	2.8	5.5
2011	JMVF	GS11A-CTD3-6	71°17.86`N, 5°46.30`W	289	4.5	5.3	2.7	1.5
2011	JMVF	GS11A-CTD3-7	71°17.86`N, 5°46.30`W	258	106.8	7.7	2.5	-0.2
2011	JMVF	GS11A-CTD3-8	71°17.86`N, 5°46.30`W	229	36.0	4.3	2.6	0.0
2011	JMVF	GS11A-CTD3-9	71°17.86`N, 5°46.30`W	199	61.3	5.4	2.5	-0.9
2011	JMVF	GS11A-CTD3-10	71°17.86`N, 5°46.30`W	169	0.5	2.7	2.6	0.3
2011	JMVF	GS11A-CTD3-11	71°17.86`N, 5°46.30`W	140	0.1	2.7	2.5	-0.6
2011	JMVF	GS11A-CTD3-12	71°17.86`N, 5°46.30`W	110	74.1	6.6	2.6	-1.1
2011	JMVF	GS11A-CTD9-1	71°15.70`N, 5°48.81`W	630	5.5	15.2	3.0	16.0
2011	JMVF	GS11A-CTD9-2	71°15.70`N, 5°48.81`W	599	3.0	11.8	3.1	15.0
2011	JMVF	GS11A-CTD9-3	71°15.70`N, 5°48.81`W	550	3.2	9.2	2.8	6.2
2011	JMVF	GS11A-CTD9-4	71°15.70`N, 5°48.81`W	500	0.1	9.0	2.7	5.1
2011	JMVF	GS11A-CTD9-5	71°15.70`N, 5°48.81`W	449	0.0	4.7	2.7	3.1
2011	JMVF	GS11A-CTD9-6	71°15.70`N, 5°48.81`W	399	4.9	0.4	2.7	2.1
2011	JMVF	GS11A-CTD9-7	71°15.70`N, 5°48.81`W	349	4.0	6.6	2.6	1.0
2011	JMVF	GS11A-CTD9-8	71°15.70`N, 5°48.81`W	299	3.8	2.2	2.7	0.6
2011	JMVF	GS11A-CTD9-9	71°15.70`N, 5°48.81`W	249	3.8	2.6	2.6	0.9
2011	JMVF	GS11A-CTD9-10	71°15.70`N, 5°48.81`W	199	1.3	2.8	2.6	-0.2
2011	JMVF	GS11A-CTD9-11	71°15.70`N, 5°48.81`W	149	4.8	3.4	2.6	-0.4
2011	JMVF	GS11A-CTD9-12	71°15.70`N, 5°48.81`W	99	0.0	3.4	2.5	-0.7
2011	JMVF	GS11A-CTD10-1	71°17.84`N, 5°46.41`W	495	6.6	34.0		
2011	JMVF	GS11A-CTD10-2	71°17.84`N, 5°46.41`W	460	9.2	36.9		
2011	JMVF	GS11A-CTD10-3	71°17.84`N, 5°46.41`W	429	6.4	32.1		
2011	JMVF	GS11A-CTD10-4	71°17.84`N, 5°46.41`W	400	5.5	23.1		
2011	JMVF	GS11A-CTD10-5	71°17.84`N, 5°46.41`W	370	1.8	12.3		
2011	JMVF	GS11A-CTD10-6	71°17.84`N, 5°46.41`W	340	4.7	6.0		
2011	JMVF	GS11A-CTD10-7	71°17.84`N, 5°46.41`W	309	5.5	3.2		
2011	JMVF	GS11A-CTD10-8	71°17.84`N, 5°46.41`W	279	7.5	2.5		
2011	JMVF	GS11A-CTD10-9	71°17.84`N, 5°46.41`W	249	8.4	3.4		
2011	JMVF	GS11A-CTD10-10	71°17.84`N, 5°46.41`W	218	8.6	2.5		

Appendix

Year	Location	CTD-btl	Coordinates	Depth(m)	H_2 (nM)	CH_4 (nM)	^{3}He (fM)	Delta ^{3}He (%)
2011	JMVF	GS11A-CTD10-11	71°17.84`N, 5°46.41`W	190	8.6	2.5		
2011	JMVF	GS11A-CTD10-12	71°17.84`N, 5°46.41`W	159	8.7	9.5		
2011	JMVF	GS11A-CTD11-1	71°17.154`N, 6°14.192`W	439	4.2	3.1		
2011	JMVF	GS11A-CTD11-2	71°17.154`N, 6°14.192`W	409	7.4	2.2		
2011	JMVF	GS11A-CTD11-3	71°17.154`N, 6°14.192`W	379	4.5	6.8		
2011	JMVF	GS11A-CTD11-4	71°17.154`N, 6°14.192`W	349	6.5	2.9		
2011	JMVF	GS11A-CTD11-5	71°17.154`N, 6°14.192`W	319	9.8	2.6		
2011	JMVF	GS11A-CTD11-6	71°17.154`N, 6°14.192`W	289	6.9	2.0		
2011	JMVF	GS11A-CTD11-7	71°17.154`N, 6°14.192`W	259	0.5	2.3		
2011	JMVF	GS11A-CTD11-8	71°17.154`N, 6°14.192`W	229	0.3	5.2		
2011	JMVF	GS11A-CTD11-9	71°17.154`N, 6°14.192`W	200	1.4	2.8		
2011	JMVF	GS11A-CTD11-10	71°17.154`N, 6°14.192`W	169	5.5	3.5		
2011	JMVF	GS11A-CTD11-11	71°17.154`N, 6°14.192`W	139	1.6	2.8		
2011	JMVF	GS11A-CTD11-12	71°17.154`N, 6°14.192`W	109	0.3	3.0		
2012	JMVF	GS12B-CTD4-1	71°17.875`N,05°46.316`W	520	4.3	118.0	3.8	38.8
2012	JMVF	GS12B-CTD4-2	71°17.875`N, 05°46.316`W	490	0.0	111.3	3.4	26.9
2012	JMVF	GS12B-CTD4-4	71°17.875`N, 05°46.316`W	459	0.6	95.0		
2012	JMVF	GS12B-CTD4-5	71°17.875`N, 05°46.316`W	429	1.0	112.3		
2012	JMVF	GS12B-CTD4-6	71°17.875`N, 05°46.316`W	399	0.0	163.0	3.5	29.5
2012	JMVF	GS12B-CTD4-7	71°17.875`N, 05°46.316`W	339	1.0	114.8		
2012	JMVF	GS12B-CTD4-8	71°17.875`N, 05°46.316`W	309	0.0	13.3	3.4	27.8
2012	JMVF	GS12B-CTD4-9	71°17.875`N, 05°46.316`W	280	0.0	1.7		
2012	JMVF	GS12B-CTD4-10	71°17.875`N, 05°46.316`W	249	1.3	1.5	2.5	0.3
2012	JMVF	GS12B-CTD4-11	71°17.875`N, 05°46.316`W	219	1.3	1.4		
2012	JMVF	GS12B-CTD4-12	71°17.875`N, 05°46.316`W	189	2.1	2.0		
2012	JMVF	GS12B-CTD4-13	71°17.875`N, 05°46.316`W	160	1.1	0.0		
2012	JMVF	GS12B-CTD4-14	71°17.875`N, 05°46.316`W	129	0.0	1.5		
2012	JMVF	GS12B-CTD4-15	71°17.875`N, 05°46.316`W	99	0.0	1.1		
2012	JMVF	GS12B-CTD4-16	71°17.875`N, 05°46.316`W	70	0.0	0.0		
2012	JMVF	GS12B-CTD4-17	71°17.875`N, 05°46.316`W	39	0.4	0.4		
2012	JMVF	GS12B-CTD4-18	71°17.875`N, 05°46.316`W	9	0.0	1.3		
2012	JMVF	GS12B-CTD6-1	71°17.875`N, 05°46.191`W	451	0.0	90.6		
2012	JMVF	GS12B-CTD6-2	71°17.875`N, 05°46.191`W	400	0.0	92.9		
2012	JMVF	GS12B-CTD6-4	71°17.875`N, 05°46.191`W	300	2.1	14.4		
2012	JMVF	GS12B-CTD6-5	71°17.875`N, 05°46.191`W	250	1.3	2.9		
2012	JMVF	GS12B-CTD6-6	71°17.875`N, 05°46.191`W	200	2.0	2.6		
2012	JMVF	GS12B-CTD6-7	71°17.875`N, 05°46.191`W	149	0.7	2.1		
2012	JMVF	GS12B-CTD6-8	71°17.875`N, 05°46.191`W	99	0.0	2.0		
2012	JMVF	GS12B-CTD6-9	71°17.875`N, 05°46.191`W	49	0.5	1.7		

Appendix

Year	Location	CTD-btl	Coordinates	Depth(m)	H_2 (nM)	CH_4 (nM)	^{3}He (fM)	Delta ^{3}He (%)
2012	JMVF	GS12B-CTD7-1	71°17.840`N, 05°46.246`W	454	1.9	102.3		
2012	JMVF	GS12B-CTD7-2	71°17.840`N, 05°46.246`W	399	0.7	105.1		
2012	JMVF	GS12B-CTD7-4	71°17.840`N, 05°46.246`W	347	0.0	62.6		
2012	JMVF	GS12B-CTD7-5	71°17.840`N, 05°46.246`W	299	0.0	11.9		
2012	JMVF	GS12B-CTD7-6	71°17.840`N, 05°46.246`W	249	0.0	1.9		
2012	JMVF	GS12B-CTD7-7	71°17.840`N, 05°46.246`W	199	0.6	0.7		
2012	JMVF	GS12B-CTD7-8	71°17.840`N, 05°46.246`W	149	1.1	0.7		
2012	JMVF	GS12B-CTD7-9	71°17.840`N, 05°46.246`W	99	0.0	1.2		
2012	JMVF	GS12B-CTD7-10	71°17.840`N, 05°46.246`W	49	0.0	2.5		
2012	JMVF	GS12B-CTD8-1	71°17.919`N, 05°46.177`W	460	0.0	76.1		
2012	JMVF	GS12B-CTD9-1	71°17.920`N, 05°46.322`W	565	5.7	92.5		
2012	JMVF	GS12B-CTD10-1	71°17.919`N, 05°46.493`W	580	0.8	63.4		
2012	JMVF	GS12B-CTD10-2	71°17.919`N, 05°46.493`W	268	0.0	8.8		
2012	JMVF	GS12B-CTD11-1	71°17.892`N, 05°46.322`W	515	0.0	52.6		
2012	JMVF	GS12B-CTD11-2	71°17.892`N, 05°46.322`W	319	0.4	33.8		
2012	JMVF	GS12B-CTD12-1	71°17.862`N, 05°46.100`W	548	3.6	121.6		
2012	JMVF	GS12B-CTD12-2	71°17.862`N, 05°46.100`W	468	1.9	88.8		
2012	JMVF	GS12B-CTD12-4	71°17.862`N, 05°46.100`W	298	0.6	1.0		
2012	JMVF	GS12B-CTD13-1	71°17.801`N, 05°46.436`W	548	0.0	89.1		
2012	JMVF	GS12B-CTD13-2	71°17.801`N, 05°46.436`W	468	0.2	100.7		
2012	JMVF	GS12B-CTD13-4	71°17.801`N, 05°46.436`W	298	0.0	35.2		
2012	JMVF	GS12B-CTD20-1	71°17.880`N, 05°46.312`W	510	6.3	122.7		
2012	JMVF	GS12B-CTD20-2	71°17.880`N, 05°46.312`W	499	6.9	180.2		
2012	JMVF	GS12B-CTD20-19	71°17.880`N, 05°46.312`W	448	1.4	62.6		
2012	JMVF	GS12B-CTD20-4	71°17.880`N, 05°46.312`W	398	0.5	92.4		
2012	JMVF	GS12B-CTD20-5	71°17.880`N, 05°46.312`W	349	3.1	43.1		
2012	JMVF	GS12B-CTD20-6	71°17.880`N, 05°46.312`W	298	0.1	23.1		
2012	JMVF	GS12B-CTD20-7	71°17.880`N, 05°46.312`W	248	0.2	5.9		
2012	JMVF	GS12B-CTD20-8	71°17.880`N, 05°46.312`W	199	0.5	2.6		
2012	JMVF	GS12B-CTD20-9	71°17.880`N, 05°46.312`W	149	1.5	2.2		
2012	JMVF	GS12B-CTD20-10	71°17.880`N, 05°46.312`W	98	1.3	1.8		
2012	JMVF	GS12B-CTD20-11	71°17.880`N, 05°46.312`W	48	1.3	1.5		
2012	JMVF	GS12B-CTD20-12	71°17.880`N, 05°46.312`W	9	0.0	2.9		

Appendix

Year	Location	CTD-btl	Coordinates	Depth(m)	H_2 (nM)	CH_4 (nM)	^3He (fM)	Delta ^3He (%)
2012	JMVF	GS12B-CTD22-1	71°17.825`N, 05°46.683`W	590	0.0	53.7	3.2	20.7
2012	JMVF	GS12B-CTD22-2	71°17.825`N, 05°46.683`W	549	1.4	59.8	3.1	21.0
2012	JMVF	GS12B-CTD22-4	71°17.825`N, 05°46.683`W	498	1.5	56.8		
2012	JMVF	GS12B-CTD22-5	71°17.825`N, 05°46.683`W	449	0.3	65.8		
2012	JMVF	GS12B-CTD22-6	71°17.825`N, 05°46.683`W	398	0.0	56.4	3.1	19.1
2012	JMVF	GS12B-CTD22-7	71°17.825`N, 05°46.683`W	349	0.1	61.9		
2012	JMVF	GS12B-CTD22-8	71°17.825`N, 05°46.683`W	297	0.0	15.5		
2012	JMVF	GS12B-CTD22-9	71°17.825`N, 05°46.683`W	249	0.8	3.3	2.7	6.4
2012	JMVF	GS12B-CTD22-10	71°17.825`N, 05°46.683`W	199	1.2	1.9		
2012	JMVF	GS12B-CTD22-11	71°17.825`N, 05°46.683`W	149	0.8	0.9		
2012	JMVF	GS12B-CTD22-12	71°17.825`N, 05°46.683`W	99	0.4	2.1		
2012	JMVF	GS12B-CTD22-13	71°17.825`N, 05°46.683`W	49	0.0	3.2		
2012	JMVF	GS12B-CTD22-14	71°17.825`N, 05°46.683`W	7	0.6	2.3		
2012	JMVF	GS12B-CTD23-1	71°15.558`N, 05°48.902`W	709	o.o	79.6		
2012	JMVF	GS12B-CTD23-2	71°15.558`N, 05°48.902`W	629	0.9	22.5		
2012	JMVF	GS12B-CTD23-4	71°15.558`N, 05°48.902`W	559	0.0	22.0		
2012	JMVF	GS12B-CTD23-5	71°15.558`N, 05°48.902`W	489	1.0	70.4		
2012	JMVF	GS12B-CTD23-6	71°15.558`N, 05°48.902`W	419	0.1	34.3		
2012	JMVF	GS12B-CTD23-7	71°15.558`N, 05°48.902`W	349	2.2	2.1		
2012	JMVF	GS12B-CTD23-8	71°15.558`N, 05°48.902`W	278	0.0	3.4		
2012	JMVF	GS12B-CTD23-9	71°15.558`N, 05°48.902`W	207	0.0	2.6		
2012	JMVF	GS12B-CTD23-10	71°15.558`N, 05°48.902`W	139	0.0	4.7		
2012	JMVF	GS12B-CTD23-11	71°15.558`N, 05°48.902`W	69	1.0	2.6		
2012	JMVF	GS12B-CTD23-12	71°15.558`N, 05°48.902`W	10	2.3	2.6		
2012	JMVF	GS12B-CTD25-1	71°04.766`N, 07°25.272`W	1 677	0.0	2.7		
2012	JMVF	GS12B-CTD25-2	71°04.766`N, 07°25.272`W	1 332	0.2	0.9		
2012	JMVF	GS12B-CTD25-4	71°04.766`N, 07°25.272`W	1 035	0.4	0.3		
2012	JMVF	GS12B-CTD25-5	71°04.766`N, 07°25.272`W	991	0.0	0.0		
2012	JMVF	GS12B-CTD25-6	71°04.766`N, 07°25.272`W	890	0.0	1.0		
2012	JMVF	GS12B-CTD25-7	71°04.766`N, 07°25.272`W	790	3.0	0.9		
2012	JMVF	GS12B-CTD25-8	71°04.766`N, 07°25.272`W	691	2.4	2.3		
2012	JMVF	GS12B-CTD25-9	71°04.766`N, 07°25.272`W	592	0.0	1.1		
2012	JMVF	GS12B-CTD25-10	71°04.766`N, 07°25.272`W	444	0.3	2.3		
2012	JMVF	GS12B-CTD25-11	71°04.766`N, 07°25.272`W	197	0.0	0.4		
2012	JMVF	GS12B-CTD25-12	71°04.766`N, 07°25.272`W	99	0.0	1.6		
2012	JMVF	GS12B-CTD25-13	71°04.766`N, 07°25.272`W	9	0.0	3.1		

*not measured.

Appendix